

A Comprehensive Review of Artificial Intelligence Applications in Major Retinal Conditions

Hina Raja · Taimur Hassan^{*} · Bilal Hassan · Muhammad Usman
Akram · Hira Raja · Alaa A Abd-alrazaq · Siamak Yousefi · Naoufel
Werghi

Received: date / Accepted: date

Abstract This paper provides a systematic survey of retinal diseases that cause visual impairments or blindness, emphasizing the importance of early detection for effective treatment. It covers both clinical and automated approaches for detecting retinal disease, focusing

on studies from the past decade. The survey evaluates various algorithms for identifying structural abnormalities and diagnosing retinal diseases, and it identifies future research directions based on a critical analysis of existing literature. This comprehensive study, which reviews both clinical and automated detection methods using different modalities, appears to be unique in its scope. Additionally, the survey serves as a helpful guide for researchers interested in digital retinopathy.

Keywords Artificial intelligence, Optical Coherence Tomography (OCT), Fundus, Diabetic Retinopathy (DR), Glaucoma, Age-related Macular Degeneration (AMD)

Hina Raja
Department of Ophthalmology, University of Tennessee
Health Science Center, Memphis, USA
E-mail: h.raja@uthsc.edu

Taimur Hassan (*Corresponding Author)
Department of Electrical, Computer, and Biomedical Engineering, Abu Dhabi University, Abu Dhabi, UAE
E-mail: taimur.hassan@adu.ac.ae

Bilal Hassan
Department of Electrical Engineering and Computer Science, Khalifa University, Abu Dhabi, United Arab Emirates.
E-mail: bilal.hassan@ku.ac.ae

Muhammad Usman Akram
Department of Computer and Software Engineering, National University of Sciences and Technology, Pakistan
E-mail: usman.akram@ceme.nust.edu.pk

Hira Raja
Margalla Institute of Health Sciences, Rawalpindi, Pakistan
E-mail: dhanyalhira@gmail.com

Alaa A. Abd-alrazaq
AI Center for Precision Health, Weill Cornell Medicine-Qatar, Doha, Qatar
E-mail: aaa4027@qatar-med.cornell.edu

Siamak Yousefi
Department of Ophthalmology, University of Tennessee Health Science Center, Memphis, USA
E-mail: siamak.yousefi@uthsc.edu

Naoufel Werghi
Center for Cyber-Physical Systems (C2PS), Department of Electrical Engineering and Computer Science, Khalifa University, Abu Dhabi, United Arab Emirates
E-mail: naoufel.werghi@ku.ac.ae

1 Introduction

Vision is the most important of all the senses and plays a key part in everyone's life. According to a report by the World Health Organization (WHO) in 2012, the number of individuals with visual impairment (VI) was estimated to be 285 million (Pascolini and Mariotti, 2012). Among the total population of 285 million individuals, a significant proportion of 246 million were observed to have low vision (LW), while 39 million were identified as being blind. The population of visually impaired individuals experienced an increase to 2.2 billion in the year 2019, with approximately one billion cases potentially preventable through timely and accurate diagnosis (ref, 2020 (accessed December 24, 2020) (Figure 1). The leading causes of vision impairment and blindness are retinal diseases, which include trachoma (2 M), diabetic retinopathy (3 M), corneal opacities (4.2 M), glaucoma (6.9 M), cataract (65.2 M), and refractive error (123.7 M). The retinal disease slowly progresses; initially, there are often no symptoms, so it is difficult

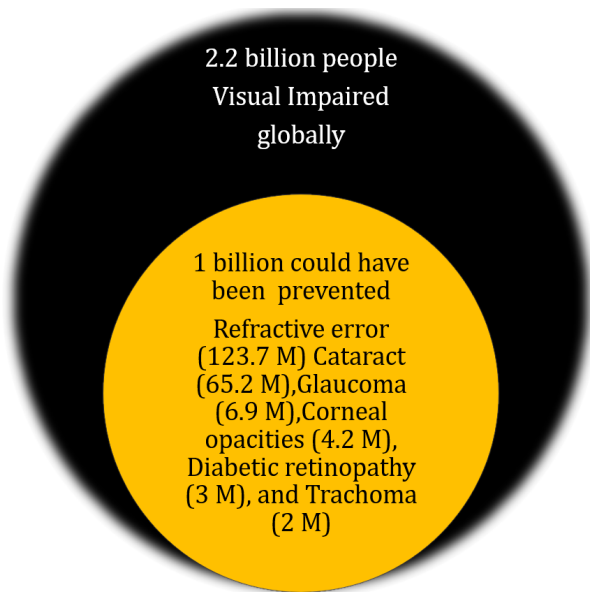


Fig. 1: Global prevalence of people with vision impairment and preventable diseases, as depicted by WHO statistics.

for most of the subjects to detect the early symptoms. According to the report, fifty percent of the patients in the United States were found to be uninformed about their ocular condition (Tham et al., 2014). As the early symptoms are left undetected so these VI subjects lead towards permanent blindness. The goal of the global community is to uplift eye care facilities by providing early detection of retinal diseases to halt the progression through appropriate treatment in order to preserve vision. Due to the high correlation between retinal diseases and blindness, a lot of clinical research is going on for screening retinal diseases in the early stages. Due to the subjective nature and time expenditure of manually extracting the retinal lesion, automated methods are used to aid ophthalmologists. Improvements to these automated procedures are the subject of ongoing research. In this paper, we are discussing clinical pathophysiology of retinal diseases and various modalities which have been used to detect them. Optical coherence tomography (OCT), Optical coherence tomography angiography (OCTA), color fundus photography (CFP), fundus fluorescein angiography (FFA), and ultrawide-field photography (UWFP) modalities have been used for diagnosis of retinal abnormalities. CFP has been widely employed for the initial screening of various retinal abnormalities. However, OCT is extensively used by ophthalmologists for the detection of ocular disorders and to monitor their progression. In addition to this, a comprehensive review of automated studies related to the detection of retinal diseases is presented.

1.1 Existing Surveys

Retinal image analysis is a wide research area where clinicians and researchers work together to devise techniques for the early detection of retinopathies. We critically reviewed survey studies related to retinal analysis in the context of clinical and automated literature. However, most of the review articles are either disease-specific or modality-specific. The next section summarizes each category of review papers found in the literature.

1.1.1 Disease-specific survey papers

Nicholson et al. (Nicholson et al., 2013) performed a systematic review to analyze the pathogenesis of central serous chorioretinopathy (CSR). The study (Khalil et al., 2014) presented a survey to detect glaucoma changes through fundus images. Preprocessing, feature extraction, feature selection, and machine learning (ML) techniques were discussed. Gupta et al. (Gupta and Karandikar, 2015) reported a survey study that analyzes the automated techniques for DR diagnosis. A comparison was made between the algorithm that detects the various structural changes through fundus images. A total of 13 studies were included in the survey. The review study (Das et al., 2016) was presented in the literature that analyzed diabetic macular edema (DME) management in Indian subjects. Muramatsu et al. (Muramatsu et al., 2018) presented the survey for the treatment of DME in Japanese subjects. The clinical and technical review was presented for glaucoma diagnosis through fundus and OCT images (Naveed et al., 2017). Pead et al. (Pead et al., 2019) presented a review study that evaluated the ML and deep learning (DL) techniques for automated drusen detection in the context of AMD. The paper included only those studies which detected the drusen in color fundus photography. A total of 14 articles were reviewed and only compared the ML and DL methods presented in those studies. Araki et al. (Araki et al., 2019) presented a survey to analyze the effect of steroids on Japanese CSR subjects. Another clinical review (Van Rijssen et al., 2019) investigated the different treatments related to CSC, which included photodynamic therapy, laser treatment, and pharmacology. The survey (Lakshminarayanan et al., 2021) was conducted over the period of five years, from 2016 to 2021, to investigate the automated techniques, which includes ML and DL approaches, for the detection of DR in fundus and OCT images. A total of 114 papers were comprehensively reviewed from the open literature. Another review study (Ab-

dullah et al., 2021) was presented that compared the automated ML techniques to detect the structural changes in fundus images. In addition to this, the author discussed the various fundus-related datasets (public and private). Rubina et al. (Sarki et al., 2020) comprehensively reviewed state-of-the-art approaches for the detection of diabetic and glaucomatous changes through fundus images. Image processing, ML, and DL techniques were explored. The author also reported available datasets. The paper (Bala et al., 2021b) presented the clinical and technical survey for glaucoma diagnosis. It reported DL techniques for detecting pathological changes in fundus and OCT images. The study (Shahriari et al., 2022) discussed how artificial intelligence (AI) is being used to screen, diagnose, and categorize DME.

1.1.2 Modality-specific survey papers

Michael et al. (Abramoff et al., 2010) presented a clinical review of the retinal imaging trends. Besides this, the paper summarized the most prevalent causes of blindness, which include AMD, DR, and glaucoma. The review was about 2-D fundus imaging and 3-D OCT imaging techniques. Another study (Das and Malathy, 2018) in the literature presented the clinical review of fundus images for detecting retinal diseases. The study (Kafieh et al., 2013) is modality specific, where image segmentation methods were reviewed for processing the retinal OCT images. The OCT segmentation approaches were classified into five categories, such as A-scan, B-scan, active contour, AI methods, 3D graphs, and 3D OCT volumetric. Baghaie et al. (Baghaie et al., 2015) reported the major issues related to OCT image analysis. More specifically, different techniques for noise reduction, image segmentation, and registration were discussed. Usman et al. (Usman et al., 2017) provided an exhaustive review of various class image processing and computer vision techniques for detecting glaucoma, DR, and pathological myopia. The authors also reported the causes, symptoms, and pathological alterations of these diseases in OCT images, which can aid in the development of an automated system for the detection of retinal disorders. The precision of algorithms determined performance after an exhaustive examination and evaluation of various methods. Khan (Khan et al., 2019) presented a survey that is also modalities-specific. The survey comprehends the automated techniques for extracting retinal vessels in fundus images. The techniques are categorized into supervised and unsupervised groups. Supervised approaches are further classified into ensemble classification and neural network-based

approaches. However, unsupervised techniques are grouped into four classes: matched filtering, mathematical morphological, multi-scale-based techniques, and region-growing methods. A valuable comparison was made among the techniques which were reported on the publicly available datasets. In the article (Nuzzi et al., 2021), a clinical review was reported on the state-of-the-art applications for AI in ophthalmology, which helps clinicians to have an overview of growing trends. The paper (Badar et al., 2020) was modality specific, focusing on DL techniques for retinal analysis through fundus images. The review includes automated disease classification methods based on retinal pathological landmarks. The methods were evaluated using accuracy, F score, sensitivity, specificity, and area under ROC curve on publicly available datasets. Angiography has gained popularity in the field of ophthalmology for the diagnosis of ocular diseases. Boned (Boned-Murillo et al., 2022) presented the survey study related to OCTA in diabetes subjects. Deep learning techniques were reported for the detection of retinal vascularization. Stolte et al. (Stolte and Fang, 2020) performed a comprehensive survey for DR diagnosis covering the clinical and technical aspects. The paper also described the publicly available datasets of the fundus and OCT modalities. In addition to this, ML and DL frameworks were reviewed for the detection and classification of DR. However, fundus-related literature was more critically reviewed as compared to OCT and OCTA modalities. A systematic review of clinical and technical studies across many disorders and modalities, represented as a chord diagram (Figure 2) illustrating the relationship between different categories.

There are other review studies reported in the literature that are either modality specific (Amini and Rabbani, 2016) (Salehi et al., 2022) (Raja et al., 2022) (Im et al., 2022) (Ye et al., 2023) (Vujosevic et al., 2023) (Khalili et al., 2023) (Pavithra et al., 2023), or disease-specific (Keenan et al., 2022) (Jimenez-Carmona et al., 2022) (Aboobakar and Wiggs, 2022) (Ong and Fawzi, 2022) (Mauschitz and Finger, 2022) (Chou et al., 2022) (Patel et al., 2022) (Fea et al., 2022) (Yuksel Elgin et al., 2022) (Wang et al., 2022c) (Huang et al., 2022b) (Chauhan et al., 2022) (Srivastava et al., 2023) (Iannucci et al., 2023) (Saeed et al., 2023), but a single study is not to be considered as a comprehensive survey for retinal analysis of various diseases.

1.2 Our contribution

Following are the major contributions of this survey.

1. To the best of our knowledge, this is the first study that presents a comprehensive review of clinical and

Table 1: Summary of review studies related to retinal diseases. The abbreviation are: CL: Clinical, TEC: Technical, CVAS: Cardiovascular, SJG: Surgery, MAG: Management NeuroD: Neurodegeneration, TRT: Treatment, PMED: Precision Medicine, CAT: Cataract, and GLA: Glaucoma

Study	Modality	Timeline	Disease	Category
Abramoff et al. (2010)	Fundus, OCT	till 2010	Glaucoma, AMD, DR	TEC
Kafieh et al. (2013)	OCT	1997 to 2012	-	CL, TEC
Nicholson et al. (2013)	FFA, OCT, Adaptive Optics	till 2012	CSR	CL
Gupta and Karandikar (2015)	Fundus	2009-2013	DR	TEC
Baghaie et al. (2015)	OCT	1980 to 2015	-	TEC
Das et al. (2016)	FFA, OCT	till 2015	DME	CL
Usman et al. (2017)	OCT	till 2015	GLA, DR, Myopia	CL, TEC
Muramatsu et al. (2018)	-	till 2017	DME	CL
Khan et al. (2019)	Fundus	till 2017	GLA, DR, AMD	TEC
Peard et al. (2019)	Fundus	2018	AMD	TEC
Araki et al. (2019)	-	till 2018	CSR	CL
Van Rijssen et al. (2019)	-	till 2019	CSR	CL
Stolte and Fang (2020)	Fundus, OCT, OCTA	till 2020	DR	CL, TEC
Lakshminarayanan et al. (2021)	Fundus, OCT	2016-2021	DR	TEC
Abdullah et al. (2021)	Fundus	till 2021	GLA	TEC
Sarki et al. (2020)	Fundus	2016-2020	GLA, DR	TEC
Bala et al. (2021b)	Fundus, OCT	till 2021	GLA	CL, TEC
Badar et al. (2020)	Fundus	till 2018	GLA, AMD, DR	TEC
Nuzzi et al. (2021)	-	till 2021	GLA, AMD, CAT, DR	CL
Boned-Murillo et al. (2022)	OCTA	till 2021	DR	TEC
Elsharkawy et al. (2022)	Fundus, FFA, OCT, OCTA	till 2021	DR	CL, TEC
Salehi et al. (2022)	OCT	till 2021	AMD	CL
Chou et al. (2022)	-	2021	GLA	CL
Aboobakar and Wiggs (2022)	-	2021	GLA	CL (Gene)
Shahriari et al. (2022)	Fundus, OCT	till July 2021	DME	TEC
Mauschitz and Finger (2022)	-	Oct 2021	AMD	Clinical
Patel et al. (2022)	-	2021	GLA	Clinical (TRT)
Raja et al. (2022)	OCT	till 2021	GLA	CL, TEC
Fea et al. (2022)	-	2021	GLA	CL (TRT)
Yuksel Elgin et al. (2022)	-	2020	GLA	CL
Wang et al. (2022c)	-	2020	GLA	CL (Gene)
Huang et al. (2022b)	-	2021	DME	CL (TRT)
Im et al. (2022)	-	2021	DME	CL
Chauhan et al. (2022)	-	2021	DME	CL (TRT)
Pavithra et al. (2023)	Fundus	2022	DME	TEC
Srivastava et al. (2023)	-	2022	GLA, DR, AMD, CAT	TEC
Sharma et al. (2023)	-	2021	GLA	CL (MAG)
Iannucci et al. (2023)	-	-	Uveitic GLA	CL (MAG)
Fea et al. (2023)	-	Aug 2022	GLA	CL (PMED)
Saeed et al. (2023)	-	-	GLA	CL (SJG)
Ye et al. (2023)	OCT, Fundus	-	DR GLA	TEC
Vujosevic et al. (2023)	OCT	-	-	CL (NeuroD)
Khalili et al. (2023)	OCTA	Nov 2020	-	CL

automated literature related to various retinal diseases, which are major causes of blindness.

2. This paper presents a detailed survey of fundus and OCT modalities for retinal analysis, reporting almost all the significant aspects.
3. To the best of our knowledge, this review is the novel that targets most retinal diseases such as AMD, glaucoma, DR, and DME.

The rest of the paper is organized as section II presents the methods used for conducting this review study, section III describes the anatomy of the human eye,

and section IV presents the significance of retinal diseases toward blindness. Section V discusses the different modalities used to detect retinal disorders. Sections VI and VII highlight the pathological changes and clinical severity of major retinal diseases, respectively. The clinical literature related to retinal disorders is discussed in section VIII. Whereas section IX presents a review of automated algorithms for detecting different biomarkers and classification of retinal disorders based on image processing techniques, ML, and DL techniques. Section X discusses the

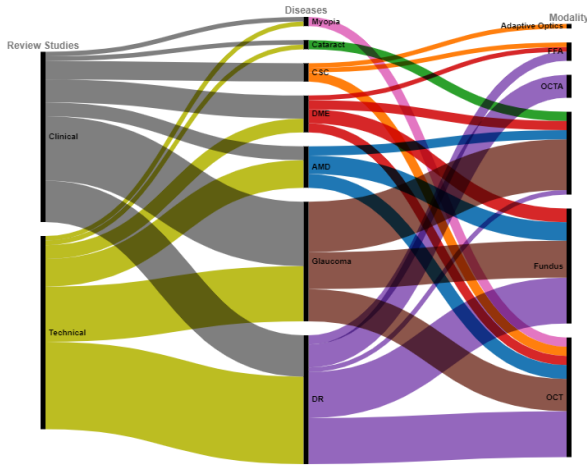


Fig. 2: Chord diagram showing the interactions between categories in a systematic review of clinical and technical studies across multiple diseases and modalities. The diagram highlights the relationships between subcategories of diseases (e.g., glaucoma, DR, AMD, DME, Cataract, and CSR) and modalities (e.g., Fundus, OCT, OCTA, Adaptive optics, and FFA). The thickness of the chords represents the strength of the connections between the categories, with thicker chords indicating stronger connections.”

advanced DL techniques and related work found in the literature. The publicly available dataset for fundus and OCT have summarised in section XI. Finally, future directions are discussed in section XI.

2 Methods

2.1 Timeline

We included studies published only in the last decade (i.e., January 2013- January 2023).

2.2 Eligibility Criteria

The following descriptions serve as eligibility criteria for the studies that were included in the review: (1) studies include clinical and experimental findings related to ocular diseases (diabetic retinopathy (DR), glaucoma, age-related macular degeneration (AMD), macular edema (ME)), (2) studies presented an automated algorithm for detection of different retinal lesions, (3) segmentation and classification techniques, (4) image processing techniques, classic

machine learning techniques, deep learning models, (5) modalities fundus, FFA, OCT, and OCTA). The main exclusion criteria were studies that were not related to the above-mentioned disease and data from conference reports, communications, or letters.

2.3 Search Strategy

The studies were retrieved from secondary sources, which included internet sources, reports, conferences, and journal articles. Sampling is purposive, aimed at having a review study on diagnosing and detecting the retinal lesion. The review was performed by searching articles on retinal diseases from PubMed, Science Direct, IEEE Xplore Digital Library, Springer Link, and Google Scholar. The search was carried out with a combination of different keywords, which included retinal diseases, diabetic retinopathy (DR), glaucoma, age-related macular degeneration (AMD), macular edema (ME), automated detection, machine learning model, deep learning model, and advanced deep learning techniques. The search criteria were intentionally broad in order to encompass all studies that could potentially meet the eligibility criteria. Original peer-reviewed articles were considered regardless of publication status.

2.4 Study selection process

Articles found in the primary search were evaluated for eligibility to be included in the review based on their relevance to the research question or topic. We follow the review protocol of Systematic Reviews and Meta-analysis (PRISMA), shown in table 3.

2.5 Data extraction and Synthesis

Following a thorough reading and summary of the chosen publications, the key points and arguments from each were extracted and synthesized in a separate file. The following findings were extracted from selected studies: pathological association from clinical or experimental articles, techniques, datasets, and results from technical literature. Results include evaluation metrics such as accuracy, sensitivity, specificity, precision, recall, F1 score, and intersection over union. However, some of the discussed studies have limited data, as we could not access the full paper.

3 Eye anatomy

Vision is the most preponderant sense and plays a pivotal role. The human visual system consists of the sensor organ eye and parts of the central nervous system,

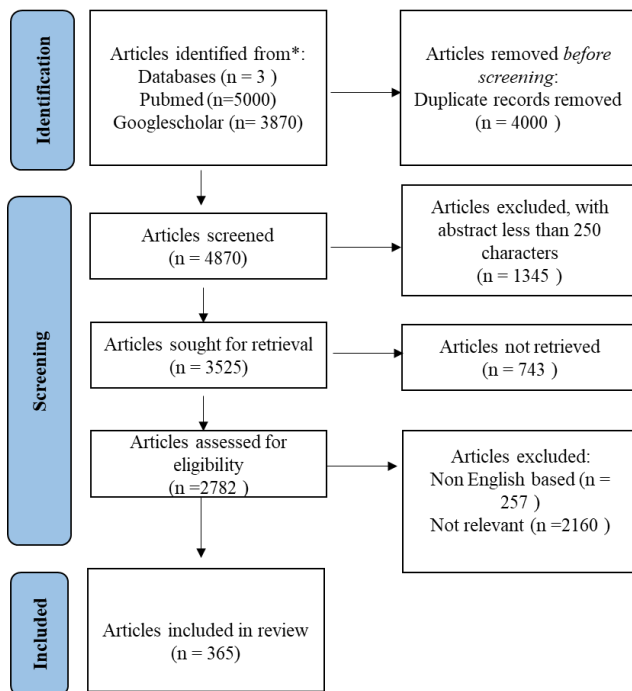


Fig. 3: PRISMA Flowchart for the Inclusion of studies in a review study of retinal diseases. The flowchart outlines the process of study selection and inclusion in the review, including the number of articles retrieved, screened, excluded, and included at each step.

which are the optic nerve, optic track, and visual cortex. The eye is a sensory organ that receives visual data and sends it to the brain. Eye is the most complicated structure in the human body; it is spherical in shape and consists of three layers (Willoughby et al., 2010). The outermost layer of eye is made up of the sclera and cornea (see Figure 4). The sclera is composed of connective tissues, which helps in maintaining the eye shape and it also provides protection to the whole eyeball. The anterior most part of an eye is cornea, which is a protective transparent membrane that covers the iris and pupil. The human cornea has an average horizontal and vertical diameter of 11.5mm and 10.5mm, respectively. Beneath the sclera, a choroid lies that contains blood vessels that provide oxygen and nourishment to the whole eyeball (Hassan et al., 2016b). Moreover, the third and innermost layer of an eyeball is the retina, which contains light-sensitive tissues responsible for producing vision. The retina comprises two main regions, i.e., the macular region (also known as the macula of the retina) and the peripheral region (Hassan et al., 2018b). Light enters the eye through the pupil, is focused by the biconvex lens, and lands on the retina, where the macular region uses rod and cone cells in the macular center (called the fovea) to produce central vi-

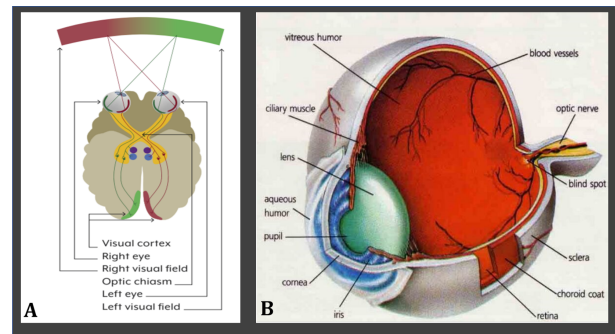


Fig. 4: A. Visual system of the human eye. It consists of the eye, optic nerve, and visual cortex (Gilbert et al., 2019). B. The structure of the human eye consists of three layers (ref (2019 (accessed Nov 5, 2020)).

sion. The peripheral region is responsible for producing side vision (Raja et al., 2020c). The other parts of the eye's middle layer are the choroid, the ciliary body, and the iris. The ciliary body provides support to the lens and also produces the aqueous humor. Also, the movement of the pupil is regulated by the iris, which controls the amount of light that gets into the eye through contraction and relaxation process (Hassan et al., 2015). Furthermore, the retina has ten layers that help translate visual data into the electrical signals that are sent to the brain. The electrical signals are transmitted from the retina to the brain through the optic nerve situated near the optic nerve head (ONH) region of the peripheral retina.

4 Significance of retina & retinal diseases towards blindness

The retina is the light-sensitive innermost layer of the eye, which transmits visual information to the brain for interpretation. These neural impulses reach the brain, where they are combined with stored knowledge to generate a complete picture of the object's context. Because the retina and optic nerve protruded from the developing brain, it is regarded to be a member of the brain's central nervous system (CNS). Because of this, it is the only region of the central nervous system that may be visualized without resorting to invasive procedures. There are ten layers to the retina (see Figure 5), and each layer is responsible for a certain function, such as transforming light into electrical signals. The inner limiting membrane (ILM), which is made up of astrocytes and müller cells, is the first retinal layer beneath the vitreous body. Retinal ganglion cells (RGCs) with axons make up the retina's second layer, the retinal nerve fiber (RNFL). The 1.5 million retinal ganglion cell axons in the human eye converge at the optic nerve

head (ONH), travel through the inner and outer neural canals, and finally exit the eye and enter the brain (Medeiros et al., 2012). Lamina cribrosa (LC) and bruch opening membrane (BMO) refer to the inner and outer neural canals, respectively. The LC is an inmost layer of the ONH and, thus a posterior sclera. It is a network of capillaries that provide nourishment to RGCs and a 3D network of elastic porous connective tissues (Park and Park, 2013). The fenestrated trabeculae create a pathway for the egress of RGC axons and vascular tissue. The ganglion cell layer (GCL) follows the RNFL and contains the bodies of ganglion cells. The inner plexiform layer (IPL) is situated posterior to the GCL and encompasses the synaptic connections between the dendrites of the ganglion, amacrine, and bipolar cells. The fifth position within the ocular anatomy is occupied by the inner nuclear layer (INL). It consists of the cell bodies of amacrine, bipolar, and horizontal cells. The next layer of the retina is the outer plexiform layer (OPL), which consists of a dense network of neuronal synapses between the dendrites of horizontal, bipolar cells (from INL) and photoreceptor cells. The outer nuclear layer (ONL) consists of the rod and cone nuclei responsible for visual phototransduction. The human retina contains approximately 7 million cones and 75-150 million rods. Cones correspond to photopic vision, whereas rods are responsible for scotopic vision. Cones are concentrated in the fovea, while rods are distributed throughout the retina, with the exception of the fovea. Cones and rods undergo a chemical transformation that transmits electrical impulses to the nerves. Initially, signals travel through bipolar and horizontal cells, then amacrine and ganglion cells, and finally, optic nerve fibers to the brain. These neural layers are responsible for processing the incoming picture data. The rod is the source of the signals, while the cones are the unprocessed data from individual points that are used to identify more complex features, including shapes, colors, contrasts, and motion. In contrast, photoreceptor cells' nucleus and inner segments are separated by an outer limiting membrane (OLM). Each photoreceptor cell's inner and outer segments can be found in the IO/OS layer. Retinal pigment epithelium (RPE) is located between IO/OS and choroid and is the outermost layer of the retina.

5 Retinal Imaging Modalities

Several examinations have been performed to identify and track the advancement of ocular disorders. The perimeter has been utilized to assess visual field (VF) impairments. Fundoscopy is a primary diagnostic tool employed by ophthalmologists to examine the eye. The

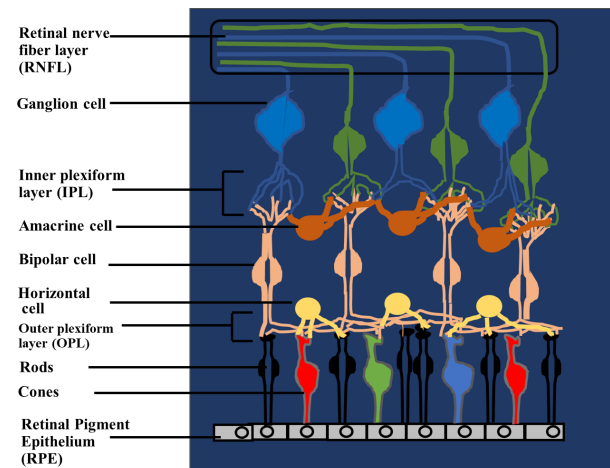


Fig. 5: Systemic view of retinal layers of the human eye.

key areas of interest that can be evaluated through this technique include the ONH, macula, peripheral retina, and central retina. The fundus image, however, does not reveal any information about the retinal layers' pathological changes. Imaging techniques like OCT/OCTA, scanning laser polarimetry, and confocal scanning laser ophthalmoscopy are utilized to evaluate the retinal layers, macula, and ONH quantitatively. OCT provides assessments of both the retinal layers and the optic disc, in contrast to CSLO, SLP, and other methods that test only the optic disc. However, OCT has seen widespread usage as an imaging tool for identifying structural retinal abnormalities and tracking the number of ocular illnesses. A variety of imaging modalities are available for the screening and diagnosis of ocular illnesses, and the following sections provide an introduction to them.

5.1 Fundus Imagery

Fundus photography is used to analyze the rear of eye known as fundus (Tran et al., 2012). In fundus photography, specialized fundus cameras are utilized that are comprised of an intricate microscope and it is connected to a flash-enabled camera. The principle of fundus cameras is based on the concept of monocular indirect ophthalmoscopy (ref, 2022 (accessed Jan 25, 2022)). A fundus camera shows a magnified view of the fundus region. A typical camera shows 30 to 50° of the retinal area with a 2.5x magnification. This relationship can be changed with zoom or auxiliary lenses from 15°, which gives a 5x magnification, to 140°, which gives a 0.5x magnification with a wide-angle lens. The objective lens of the camera focuses the light from the observer's retina using a set of lenses formed like a doughnut with a central aperture and an annulus in the center. The

light that is reflected from the retina goes through the hole in the doughnut that isn't lit up by the lighting system. As each system's light path is separate, the resulting image contains very few reflected rays. The light that forms a picture travels onward into the modest magnification telescopic eyepiece. When the shutter release is activated, a mirror moves into the light path, reflecting the flash bulb's light into the subject's eye. At the same time, a mirror drops in front of the observation telescope, focusing the incoming light onto the film or digital CCD.

Fundus photography can be conducted utilizing chromatic filters or specialized contrast agents such as fluorescein and indocyanine green [ref \(2022 \(accessed Jan 25, 2023\)\)](#). Color fundus photograph (CFP) is acquired when the retina is illuminated by white light. A filter is utilized during the process of red-free fundus photography so that superficial lesions and certain vascular anomalies inside the retina and the surrounding tissue can be observed more clearly. The wavelengths of light between 540 and 570 nanometers are blocked by using a green filter. This provides a stronger contrast for viewing retinal blood vessels and accompanying hemorrhages, yellowish lesions such as exudates and drusen, and abnormalities in the nerve fiber layer and epiretinal membranes. This technique can be used to evaluate the course of DR by better monitoring intraretinal microvascular anomalies and disc and other areas of neovascularization. In addition, red-free photography is frequently utilized as a baseline photo before angiography is performed [Lim et al. \(2020\)](#). By injecting a fluorescent dye into a patient's bloodstream, an angiographer can take pictures and make recordings of the blood flow within the retina and surrounding tissue. When exposed to light of a certain wavelength (excitation color), this dye fluoresces in a distinct color. The autofluorescent light is then isolated by a barrier filter, preventing the passage of any other light. Sodium fluorescein angiograms (known as FAF) are used to visualize retinal vascular disease; they require a blue excitation and fluoresce a yellow light of around 490nm 530nm, respectively. CME and DR are two of the many eye diseases for which FAF is commonly utilized. Indocyanine Green Angiography, or ICG, is utilized primarily to analyze deeper choroidal diseases. It uses a near-infrared diode laser of 805 nm and barrier filters that allow light of 500nm and 810nm. Choroidal vascular outpouching can be observed with ICG in a variety of diseases, including CSC, ocular malignancies, and hyperpermeable vessels.

Structures such as the macula, OD, and central retina are easily discernible on a fundus photograph. Fundus images are widely used by ophthalmologists for

initial screening of retinal diseases, such as DR, glaucoma, AMD, and DME [Son et al. \(2022\)](#). As the fundus photograph is two-dimensional, it does not provide a detailed analysis of retinal layers. For detecting and diagnosing common eye illnesses, fundus photography can be used to track the effects of anti-malarial treatment on patients by documenting any changes in the fundus during routine screening. Fundus photography had a remarkable period of development and evolution over the last decade. The fundus camera market is very competitive, with brands including Welch Allyn, Kowa, Zeiss, Digisight, Topcon, Canon, Nidek, CSO, CenterVue, Ezer, and Optos. Amazing advancements in telecommunications and smartphone technology have made ophthalmology screening in remote areas a practical option. Therefore, recently portable fundus cameras are gaining popularity for initial screening of retinal diseases [\(Yao et al., 2022\)](#). These portable cameras are beneficial in rural areas and especially in developing countries where ophthalmologist to patient ratio is low and where access to healthcare facilities are limited [\(Panwar et al., 2016\)](#).

5.2 Fundus Autofluorescence (FAF)

Fundus autofluorescence (FAF) is a non-invasive imaging modality that has gained popularity in research and clinical applications due to its capacity to map naturally and pathologically occurring fluorophores in the posterior pole of the eye. FAF was first used for in vivo fundus imaging in 1995, when Delori et al. [\(Delori et al., 1995\)](#) characterized the intrinsic autofluorescent properties of the human retina using a novel fundus spectrophotometer. The fluorescence utilized the characteristics of lipofuscin within the RPE to produce an image. Fluorophores stored as lipofuscin in postmitotic RPE cells' lysosomal storage bodies provide the majority of the excitation light, while photopigments in the outer photoreceptor segments filter it. Lipofuscin is made up of many different bisretinoids, such as A2E, A2PE, isoA2E, and A2-DHP-PE, and is a result of the lysosomal degradation of photoreceptor outer segments [\(Pole and Ameri, 2021\)](#). Bisretinoids, depending on the lipofuscin's chemistry, absorb blue light with a peak excitation wavelength of 470 nm and produce yellow-green light with a peak wavelength of 600 nm when exposed to a light source. After a detector has recorded the emission signals, the image can be interpreted as a density map of lipofuscin, with darker areas denoting lower density [\(Schmitz-Valckenberg et al., 2021\)](#). In addition, the detected signal can be disrupted by any fluorophore or filter present in the light path, even under healthy conditions. Abnormal patterns of autofluorescence (AF) on

FAF imaging can serve as indicators for retinal disease since numerous retinal disorders frequently lead to RPE dysfunction and buildup of lipofuscin. Blood is able to substantially absorb the blue (488nm) or green (514nm) light that is generally employed in FAF imaging, therefore blood vessels appear black in a normal fundus without retinal disease. Since there is no retinal pigment epithelium (RPE) or lipofuscin in the optic nerve, it may appear dark depending on the imaging device. The high concentration of light-absorbing xanthophyll pigment in the fovea makes it visible as a spot of hypo-AF with blue or green short-wavelength FAF. Abnormal areas of hyper-autofluorescence (AF) develop when there is either an abnormally high concentration of lipofuscin or other substances with a comparable autofluorescent spectrum, or abnormally high fluorescence transmission. Notable causes of hyper-AF include: optic disc drusen, loss of macular photopigment, presence of subretinal autofluorescent material, and increased RPE lipofuscin.

Particularly with progressive nuclear cataracts and when employing short-wavelength light (i.e., blue light) for excitation, the lens is a significant confounder of the signal. Actually, the brownish-yellowing of the lens, which usually develops with age, is a strong absorber of blue excitation light. It blocks the excitation light on its way to the posterior pole and makes its own fluorescence light, which is then scattered in the light path and interferes with the FAF detection of signals from the ocular fundus. Blocking can also be seen with retinal hemorrhages, but the signal at the site of the hemorrhages may become much stronger over time as a result of the metabolic breakdown of blood chemicals (Sawa et al., 2006). At the fovea and parafovea, a rise in the optical density of melanin and the buildup of macular pigment in the inner retinal layers when blue light is used to excite the eye reduce the FAF signal (Delori et al., 1995). When the RPE degenerates and loses its fluorophores, more fluorophores at the top of the choroid may add to the FAF signal. This could be because of melanolipofuscin at this anatomical level or because of other minor fluorophores like elastin and collagen in the walls of choroidal blood vessels and the sclera. Factors contributing to increased FAF include the bleaching phenomenon and loss of photopigment, which causes decreased absorbance anterior to the RPE level (Bindewald-Wittich et al., 2023).

Many different types of FAF devices have become commercially available as a result of technological advancements; these devices vary in their excitation wavelength (e.g., green short-wavelength, blue short-wavelength), the type of imaging they employ (e.g., confocal scanning laser ophthalmoscope, ultra-widefield confocal scanning

laser ophthalmoscope, broad line fundus imaging, fundus camera), and other factors. The basic mechanism is the same as that used in fluorescein or indocyanine green angiography (i.e., molecules are excited by light in a specific wavelength range, and the emitted light has a longer wavelength than the excitation light). Dye-based angiography detects foreign molecules, whereas FAF imaging relies on the visualization of endogenous fluorophores. Because the necessary molecules for FAF imaging are endogenous, there is no need to inject a contrast agent into a vein.

5.3 Fluorescein Angiography

Fluorescein angiography (FA) has been the gold standard for the identification of retinal vascular abnormalities since 1961 (Weinhaus et al., 1995). Capillaries and deep retinal vasculature are not easily visible, however, even using traditional cameras or even the most cutting-edge scanning laser ophthalmoscope (Keane and Sadda, 2014). Although FA is mainly used for qualitative evaluation of retinal perfusion, the principle of dye dilution tracking has been described for quantifying blood flow. A dye dilution curve is generated by plotting the fluorescein dye concentration in the blood at a given time point against time. In 1965, Hickam and Frayser (Hickam and Frayser, 1965) published the first work utilizing this concept to estimate retinal blood flow. From a series of fluorescein photographs taken 1.5 seconds apart, they determined the mean retinal circulation time, providing a rough estimate of retinal perfusion. A special fundus camera with excitation and barrier filters is needed for FA. High contrast images of the early stages of the angiography are obtained by rapidly injecting fluorescein dye intravenously, typically through an antecubital vein (Hansen et al., 2013). A blue excitation filter is used to modify the white light from a flash. When exposed to blue light (465-490 nm), free fluorescein molecules absorb the energy and fluoresce, emitting yellow-green light (520-530 nm). Excited fluorescein emits light between 520 and 530 nm, which a barrier filter can block. The imaging process begins immediately following the injection and typically lasts for ten minutes. Photographs can be shot digitally or on 35mm film.

5.4 OCT Imagery

OCT is a noninvasive imaging modality that employs low-coherence light to produce a higher-resolution cross-sectional image. (Huang et al., 1991) (Wolfgang and G, 2008). The OCT method is extensively utilized

in ophthalmology, but it also has numerous clinical applications in cardiology, dermatology, oncology, and gastrointestinal Adam et al. (2007). In dermatology, it holds great promise for the early diagnosis of skin cancer and other illnesses. Intravascular OCT also helps detect atherosclerotic lesions in their earliest stages. Future investigations in several clinical domains are likely to include OCT.

OCT imaging is rapidly becoming an essential tool for getting a 3-D image of the retina and is, therefore, the most common application for OCT. The Michelson Interferometer is the apparatus used to acquire an OCT image; it measures the sample's spatial location not through the passage of time but by means of light waves (near the infrared spectrum). The utilization of a super luminescent diode as a source is favored due to its broadband spectrum, which is conducive to the acquisition of deeper structures. The coherence length of the emitted light is a determining factor for the resolution of the OCT machine. Tomography is a method that involves the acquisition of 2D or 3D images of an object through the use of a penetrating wave, which allows for imaging by sections or slices. The fundamental concept underlying OCT technology is rooted in the interference phenomena of light. Specifically, when the depth of a sample corresponds to the time delay of flight of the referencing mirror, they undergo coherent interference, resulting in the production of a detectable signal. This phenomenon is commonly referred to as coherence. An axial scan (A-scan) was generated by calculating the time delay of the reflected light wave from the sample. The reflected signals' intensities are represented using a color scale that mimics the colors of a rainbow. The process of determining color is predicated on the sequence of reflectivity, wherein the color spectrum progresses from black to white, with a corresponding escalation in reflectivity (Thomas and Duguid, 2004). The acquisition of numerous axial scans at consecutive lateral positions can produce a two-dimensional representation, commonly referred to as a B-scan, that depicts a cross-sectional view of the specimen. The 2D map estimates the microstructure's transverse position and depth (Huang et al., 1991). Time-domain optical coherence tomography (TD-OCT) is the standard OCT technique. The depth range is sampled one point at a time by shifting the location of the reference mirror in order to create a longitudinal scan (A-scan). However, in order to achieve an axial scan, the reference mirror must be displaced mechanically by one cycle at a time. The utilization of Fourier transformation facilitated the transition from the conventional TD-OCT technique to the spectral domain OCT (SD-OCT) implementation, owing to

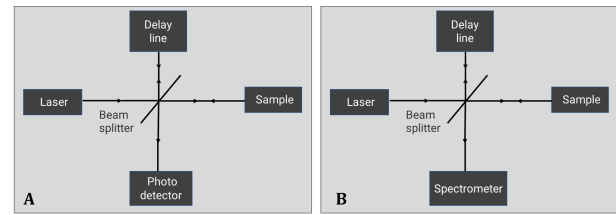


Fig. 6: Illustration of time domain and spectral domain OCT principle. (A) In TD-OCT, the reference mirror moves across a distance. In (B) SD-OCT, the reference mirror remains fixed, and a spectrometer detects the spectral variation.

its technical proficiency. In order to quantify the spectral modulations caused by interference between the reference reflection and the sample reflection, a spectrometer has been utilized in place of a single detector, and the reference mirror has been kept fixed (Huang, 2009). Additionally, a Fourier transform was used to convert the spectrum modulations to depth information in order to capture an axial scan. Schematics of both TD-OCT and SD-OCT are shown in Figure 6 (A and B), respectively. Topcon 3D-OCT 2000 (FD-OCT), Cirrus HD-OCT (FD-OCT), Carl Zeiss Meditec, and Heidelberg Engineering's Spectralis OCT are the commercially available OCT devices.

5.5 Optical Coherence Tomography Angiography

Optical coherence tomography angiography (OCTA) is a noninvasive imaging modality; it is dye-free OCT-based that provides volumetric visualization of retinal and choroidal vasculature (CNV) (Park et al., 2016). OCTA relies on repeated scans of the same area to identify movement. Therefore, time-domain systems with lower speeds prevented the creation of OCTA. Fourier-domain OCT systems initially introduced a factor 50 improvement in scanning speed for OCT, allowing for advanced OCT applications. In 2006, Makita et al. Makita et al. (2006) initially described OCTA utilizing an SD-OCT device with a spectral resolution of 18.7 kHz. With further improvement of OCT hardware and advancement in data processing techniques, higher quality OCT angiograms could be generated with fewer image artifacts.

OCTA is a novel variant of OCT; it has the capability to generate 3D angiograms of the retina and choroid with high resolution. Additionally, it can detect sub-retinal neovascular blood vessels. To analyze structural changes in various retinal illnesses, ophthalmologists are increasingly turning to OCTA, which is rapidly becoming one of the most important diagnostic tools in

the field. Successive OCT-B scans are rapidly acquired and subsequently compared to generate 3D angiograms of the retinal and choroidal vasculature. The decorrelation signal is created by the movement of blood cells from one scan to the next. We currently know that four vascular plexuses provide blood to the retina. The blood flow from the central retinal artery enters the superficial capillary plexus (SCP), which subsequently divides into the intermediate capillary plexus (ICP) and the deep capillary plexus (DCP). SCPs are found in the ganglion, inner plexiform, and RNFL. In contrast to the DCPs, which are below the inner nuclear layer, the ICPs are situated above it (Campbell et al., 2017). Photoreceptors and the outer plexiform layers do not have any blood vessels. Radial peripapillary capillary plexus (RPC) is the fourth retinal plexus, and it is aligned with the axons of the nerve fiber layer. When compared to the DCP, the RPC lacks a lobular structure. OCTA's 3D and higher resolution for visualizing the eye's microvasculature are two of its main benefits over FA. This permits the capillary plexus to be dissected into its superficial and deep components and the latter to be shown in exquisite detail. OCTA is helpful in detecting retinal diseases like CNV (Roisman and Goldhardt, 2017), changes in flow around the optic disc in glaucoma Igarashi et al. (2017), capillary dropouts in DR Schaal et al. (2019), macular malformations in telangiectasia and perfusion loss in vessels occlusions Suzuki et al. (2016). To effectively evaluate the retinal and choroidal vasculature and distinguish between healthy and diseased retina, accurate structural image segmentation is required. Scanning results typically include depth information on vascular anomalies such retinal or choroidal neovascularization (CNV) by coordinating the 3D flow data, provided as 2D images, with the structural data. Table 2 shows the summarised the above-discussed imaging modalities.

6 Major retinal diseases

6.1 Diabetic Retinopathy

Diabetic Retinopathy (DR) is a pathological condition of the eye that results from elevated levels of insulin in the bloodstream, leading to abnormalities in the retina Klein et al. (1984). DR is the leading cause of visual impairment and blindness. DR is a chronic and degenerative ailment that poses a significant challenge due to its asymptomatic nature during the early stages of the disease. Figure 7 (B) shows the visual field of the DR subject. The determination of the severity of DR is contingent upon the quantity and classifications of lesions that are observable on the retinal surface. The

human retina comprises diverse constituents, including blood vessels, the fovea, the macula, and the optic disc (OD). DR is commonly categorized into two stages: non-proliferative DR (NPDR) and proliferative DR (PDR). NPDR is characterized by the impairment of blood vessels within the retina, leading to the leakage of fluid onto the retinal surface (Crick and Khaw, 2003). This results in the swelling and moistening of the retina. NPDR may present with various manifestations of retinopathy, including microaneurysms (MAs), hemorrhages (HMs), exudates (both hard and soft), and inter-retinal microvascular abnormalities (IRMA) (Robert, 1995). PDR is a severe form of DR in which new aberrant blood vessels sprout in various parts of the retina, potentially causing complete blindness. As it is shown in Figure 8, the NPDR lesions can be either MAs, HMs, or EXs. MAs are the earliest detectable indication of DR, and they form when fluid leaks out of the retina's tiny blood capillaries. Their size is smaller, they have a round form, and they are red in color. The breakdown of MA walls results in HMs. Blot HMs are bigger red lesions, while hemorrhages seem like bright red dots (Sjölöe et al., 1997). EXs are yellow spots on the retina caused by blood leakage containing lipids and proteins. If the lipid accumulation is on or close to the macula, it can result in permanent blindness. Both MAs and HMs are classified as dark lesions, while EXs are considered brilliant lesions (Robert, 1995).

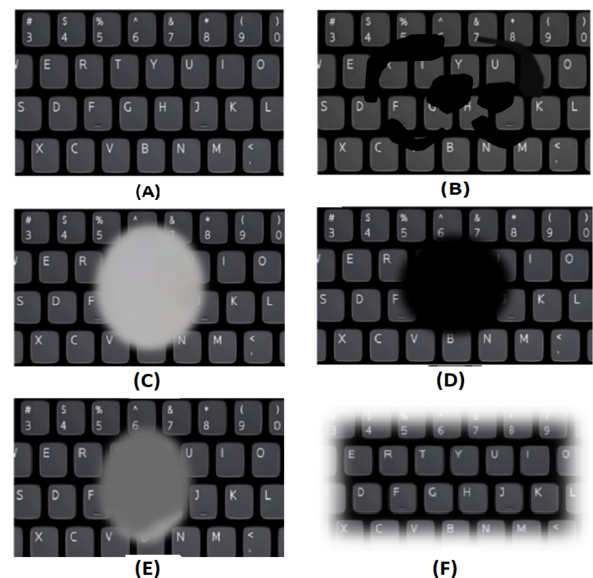


Fig. 7: Visual field of retinal diseases, (A) normal vision, (B) DR VF, (C)DME affected vision, (D) AMD subject's field of view (E) CSCR affected vision (F) Glaucoma affected vision.

Table 2: Summary of imaging modalities used in clinical practice for the screening, diagnosis, and progression monitoring of various ocular diseases. The abbreviation are: INV: Invasive, and NINV: Non-invasive.

Modality	Technique	Information	INV/ NINV	Application	Devices
Fundus	Wide-angle photograph of the retina using specialized cameras	2D view of the retina, visualization of retinal structures, blood vessels, OD, and macula	NINV	Screening, documenting retinal diseases, monitoring progression, general eye examination	Optos Daytona, Topcon Triton, Zeiss Visucam, Nidek AFC-330
OCT	Low-coherence interferometry	High-resolution, three-dimensional imaging of retinal layers	NINV	Diagnosing and monitoring retinal diseases	Cirrus HD-OCT, Spectralis OCT, Topcon 3D OCT, Zeiss Cirrus
OCTA	Combination of OCT and motion contrast imaging	Visualization of retinal and choroidal blood flow, microvascular networks	NINV	Diagnosing and monitoring retinal vascular diseases, including DR, retinal vein occlusion, and macular degeneration	AngioVue, Triton OCT Angio, XR Avanti AngioVue, Cirrus HD-OCT
FA	Intravenous injection of fluorescent dye	Dynamic imaging of retinal circulation, blood flow, leakage	INV	Diagnosing and monitoring retinal vascular diseases, including DR, retinal vein occlusion, and macular degeneration	Spectralis HRA+OCT, Optos Daytona, Topcon TRC-50DX
FAF	Detection of natural autofluorescence emitted by molecules in the RPE	Visualization of metabolic health and integrity of the RPE	NINV	Diagnosing and monitoring retinal disorders involving RPE, including AMD, CSR, and inherited retinal dystrophies	Spectralis HRA+OCT, Optos Daytona, Heidelberg Retina Angiograph 2

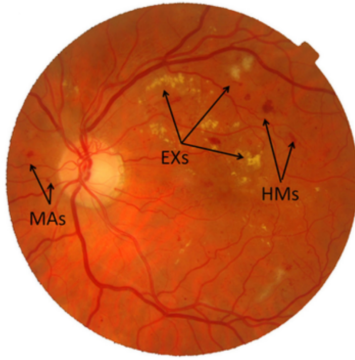


Fig. 8: A fundus scan of DR subject, showing MAS, EXs, and HMs.

sulting in blood leakage within the retina and subsequent formation of cyst segments, as depicted in Figure 9 (A). During advanced stages, the presence of yellowish lipids, commonly referred to as hard exudates, becomes apparent on the superficial layers of the retina. This manifestation can be visualized on fundus images, as depicted in Figure 9 (A).

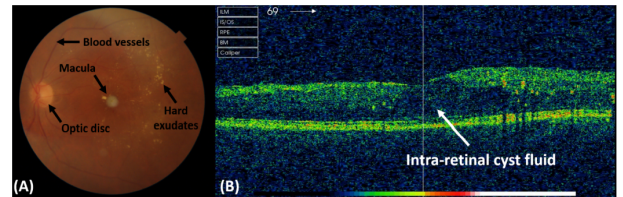


Fig. 9: (A) Fundus scan with hard exudates, (B) corresponding foveal B-scan with intra-retinal cyst fluid

6.2 Diabetic Macular Edema

Diabetic Macular Edema is the most severe form of maculopathy, mainly caused by diabetes. As can be seen in Figure 7, a person's central vision is affected by DME, and it becomes increasingly difficult to regain lost eyesight as the disease progresses. Hyperglycemia causes thinning of the blood vessels in the retina, re-

6.3 Age-related Macular Degeneration

Age-related Macular Degeneration (AMD) is a chronic medical condition that typically impacts both eyes and arises from a metabolic disorder (de Jong et al., 2020).

The condition manifests within the macula, a region of the ocular apparatus that holds particular significance in the process of visual acuity. The etiology of this particular type of maculopathy, which ranks second in terms of prevalence, remains incompletely elucidated. Experts believe that macular degeneration develops when there is an issue with the extremely high-energy metabolic processes that occur in the retina's sensory cells. The body has evolved to handle these reactions and eliminate the metabolic byproducts. If the body is unable to process these compounds, however, they accumulate in the form of drusen. The retina doesn't get enough oxygen and nutrients because of these deposits. Drusen growth behind the retina causes age-related macular degeneration, which typically affects the elderly. Due to the RPE layer thinning or atrophying because of these drusen, central vision blurs, straight lines appear vivid and blind spots develop in the central visual field as the condition progresses, as seen in Figure 7 (D). Pathological AMD symptoms on fundus and OCT images are depicted in Figure 10. AMD can cause significant visual deficits or even irreversible loss of central vision, but it does not cause blindness on its own (Seltman, 2021 (accessed March 5, 2022)). The clinical classification of AMD divides the condition into two subtypes: dry AMD and wet AMD. Under the retina, drusen can form when a patient has dry AMD, also known as non-exudative AMD. In the early stages of the disease, small drusen deposits do not impair vision; nevertheless, they do promote RPE atrophy and the creation of scars, both of which contribute to the gradual dimming and distortion of central vision as the disease advances. If dry AMD isn't treated, it might progress to wet AMD, also known as exudative AMD. Wet AMD, also known as choroidal neovascularization, occurs when aberrant blood vessels in the choroid leak fluid and blood into the retina near the macula. Fluid leakage causes peripheral blind spots and a wavy appearance of straight lines.

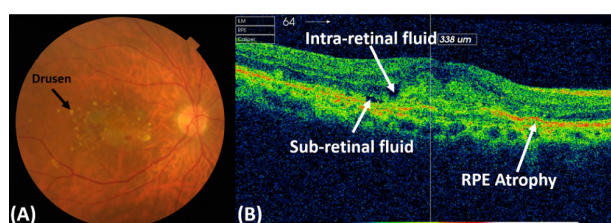


Fig. 10: (A) fundus scan with drusen, (B) corresponding foveal B-scan with intra-retinal fluid (IRF), sub-retinal fluid (SRF), and RPE atrophy

6.4 Glaucoma

Glaucoma is a multifaceted and intricate ocular condition that can result in irreversible vision loss if not addressed. The condition is typically attributed to elevated intraocular pressure (IOP) exceeding 24mm, although it can manifest in eyes with IOP levels within the normal range of less than 20mm. Figure 7(F) depicts the gradual onset and eventual symptomatology of glaucoma. Almost 40% of retinal neurons were lost before there was any detectable VF loss. The ciliary body secretes aqueous humor into the anterior chamber of the eye for its sustenance. The aqueous humor constantly creates and releases fluid through the trabecular meshwork in the anterior chamber angle to maintain a constant IOP (Boyd, Sep 2020 (accessed Nov 9, 2020)). The uveoscleral pathway is responsible for a minor amount of drainage. In the adult population, there is a nearly equivalent ratio of drainage between both tracks. The primary route of drainage in the process of aging is via the trabecular meshwork. The drainage pathways exhibit not only a passive mechanical function but also involve dynamic physiological processes. The elevation of intraocular pressure within the anterior chamber is attributed to the obstruction of fluid outflow or a narrowing of the angle at the point of drainage. When there is an obstruction in the trabecular meshwork, fluid accumulates in the anterior chamber, resulting in increased pressure on the posterior chamber. The nerve fibers are pressurized by the vitreous body, leading to the eventual loss of ganglion cells. This results in the thinning of the ganglion cell complex (GCC) and the enlargement of the optic cup, as depicted in the linked Figure 11. The detection of glaucoma is facilitated by utilizing the thickness profiles of the RNFL, GCL, and IPL layers, which are encompassed by GCC as illustrated in Figure 11 (B).

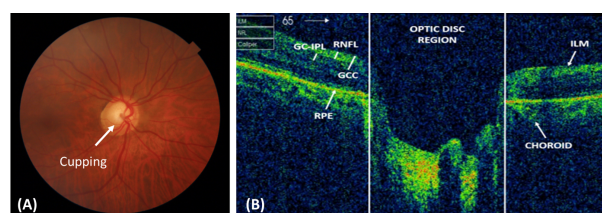


Fig. 11: The structural changes due to glaucoma are shown in the fundus and OCT scans.

7 Clinical severity grading of retinal diseases

7.1 Diabetic Retinopathy

DR is a chronic eye condition that worsens over time. NPDR describes the first stages of the disease, while PDR describes its more advanced phases (Diaz, 2021 (accessed May 22, 2022)). Tiny regions of enlargement in the retinal blood vessels indicate mild NPDR, the initial stage of DR. Microaneurysms are the medical term for these enlarged regions. The macula can expand if even a small amount of fluid leaks into the retina at this stage. When the enlargement of blood vessels is moderate, it begins to obstruct blood flow to the retina, so impairing its ability to receive adequate nutrition. As a result, fluids and blood collect in the macula. When a larger number of blood vessels in the retina become clogged, blood flow to the retina is drastically reduced. Severe NPDR is characterized by the initiation of angiogenesis signaling in the retina, prompting the growth of new blood vessels. PDR occurs when the illness has progressed to an advanced stage and new blood vessels have begun to grow in the retina. The danger of fluid leakage is increased due to the fragility of these blood arteries. This can lead to a variety of vision issues, including blurriness, a diminished field of vision, and even complete blindness.

7.2 Macular Edema

Cystoid macular edema (CME) can occur in non-diabetic patients as a result of macular fluid accumulation, which causes swelling and thickening of the macula. CME is typically caused by conditions such as retinal vein occlusion (RVO), uveitis, cataract, and laser surgeries (Wong, (accessed April 5, 2022)). The clinical grading of DME is based on the extent of retinal thickness, as established by the early treatment diabetic retinopathy study (ETDRS), and is categorized into two stages. Edema that occurs within a 500-micrometer diameter of the fovea is deemed severe due to its significant impact on visual impairment or blindness. The medical term used to describe this stage is clinically significant macular edema (CSME). Non-clinically significant macular edema (non-CSME) refers to the thickening of the retina beyond the specified limit. The visual representation depicted in Figure 12 displays the graded fundus and OCT scans of both CSME and non-CSME cases.

7.3 Age-related Macular Degeneration

The prevalence of AMD rises with age, affecting roughly 1 in 100 people aged 65–75 and 10–20 percent of those

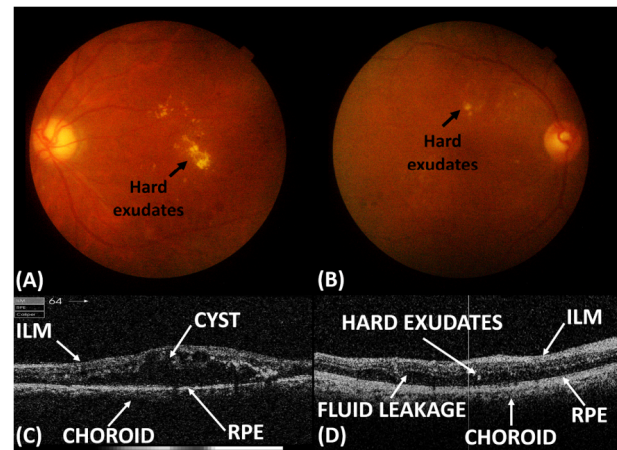


Fig. 12: (A) Fundus scan of CSME subject, (B) fundus scan of non-CSME subject, (C) foveal B-scan of CSME affected subject, (D) foveal B-scan of non-CSME subject

aged 85 and more (Seltman, 2021 (accessed March 5, 2022)). Macular degeneration is the leading cause of significant vision loss among older persons in industrialized countries. In the first of AMD's three stages, when the drusen deposits are still very small, and there has been no loss of pigment, normal vision is maintained. Some persons may experience minor vision loss at the intermediate stage of AMD when big drusen and/or pigment alterations are present. Wet or dry macular degeneration in its advanced stages is the leading cause of blindness in the elderly. Dry AMD is less severe than wet AMD and has a considerably slower progression rate; therefore, it is less likely to result in blindness or other vision impairments. People with advanced AMD typically suffer from wet AMD. The duration of the disease progression towards advanced-stage AMD leading to visual impairment is contingent upon several factors, encompassing the magnitude of the deposits that have accumulated in the retina. Approximately 1-3% of individuals with small drusen encounter visual impairments within a span of five years, while roughly 50% of those with larger drusen develop advanced AMD and suffer from vision deterioration within the same time frame. Wet AMD develops from dry AMD and rapidly worsens if untreated, but its progression can be halted or reduced by a number of treatments. Patients with advanced AMD can struggle to read or recognize familiar faces. Central vision loss is a possible long-term complication of this condition (Seltman, 2021 (accessed March 5, 2022)). Figure 13 shows the fundus and OCT images of AMD subjects.

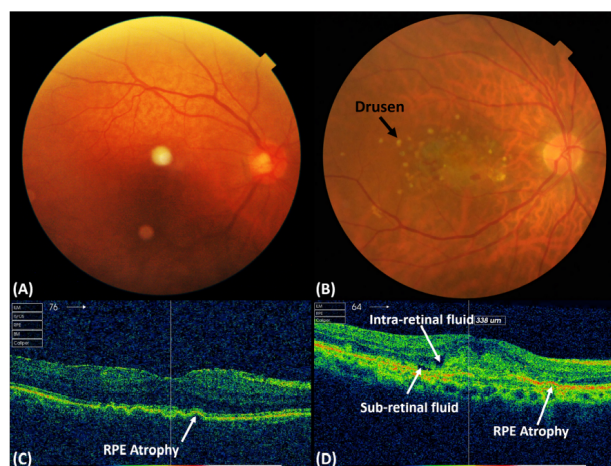


Fig. 13: (A) fundus scan of dry AMD subject, (B) fundus scan of wet AMD subject, (C) foveal B-scan of dry AMD affected subject, (D) foveal B-scan of wet AMD subject

7.4 Glaucoma

Individuals who are aged 40 years or older, have a prolonged history of steroid medication usage, and possess a familial predisposition are at an elevated risk of developing glaucoma (ref, (accessed Dec 12, 2020)). Subjects with smaller optic nerves and thinner corneas are more prone to developing glaucoma. Individuals of African and Asian descent are considered to be at an elevated risk for the development of glaucoma. Furthermore, diabetes, hypertension, migraine headaches, and inadequate blood flow may serve as underlying factors. While there are several subtypes of glaucoma, angle closure glaucoma (ACG) and open-angle glaucoma (OAG) are the most prevalent. While Asians are more likely to develop ACG, Africans are more likely to develop OAG. Each subtype of glaucoma has its own unique set of symptoms and indications. Until VF abnormalities manifest, however, OAG is asymptomatic and causes little discomfort. Pain in the eyes, severe headache, nausea, red eyes, and rapid visual disruption are some of the earliest signs of ACG. Perimeter vision loss happens in the first stage of glaucoma and lies dormant until VF abnormalities become obvious. Furthermore, early symptoms may include double vision and rainbow-colored rings surrounding bright lights. The structural alterations detected by fundus and OCT scans at various glaucoma stages are depicted in Figure 14. Figure 14 (A, B) depicts normal people, while (C, D) displays scans from patients with early-stage glaucoma. As glaucoma progresses, thinning of RNFL occurs and results in enlargement of the cup. This cupping process can easily be observed in Figure

14 (C, D, E, F). If left untreated, the disease progresses over time and results in blindness. Table 3 shows the different stages of ocular diseases.

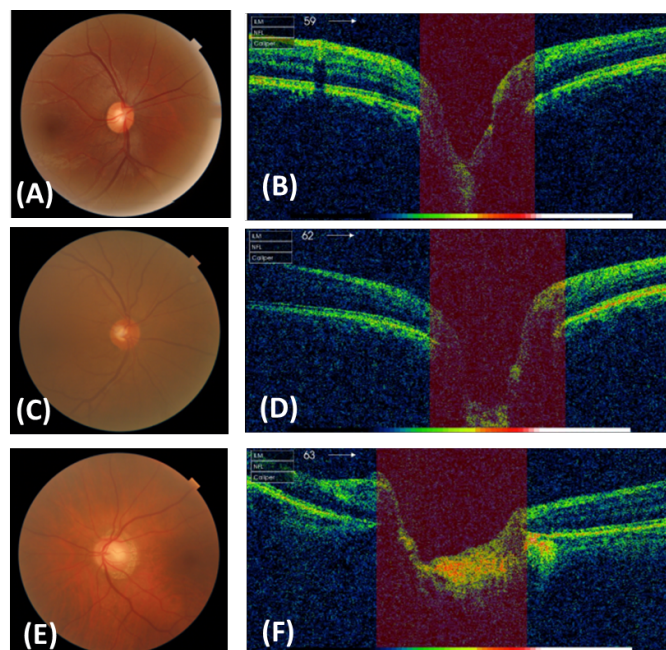


Fig. 14: Fundus and OCT scans of different stages of glaucoma (A), (B) fundus and OCT scans of health subject, (C),(D) Scan of early stage glaucoma subject, and (E)(F) Scan of advance stage glaucomatous eye

8 Clinical studies: Review

The international health care organizations aim to provide an action-oriented, results-driven approach for advancing health equity by improving the quality of care provided to minority and other underserved communities (Hill-Briggs et al., 2021). However, healthcare organizations have increasingly acknowledged the presence of healthcare disparities across race/ethnicity and socioeconomic status, but significantly fewer have made health equity for diverse patients a proper priority (Chin, 2016). The lack of financial incentives is a major barrier to achieving health equity. Now the focus of healthcare organizations is to report clinical findings based on race, ethnicity, and socioeconomic status in order to provide preventive care and primary care facilities all over the world. Social determinants of health (SDOH) have emerged as a primary focus of intervention in the quest for health equity as the healthcare system shifts toward a greater emphasis on population health outcomes and value-based treatment. Clinical ophthalmology studies have recently shifted their focus to SDOH in order to better understand and promote

Table 3: Summarizing the different stages of retinal diseases and their symptoms

Disease	Stages	Symptoms	Risk factors
Diabetes	Early NPDR	Microaneurysm	Family history, African-American, Hispanic, Native American or Asian-American, Having overweight/obesity, Age
	Moderate NPDR	Multiple microaneurysms, dot-and-blot hemorrhages, cotton wool spots	
	Severe NPDR	Microaneurysms, haemorrhages, exudates (hard and soft), and inter-retinal microvascular abnormalities	
	PDR	Neovascularization, blurriness, reduced field of vision, and even blindness	
AMD	Early AMD	Medium-sized drusen (64µm), No pigment changes, No vision loss	Age, Smoking, Family history
	Intermediate stage AMD	Large drusen (173µm), No pigment changes, Mild vision loss	
	Dry /non-exudative AMD	RPE atrophy, Blurred central vision	
	Wet AMD	Neovascular atrophy, Straight lines & blind spots in the central vision	
Glaucoma	Early	No Symptoms Loss of Ganglion cells peripheral vision loss CDR>0.5	Black, Asian or Hispanic Family history, Age, medical conditions, such as diabetes, heart disease, high blood
	Moderate	0.5<CDR>0.7, Blurred vision and rainbow-coloured circles around bright lights	
	Advanced	CDR>0.7 Blindness	

community health improvement prospects. Extensive research in clinical settings has uncovered crucial diagnostic characteristics, risk factors, phenotypic, therapy, and drug management strategies for retinal diseases. However, we are covering the latest research articles related to DR, AMD, macular edema, and glaucoma.

8.1 Diabetic Retinopathy

There are additional social and economic costs as a result of the diabetes patient's inability to work. Understanding and reducing the effects of SDOH in diabetes is a top priority due to disease incidence, economic expenses, and a disproportionate population burden (Haire-Joshu and Hill-Briggs, 2019) (Hill et al.,

2013). Hill et al. (Hill-Briggs et al., 2021) presented a systemic review, discussed associations of SDOH and diabetes risk and outcomes, as well as the results of programs designed to improve SDOH and its effect on diabetes outcomes. Initially, the article provided a brief introduction to key terms and various SDOH frameworks. The review focuses mostly on research conducted in the United States on individuals with diabetes. Recommendation for diabetic research in order to improve the healthcare facilities. The incidence of blindness caused by DR among people aged 20 to 60 years old is rising rapidly over the world. The review study (Mistry et al., 2022) examined the development of diabetes in children and adolescents over the past century and its implications for future advancements in the discipline. The study assessed etiologic factors in a birth cohort

and technology use among children and evaluated the drug management of type 2 diabetes in adolescents. Another study (Pacaud et al., 2016) presented in the literature that used the international SWEET (Better control in Pediatric and Adolescent Diabetes: working to create CEnTers of Reference) database to characterize the population of children with various forms of diabetes (non-type 1). It was concluded that Type 2 diabetes is more common but still difficult to diagnose in SWEET centers. However, better management and outcomes for patients with uncommon kinds of diabetes may be achieved through collaboration with SWEET centers sharing clinical information and outcomes. The review study (Tosur and Philipson, 2022) summarized the history of maturity-onset diabetes of the young (MODY), the most common types of MODY, the clinical features of MODY, and some tips for diagnosing and treating MODY.

The lipopolysaccharide (LPS) found on the outer membrane of gram-negative bacteria is responsible for triggering the host's immune system and leading to systemic inflammation and cellular apoptosis. Patients with advanced diabetes have been reported to have high serum LPS levels, most likely as a result of intestinal permeability and dysbiosis. Consequently, there is substantial indication that systemic LPS challenge is closely linked to the prognosis of DR. Even though the underlying molecular mechanisms are not yet fully explored, LPS-related events in the retina may render DR's vasculopathy and neurodegeneration severe. Xinran et al. (Qin and Zou, 2022) presented a review while focusing on how LPS affects the development of DR, especially how it affects the blood-retina barrier and how it affects glial activation. In the end, they summarise the recent improvements in therapeutic strategies for blocking the effects of LPS, which could be used to treat DR with good clinical promise. It has been suggested that intestinal dysbiosis plays a contributing role in the development of type 2 diabetes (T2D) (Sharma and Tripathi, 2019). The review study (Yang et al., 2021) provides an overview of the gut microbiota in T2D and associated diseases, focusing on its possible features and molecular pathways in relation to intestinal barrier breakdown, metabolic abnormalities, and chronic inflammation. The author concluded by summarising a therapeutic strategy for improving the malignant progression of type 2 diabetes and related disorders through intestinal microecology, with an emphasis on influencing gut bacteria. The goal of study (Pasini et al., 2019) was to find out how long-term exercise affects the gut flora and leaky gut in people with stable T2D. Exercise helps to control blood sugar levels by changing the gut microbiota and

its functions. This data indicates an extra way exercise works and suggests that boosting gut flora could be a key part of tailor-made treatments for T2D. The putative roles of pyroptosis-signaling pathways in the pathophysiology and impact of DR development are discussed in detail in the review study (Al Mamun et al., 2021). The review reveals briefly the pharmacological drugs might be useful in the future treatment and management of DR.

The vascular endothelial growth factor (VEGF) family consists of the five ligands for the VEGF receptor (VEGFR) (VEGF-A, -B, -C, -D, and the placental growth factor [PlGF]). However, VEGF-A binds VEGFR1 and VEGFR2, while VEGF-B and PlGF only bind VEGFR1. Even though a lot of research has been done on VEGFR2 to Figure out what its main role is in retinal diseases, recent work has shown that VEGFR1 and its family of ligands are also important and play a role in microinflammatory cascades, vascular permeability, and angiogenesis in the retina (Uemura et al., 2021). VEGFR1 signaling alone leads to the pathological changes seen in DR, retinopathy of prematurity, retinal vascular occlusions, and AMD. Anti-VEGF medicines have shown remarkable clinical efficacy in various diseases, and their effect on modulating VEGFR1 signaling remains a fertile area for future research. Upregulation of VEGF-A in the diabetic eye has been linked to DR progression. The study (Singh et al., 2019) presented a review of anti-VEGF treatments for DR that have been approved for use in the USA. An improvement of 2 steps on the DR severity scale developed for the Early Treatment Diabetic Retinopathy Study is regarded clinically meaningful. After One year of medication with ranibizumab or aflibercept, about one-third of individuals with DR and DME obtain this level of improvement. Another study (Huang et al., 2022a) presents novel concepts for the prevention and treatment of DR.

There is research going on to find the association of diabetes and its risk factors with other medical conditions. Kun et al. (Xiong et al., 2022b) investigated the IOP changes and acute angle closure (AAC) risk in diabetic patients after pupil dilatation. Diabetic patients were at a reduced risk of acquiring AAC after pupil dilatation. Increased post-dilation IOP was associated with lower pre-IOP. The study (Kjærsgaard et al., 2022) presented to determine whether or not DR is linked to and indicative of primary open-angle glaucoma (POAG). No significant links were found between DR and either the prevalence or incidence of POAG. The purpose of the study (Vergroesen et al., 2022) was to assess whether or not diabetes medication is linked to the prevalent

eye disorders of AMD, OAG, and cataract, as well as to evaluate these diseases' cumulative lifetime risks in a large cohort study. The findings of cohort analysis indicate that diabetes medication was not connected with cataracts, despite the fact that diabetes itself was definitely associated with cataracts. Metformin treatment was associated with a lower risk of OAG, and other diabetes medications were associated with a lower risk of AMD. To demonstrate the efficacy of the treatment, interventional clinical trials are required. The other studies (Cui et al., 2022), (Zhang et al., 2022f), (Jiang et al., 2022), (Yongpeng et al., 2022), (Cao et al., 2022b), (Kulshrestha et al., 2022), (Peled et al., 2022), (Eton and Newman-Casey, 2022) that found in the published research that investigates the connection between diabetes and other ocular disorders. Researchers have been looking into the effects of commonly occurring comorbidities like diabetes as a result of the rapidly spreading coronavirus disease 2019 (COVID-19) pandemic. Although diabetes does not appear to raise the incidence of COVID-19 infection, it has been proven that hyperglycemia of any degree predisposes to worse outcomes, including more severe respiratory involvement, ICU admissions, the requirement for ventilators, and mortality. Infection with COVID-19 has also been linked to the development of new-onset diabetes and hyperglycemia, as well as a worsening of glycemic control in pre-existing diabetes (Xiong et al., 2022b). Previously, researchers hypothesized that this was related to the virus damaging the pancreas directly, the body's stress response to infection, and the use of diabetogenic medicines such corticosteroids to treat severe COVID-19 infections. Patients diagnosed with mild COVID-19 may continue to take the majority of diabetes drugs while switching to insulin is the treatment of choice for those diagnosed with severe conditions. Diabetes and periodontal disease both exhibit the same pattern of inflammation. Both of these diseases, if not addressed, can cause a cytokine storm, which spreads pro-inflammatory substances all over the body (Stoica et al., 2022). Periodontitis has recently been considered to be the sixth complication of diabetes, and the most current studies point to a relationship between these two disorders that cannot be denied. Recent scientific research suggests that better glucose control in diabetes patients may be possible if their periodontal health is managed by appropriate and timely medication. New evidence of central visual system damage in diabetes patients was revealed in the recently published study (Chen et al., 2022b). Diabetes can cause damage to the peripheral sensory organs and the central visual system, which can result in decreased color vision. Adhesive capsulitis (AC) occurs more frequently and lasts longer in dia-

betic patients compared to patients with idiopathic AC. Joshua et al. presented a study (Gordon et al., 2022), the goal was to find out how gene expression is different in AC with and without diabetes mellitus. The study of RNA-sequencing data showed that 66 genes were significantly expressed between nondiabetic patients and diabetic patients with AC. Still, only three genes were differentially expressed between control patients with and without diabetes. In addition, 286 genes were found to have differential expression in patients with idiopathic AC, while 61 genes were found to have differential expression in patients with diabetic AC. The newly expressed genes provide an explanation for the dissimilarities in disease progression and provide potential therapeutic targets that could lead to alternative treatment strategies for the two groups. This study presented the use of ribonucleic acid (RNA) sequencing and analytics to examine gene expression in alveolar bone in health and diabetes subjects. The study (Zhu et al., 2020) presented to investigate the candidate genes involved in the T2D. The Gene Expression Omnibus (GEO) database was used to get the gene expression profile GSE26168. Differentially expressed genes were obtained using the online tool GEO2R. Metascape was used for annotation, visualization, and comprehensive discovery, to perform the Kyoto Encyclopedia of Genes and Genomes (KEGG) pathway and Gene Ontology (GO) term enrichment analysis. Cytoscape was used to identify prospective genes and important pathways for building the protein-protein interaction (PPI) network of DEGs. A total of 981 differentially expressed genes (DEGs) were identified in T2D, including 301 up-regulated and 680 downregulated genes. Six potential genes (PIK3R1, RAC1, GNG3, GNAI1, CDC42, and ITGB1) were selected based on the DEGs' PPI network. There are other studies investigation the genes affecting diabetes (Sufyan et al., 2021)(Lei et al., 2021) (Pujar et al., 2022) (Prashanth et al., 2021) (Dieter et al., 2021) (Chen et al., 2022c) (Oraby et al., 2022). The study (Nair et al., 2022) aims to find a strong new set of symptoms so that DR screening can be done automatically. For the automated DR detection, a new symptomatic instrument based on information-driven profound learning was made and tested. The system used a shading technique on fundus images and ranked them based on whether or not they had DR, allowing for the easy identification of medically relevant cases for referral. While the complication of DR has been extensively studied, but less attention has been given to the impact of diabetes on ocular surface health. While diabetic keratopathy can be a serious threat to one's eyesight, it can also be used as a diagnostic and therapeutic tool for other diabetic systemic problems. In

this review article (Bu et al., 2022), the current knowledge of diabetic ocular surface illness, which includes neuropathy, dry eye, and other corneal morphological alterations, was discussed. They also addressed several topics that have received less attention in the existing literature. This involves problems of the ocular surface in pre-diabetic stages as well as variances in the pathology of the ocular surface between human diabetics and animal models of diabetes. In addition to this, the author highlighted that recent breakthroughs have been made in experimental models of diabetic ocular surface problems. Finally, the most recent approaches to the diagnosis, therapy, and monitoring of ocular surface diseases caused by diabetes were analyzed. The future research prospects were described, the recent development of a technique known as protein microarrays, which has the potential to be utilized in the diagnosis and management of diabetic ocular surface disease. Traditional dilated ophthalmoscopy has been used for the initial screening of diabetic symptoms. However, as DR is a progressive disease, fundus doesn't provide details of structural changes in the retina. Technological improvements in retinal imaging have allowed for more accurate diagnosis and treatment of DR. The review study (Saleh et al., 2022) discussed the several imaging techniques that can be used to diagnose, detect, and grade DR. Vivian et al. (Schreur et al., 2022) reviewed the current imaging modalities (CFC, OCT, OCTA, FFA, UWFP) for the DR diagnosis. It was suggested that integrating data from multiple imaging techniques could lead to more precise diagnosis, treatment planning, and monitoring of disease.

Summary

DR is the leading cause of blindness in people of working age, and it is getting worse as the number of people with diabetes rises. Imaging modalities include CFC, OCT, and OCTA, which are used for DR screening and diagnosis. Existing treatments for DR focus on inflammation, angiogenesis, and oxidation, but they don't work well enough to cure the disease completely. Researchers are working on finding new genes and risk factors for DR.

8.2 Diabetic Macular Edema

DME can develop at any stage of DR and poses a severe threat to the patient's vision. DME has multiple pathways and cytokines involved in its development. The study (O'Fee et al., 2022) determined risk factors for the development of DME and described its types that occur in eyes affected by PDR. Observational and retrospective case series of patients diagnosed with PDR,

in which the patient's medical history, demographic information, ophthalmologic history, OCT, and FA image features were analyzed. The condition of DME, as well as the vitreomacular interface (VMI), was assessed using OCT images. DME was broken down into two categories, non-center-involving DME (NCI-DME) and center-involving DME (CI-DME). The result showed no significant association between VMI status and DME in this exploratory investigation of diabetic individuals with PDR; however, VMI status, younger age, and the presence of epiretinal membrane may be linked with CI-DME. Wang et al. (Wang et al., 2022b) compared the risk factors for DR and DME in people with early-onset diabetes (40 years) and people with late-onset diabetes (less than 40 years). The prevalence of any DR and DME in the EOD patients was 67.0% (95% CI: 60.3–73.7%) and 39.3% (95% CI: 32.1–46.5%), respectively, which were both substantially greater than that in the LOD patients (DME: 14.4%, 12.7–16.1%, p 0.001; DR: 41.9%, 39.6–44.2%, p 0.001). It was concluded that in the group of people with T2D, the prevalence of both DR and DME was apparently higher in patients who had diabetes before the age of 40 compared to those who developed diabetes at a later age.

Retinal anatomy and vasculature can be imaged using OCT and OCTA; however, OCT has been commonly used to track progression during treatment (Kwan and Fawzi, 2019). The study (Suciu et al., 2022) assessed the clinical, laboratory, ophthalmologic exam, and OCT parameters to explore the interconnections between them to lead to innovative pathogenetic ideas and novel treatment approaches. Patients with DME and T2D had significantly higher OCT quantitative biomarker values, whereas patients with DME and T1DM had more severe effects on systemic and laboratory biomarkers. Correlations between OCT imaging biomarkers and intraocular cytokines and VEGF therapy responsiveness suggested a potential connection to underlying pathways and their relevance to DME prognosis (Abraham et al., 2021). Sil et al. (Kar et al., 2021) determined the specific spatial compartments that contribute most relevant features for predicting therapeutic response using SD-OCT images and texture-based dermoscopic features within individual fluid and retinal tissue partitions from these images. Rebounders and non-rebounders to anti-VEGF therapy were most easily distinguished by texture-based radiomics features related to the IRF subcompartment. In DME, the response to VEGF therapy has been linked to texture patterns from OCT images, and computational imaging biomarkers (CIBs) of arterial tortuosity from UWFA. Radiogenomic analysis was used to determine the link between

underlying cytokines, OCT, and UWFA based DME CIBs (Kar et al., 2022b). The study grouped eyes with similar imaging phenotypes based on OCT CIBs and UWFA that showed similar therapy response patterns and cytokine expression. A strong link between VEGF and UWFA-derived leakage morphologic and vessel vascularity features was found. OCT and OCTA are able to detect and monitor edema while also providing a comprehensive inspection of the morphological retinal changes. The study (Li et al., 2022b) examined the OCT/OCTA morphological features and patient profiles. The correlations between best-corrected visual acuity (BCVA) and the various morphological features of both modalities were analyzed using linear mixed models. Small, round lesions seen on OCT are called hyperreflective foci (HF), and their cause is currently unknown. It was suggested that hyperreflective material might be a predictor of BCVA and a possible biomarker of dyslipidemia in DME. The results showed that hard exudates are primarily responsible for HF, while microglial cell activation is only partially responsible for hyperreflective dots (HRDs). Laura et al. (Rübsam et al., 2021) investigated the pathogenesis of HF by comparing the number and location of HF episodes in DME patients before and after treatment. The study was presented (Liu et al., 2019c) to examine the dynamic alterations of HF in Chinese patients with DME receiving intravitreal conbercept medication. Reduction of outer retinal HFs, as well as total retinal HFs, was positively correlated with improvement in BCVA ($r = 0.40$, $p = 0.043$; $r = 0.393$, $p = 0.04$). Anti-VEGF medications were considered to be the primary therapeutic option for DME. Tatsuya et al. (Yoshitake et al., 2020) evaluated the association between HF in the outer retinal layers and functional performance in DME patients who had undergone intravitreal ranibizumab (IVR) injections. In order to determine whether or not HF were related to treatment response in DME following anti-VEGF medication, the retrospective study (He et al., 2022b) was conducted. The correlations between changes in BCVA and HF, as well as changes in other biomarkers from OCT, were analyzed. Post-treatment HF count was associated with baseline hemoglobin A1C and the presence of hard exudate ($p=0.001$ and $p<0.001$, respectively). It was conducted that baseline OCT indicators, along with the amount of HF in the outer retina, may be utilized to predict the therapeutic response in DME after anti-VEGF medication. According to structural investigations, it was revealed that eyes with HF in the outer layers had a thinner central subfield and a better ellipsoid zone of photoreceptors compared to eyes without such lesions. Outer retinal HF at baseline

was declared as a reliable indicator of the therapeutic success of IVR injections for DME. It was observed patients with advanced DME or wet AMD who received a single intravitreal injection (IVT) of up to 10 g of UBX1325 experienced no adverse events during the 24-week study period. Treated patients showed statistically significant improvements in disease-related outcomes, including BCVA, CST, IR, and SR fluid. Cellular senescence is thought to play a role in the pathophysiology of the retinal microvascular network, which is the primary cause of disease in DME and wet AMD. The new small molecule Bcl-xL inhibitor UBX1325 was shown to be an effective senolytic agent. The prospective study (Bhisitkul et al., 2022) investigated how safe and well-tolerated a single IVT of UBX1325 was for people with advanced DME and wet AMD. The purpose of the (Huang et al., 2022b) review is to assess the significance of HRDs, which can be seen using an OCT, as a discriminating parameter for detecting DME. The study (Rübsam et al., 2021) suggests that dexamethasone implants have a better prognosis in individuals with HF than anti-VEGF medications. Hemolysis has been reported in primates treated with aflibercept via IgG-Fc gamma receptors. Anti-VEGF medications have not been shown to reduce inflammation or retinal cell loss in this illness (Warner et al., 2022). the result showed that the multi-cistronic rAAV2/2 gene therapy can decrease vascular leakage and inflammation via Tie2 receptor activation

Summary

Researchers have examined a large number of circulating, vitreous, and genetic biomarkers to help find diseases and make new treatments. OCT and OCTA imaging methods performed better as compared to fundus biomicroscopy and fundus photography in order to examine the structure and vasculature of the retina. Whereas OCT has been utilized to evaluate a patient's reaction to treatment. It is possible to cure DME; however, the outcomes of such treatments are frequently disappointing. As a result, it is essential to create biomarkers that can assist in the prediction of the treatment response in order to maximize the effectiveness of the treatment for specific patients. The new gene therapies are likely to become an efficient approach for the treatment of DME patients.

8.3 Age-related Macular Degeneration

The aging of the population has been a contributing factor in recent years to the rise in the number of patients diagnosed with ocular disorders. AMD is one of

the most prevalent and, if left untreated, can result in complete blindness. The purpose of study (Heesterbeek et al., 2020) is to review previous research on the phenotypic, demographic, environmental, genetic, and molecular risk factors for the development of AMD. The progression of the disease has been measured in different ways. Even though vision loss seems like a good way to measure the progression of AMD in natural history studies or clinical trials, it is often not a good idea to use visual acuity as an endpoint because vision loss can take years to happen. To account for this, most AMD studies have relied on anatomical endpoints to track the disease's development across short periods of time. Geographic atrophy (GA) and choroidal neovascularization (CNV) are the two main anatomical markers used to diagnose late AMD Schaal et al. (2016). GA, which is also known as dry AMD, is characterized by the loss of photoreceptors, RPE, and choriocapillaris, which results in a gradual loss of vision over the course of time. CFP, FAF, and OCT are the three main imaging modalities utilized for GA detection. On CFP, it can be difficult to spot early signs of GA development and establish the margins of GA in a reliable manner, whereas FAF and OCT imaging are more suited for this purpose and are more likely to produce accurate results. These new vessels expand into the retina, causing subsequent leakage and/or haemorrhage, which can lead to serous RPE detachment, which is accompanied by a rapid loss of vision, and finally causes a scar in the macula that poses a threat to the patient's vision. CFP, OCT, and FA can identify exudative nAMD by fluid leakage and haemorrhaging, however, in some circumstances, a CNV can already be detected before exudation occurs using indocyanine green angiography (ICGA) and OCTA imaging (Treister et al., 2018). This is possible because ICGA and OCTA imaging are more sensitive to CNVs than CFP, OCT, and FAG. Drusen can be a result of aging or an early sign of AMD, depending on their number, size, shape, distribution, and morphology. The goal of the study (Domalpally et al., 2022) was to determine the prevalence of drusen outside the macula as well as their contribution to the development of AMD. Drusen size, area, and placement were analysed from the macular grid using 30-degree, wide-angle, colour photos from the third baseline field. Comparisons were made between drusen found outside of the macula and those found inside. It was observed that drusen outside the macula are common in eyes with AMD, and they occur more often as the number of drusen in the macula grows. Extramacular drusen do not provide an additional risk to previously recognized risk factors in the progression of intermediate AMD to late AMD. The study (Salehi et al., 2022) presented meta-analysis and sys-

tematic review, suggested that patients with AMD have significantly reduced values for several OCT measurements, including subfoveal CT, average pRNFL thickness, and average macular GCC thickness, compared to the general population. Quantifying the relative ellipsoid zone reflectivity (rEZR) could be a structural surrogate measure for an early disease development AMD (Saßmannshausen et al., 2022). Pigmentary abnormalities, the existence of reticular pseudodrusen (RPD), and the volume of the retinal pigment epithelial drusen complex (RPEDC) were examined in relation to the rEZR using linear mixed-effects models. The results of this investigation demonstrated a connection between rEZR and the existence of iAMD high-risk characteristics as well as increasing disease severity. HF seen on OCT scans is associated with ectopic RPE and hence represents a risk factor for the development of advanced AMD (Cao et al., 2021). It was observed that HF is not predictor but rather a marker of disease severity. The process of function gain and loss begins with individual RPE cells in the in-layer and extends to all aberrant phenotypes. The presence of evidence for RPE transdifferentiation, which may have been caused by ischemia, lends support to the concept of an epithelial-mesenchymal transition.

The pathophysiology and etiology of AMD are heavily dependent on inflammation. Humanin G (HNG) is a mitochondrially derived peptide (MDP) that has been shown to be cytoprotective in AMD and to be able to defend against the mitochondrial and cellular stress that is caused by damaged mitochondria in AMD. The purpose of study (Nashine et al., 2022) was to evaluate the hypothesis that the levels of inflammation-related marker proteins are higher in AMD and that treatment with HNG lowers the levels of those proteins. It was observed that HNG functions to decrease inflammatory protein production in stressed or injured cells, which may have a role in the development of AMD. It is important to highlight that HNG does not have any deleterious effects on cells that are healthy and have proper homeostasis. The study (Bhandari et al., 2022) was presented to determine if patients who underwent incident cataract surgery were at an increased risk for acquiring late-stage AMD. Late AMD was characterized by the presence of neovascular AMD or geographic atrophy seen on annual stereoscopic fundus scans or as documented by medical records, including intravitreal injections of medication intended to inhibit the effects of vascular endothelial growth factor. It was concluded that participants with up to 10 years of follow-up having cataract surgery did not raise the chance of developing late AMD. The objective of the study (Chua et al., 2022) was to investigate the

correlations between air pollution and self-reported cases of AMD as well as in vivo measurements of retinal layer thicknesses. Greater self-reported AMD was associated with greater exposure to PM_{2.5}, while differences in retinal layer thickness were associated with PM_{2.5}, PM_{2.5} absorbance, PM₁₀, NO₂ and NO_x. Polypoidal choroidal vasculopathy is common in Asia and is considered to be a form of neovascular AMD. In a similar vein, cardiovascular disease (CVD), which is also a complex condition associated with aging, is a main cause of morbidity and mortality. Previous work (Ikram et al., 2012) (Hu et al., 2010) has shown that patients with AMD have a higher risk of cardiovascular disease, suggesting a "common soil." Smoking, poor diet, and a lack of physical activity are all risk factors for cardiovascular disease, which also contribute to the development of AMD (Mauschitz and Finger, 2022).

According to the review of many cohort studies in the general population, high levels of physical activity appear to be protective against the onset of early AMD (Mauschitz et al., 2022b). These findings confirm that physical activity is a modifiable risk factor for AMD and can help guide future efforts to minimize the public health burden of this condition. A number of pharmacologic treatments are available for neovascular AMD; however, there is currently no authorized therapy that appreciably slows the progression of dry AMD. Both dry AMD and neovascular AMD have unmet medical needs related to the development of viable treatment options. In light of these findings, it is clear that innovative methods of drug delivery are required to enhance the pharmacological effect and drug concentration at the target areas. The study (Jiménez-Gómez et al., 2022) summarised the pathophysiology and the existing therapy options for AMD, concentrating on the developing ocular sustained drug delivery techniques undergoing clinical trials. Although there is currently no cure for AMD, its symptoms can be suppressed. Current treatments for AMD are divided into four categories: device-based, anti-inflammatory drug, anti-vascular endothelial growth factor, and natural product treatment (Cho et al., 2022). All of these treatments come with side effects, but early AMD therapy combined with products has many benefits because it can stop RPE cell apoptosis at safe doses. Death of RPE cells is associated with oxidative stress, inflammation, and carbonyl stress, as well as a lack of essential cell components. Anti-oxidant, anti-inflammatory, and anti-carbonylation properties can be possessed by certain natural products. Candidates for AMD medicines derived from natural products reduce RPE cell death effectively; they have the potential to be utilized as medication for preventing

early (dry) AMD. RPE cell transplantation intends to arrest or reverse vision loss by preventing the death of photoreceptor cells. It is regarded as one of the most promising stem cell therapy applications in the field of regenerative medicine. Recent studies have focused on transplanting RPE cells produced from human pluripotent stem cells (hPSC) (O'Neill et al., 2020). Early clinical trial data indicate that transplantation of RPE cells produced from hPSCs is safe and can enhance vision in AMD subjects. Unfortunately, the techniques currently employed to generate hPSC-RPE cells for clinical studies are inefficient. Delivering RPE cells on a thin porous membrane for better integration into the retina can be one way to enhance transplantation outcomes. Another way to improve transplantation outcomes is to manipulate the outcome by controlling immune rejection and inflammatory reactions. In article (Cohn et al., 2021), author summarised the most important findings from pre-clinical studies about how different laser interventions might work to make changes that are good for the RPE, Bruch's membrane, and choriocapillaris. As laser technology has progressed toward short pulse, non-thermal delivery, such as the nanosecond laser, the most important takeaways from clinical trials of laser treatment for AMD have been summarised. Another study (Csaky et al., 2022) discussed the different treatment approaches for AMD.

Summary

AMD is considered to be the most prevalent and, if left untreated, can lead to total blindness. CFP, FAF, OCT, OCTA are the imaging modalities utilized for AMD diagnosis and progression tracking. However, OCT has been widely used by ophthalmologists to detect structural changes due to AMD. Advancements in multimodal imaging and functional testing tools, as well as continuous exploration of important disease pathways, have set the stage for future well-conducted randomized trials using nanosecond and other subthreshold short pulse lasers in AMD.

8.4 Glaucoma

The functional and anatomical changes that occur in glaucomatous eyes can be powerfully described using today's technologies for evaluating the disease's activity. However, there is still a need for innovative diagnostic tools that can diagnose glaucoma early and more precisely (Wu et al., 2022). Glaucoma has been identified by screening tests, and even though therapy was associated with a lower risk of glaucoma development, there is still no evidence that treatment improves visual outcomes and quality of life (Chou et al., 2022). The study (Aspberg et al., 2021) was

conducted to evaluate how population screening affects the rate of blindness caused by OAG. The longest-ever follow-up of an OAG screening project that lasted more than 20 years. According to the findings, the prevalence of cases of bilateral blindness in the population that was tested dropped by 50%. The study (Munteanu et al., 2022) performed an assessment of risk factors and various indicators of symptoms between POAG patients and non-glaucoma patients (NG), as well as between POAG with high intraocular pressure and normal intraocular pressure, in tertiary preventive measures. Only age ($F = 2.381$, $df = 40$, $p = 0.000$) remains statistically significant after controlling for potential confounders such as gender, place of residence, and marital status. The most common forms of pediatric glaucoma and its diagnosis and treatment were reviewed, based on the childhood glaucoma research network (CGRN) (Karaconji et al., 2022). These include juvenile open-angle glaucoma (JOAG), and primary congenital glaucoma (PCG). In addition to this, other causes of glaucoma linked to, non-acquired ocular anomalies (Peters anomaly, Axenfeld-Rieger anomaly, and aniridia), systemic disease (neurofibromatosis, Sturge-Weber syndrome) were investigated. Early diagnosis of the structural changes paves the way for earlier therapy and results in slower disease progression. Screening for glaucoma through tonometry has a significant false positive and false negative detection rate. It was observed that screening with an assessment of the optic disc is likely to identify the majority of glaucoma incidences. The study (Karvonen et al., 2020) evaluated the screening capacities of the OCT, laser polarimetry (GDx), and scanning laser ophthalmoscopy (Heidelberg Retinal Tomograph, HRT), and found that all tools were quite similar. Since the accuracy of each of the factors that were evaluated was moderate, screening with these parameters alone does not produce reliable results. The prospective study (Yu et al., 2016) demonstrates that OCT event and trend-based progression analysis programmes compare to linear mixed modeling (without relying on a normative database) and detect progression earlier than SAP. Damage to the RNFL could be detected with OCT prior to the onset of visual field abnormalities on SAP, suggesting that RNFL thickness assessment is a useful screening tool for glaucoma (Kuang et al., 2015). Luis et al. (Vazquez et al., 2021) summarized the findings of current studies that concentrate on the relevance of OCT parameters in the diagnosis and monitoring of glaucoma. It has been shown that the ONH, RNFL, and macular parameters have significant diagnostic ability. According to Wanza et al. (Mwanza et al., 2010), the maximum

allowable difference in RNFL between two visits is $4\mu\text{m}$. The thinning that is more than $4\mu\text{m}$ classified as a statistically significant progressive change from the baseline. The study (Aksoy et al., 2020) was presented to evaluate the accuracy of SD-OCT segmentation software in differentiating early glaucoma from ocular hypertension and healthy eyes. In addition to this, comparison of macular layer thicknesses between early glaucoma, ocular hypertension, and healthy eyes was performed. It was concluded that analysis of the pRNFL and macular segmentation can work together to provide a more accurate early diagnosis of glaucoma. The efficacy of SD-OCT RNFL thickness measurements in glaucoma diagnoses was evaluated (Mansoori et al., 2011), and results showed that SD-OCT could be helpful for identifying glaucoma patients in the elderly. The progression of the RNFL loss is more sensitive than the GCIP loss in patients with early to moderate glaucoma (Hammel et al., 2017). However, in a more advanced stage, GCIP remains above ground, making macular analysis the more promising method for diagnosing progression (Bowd et al., 2017). In addition to GCIP, metrics related to ONH can be used to monitor development in the advanced stages (Chen, 2009).

Despite developments in imaging technology, perimetry still plays a vital role in the diagnosis and management of glaucoma. The review article is to highlight recent developments in perimetry methods and to illustrate improvements in collecting and analyzing data on the visual field (Prager et al., 2021). The diagnosis and characterization of glaucomatous field damage have been significantly aided by the application of artificial intelligence in research settings. In addition, tablet-based techniques and virtual reality headsets show potential for the screening and remote monitoring of glaucoma patients. Research has shown that the LC plays a crucial role in the pathophysiology of glaucoma development and progression, and is thus considered an anatomic site of glaucomatous optic nerve injury (Czerpak et al., 2021). The most significant findings were the decrease in LC thickness, posterior LC displacement, and the presence of localized defects (Bastelica et al., 2022). In vivo, evaluation of LC features in both normal and glaucomatous eyes has been possible with the development of high-resolution OCT devices, most notably enhanced depth imaging OCT (EDI-OCT) and swept-source OCT (SS-OCT). The study (Kim et al., 2022) investigated whether the LC curve changes when IOP falls down after eye drops in normal tension glaucoma (NTG) subjects. It was concluded that topical glaucoma treatment resulted in a reduction in IOP from 15.7 ± 2.5 mm Hg at baseline

to 11.2–17 mm Hg. There are other clinical studies (Kim et al., 2019a) (Czerpak et al., 2022) (Bastelica et al., 2022) (Guan et al., 2022) (Glidai et al., 2022) (Mochida et al., 2022) found in the literature highlighting the significance of LC for glaucoma diagnosis and progression tracking. Despite the advancement in imaging technology, accurate analysis of the LC is still challenging (Andrade et al., 2022) (Kim et al., 2020). Increased IOP and/or glaucomatous optic neuropathy have been linked to a wide range of systemic diseases, including renal disease and hemodialysis, neurologic disorders, primary familial amyloidosis, endocrine disorders, vascular disease, collagen vascular disease, hematologic disorders, irradiation; systemic viral disease, dermatologic disorders (Funk et al., 2022). An evaluation of the systemic illness causing the elevated IOP is necessary. Per et al. presented a study (Wändell et al., 2022) intended to examine the prevalence of OAG among people in Region Stockholm in relation to other somatic comorbidities. Higher fully adjusted OR (95% confidence intervals) were found for women and men with, cancer 1.175 (1.120–1.233) and 1.106 (1.048–1.166), hypertension 1.372 (1.306–1.440) and 1.243 (1.179–1.311), diabetes 1.138 (1.074–1.207) and 1.216 (1.148–1.289). It was concluded that glaucoma is more likely to develop in people who have certain somatic disorders, most notably diabetes, hypertension, and cancer. In addition to this, the risk of glaucoma is also higher in neighborhoods with higher socioeconomic status as compared to neighborhoods with lower socioeconomic status. Jun et al. (Ro et al., 2022) conducted their research on the risk of OAG in the 12 years that followed the diagnosis of chronic kidney disease (CKD) using a cohort that was representative of the entire country. The results showed that CKD is a major contributor to the development of OAG, and that the risk of OAG increases with the severity of CKD. The purpose of study (Kolli et al., 2022) was to determine whether the genetic risk for POAG influences the correlations between cardiopulmonary diseases and glaucoma indicators. The history of common cardiopulmonary conditions and cardiopulmonary measurements were analyzed in the UK Biobank, together with history of glaucoma. The prevalence of diabetes (17.5% vs 6.5%), CKD (6.7% vs 2.0%) dyslipidaemia (31.2% vs 18.3%) were all greater in glaucoma patients than in controls (adjusted $p=0.0013$ for each) within decile 1. Contrast test p -value for difference 0.05 indicates that the extent of the connection between glaucoma and diabetes, CKD, and glycated haemoglobin varies between deciles 1 and 10. The study (Mauschitz et al., 2022a) conducted retinal layers assessment as biomarkers for brain atrophy.

They investigated the relationship between segmented retinal layers and various cerebral parameters from magnetic resonance imaging (MRI). Relationships between retinal measurements and volumetric brain measures, as well as fractional anisotropy (FA) as a marker of microstructural integrity of white matter (WM) were analyzed using multiple linear regression. Inner retinal volumes were correlated with total brain and GM volumes, and even more strongly with WM volumes and FA. It was that both the inner and outer retina were linked to hippocampal size, whereas the outer retina was most strongly associated with GM volume.

Wang et al. (Wang et al., 2022c) reviewed recent advances in the genetics of POAG. The study discussed how recent developments in research methods have led to the discovery of new risk genes, as well as how subsequent biological investigations could be conducted in order to define how the risk that is represented by a genetic sequence variant manifests itself in patients. By analysing transcriptomes from single cells with Smart-Seq2, new genes were found involved in regeneration that substantially increase axon regeneration (Li et al., 2022a). Among these, *Anxa2* is the most powerful because of the synergistic effect it has with its receptor tPA in Pten-deletion-induced axon rejuvenation. In a clinically relevant model of glaucoma, *Anxa2*, its downstream effector ILK, and *Mpp1* significantly protect RGC somata, axons and preserve vision. Nigus et al. (Asefa et al., 2022) prioritized the genes that are most likely to be "causal" and to uncover the functional properties and underlying biological pathways of POAG candidate genes. They drew on data from the GERA and UK Biobank cohorts to analyze the genetic risk factors for POAG. Systematic gene-prioritization analyses were performed based on, nearest genes, co-regulation analysis, epigenomic data, transcriptome-wide association studies, and nonsynonymous single-nucleotide polymorphisms. The study found 142 genes that should be prioritized, of which 64 were found to be new for POAG. According to at least four different lines of evidence, the genes that were given the highest priority were *BICC1*, *AFAP1*, and *ABCA1*. Another review study (Aboobakar and Wiggs, 2022) summarized the genetic relationships between various types of glaucoma and the potential roles these genes play in disease pathogenesis. There are other studies (Hamel et al., 2022) (Milanowski et al., 2022) (Choquet et al., 2022) (He et al., 2022b) presented in the literature related to glaucoma risk genes. Glaucoma treatment has been challenging, because ocular barriers have inherent mechanics that impede the entry of ophthalmic medicines. Several

carriers (inorganic, polymeric, hydrogel, and contact lens-based) with specialized chemical and physical properties have been intensively investigated as potential solutions. The review article (Patel et al., 2022) summarized the latest developments in ocular delivery formulations with a particular emphasis on glaucoma, including the different types of nanocarriers and delivery routes. IOP can be lowered with the use of the new Rho kinase inhibitor netarsudil/latanoprost FDC by enhancing trabecular outflow (Asrani et al., 2020) (Brubaker et al., 2020). A very promising platform for the treatment of glaucoma and simultaneous protection of the ocular surface would be the combination of hypotensive liposomal formulations with osmoprotective agents (González-Cela-Casamayor et al., 2022). Drug delivery systems for the ocular surface, like contact lenses and nanotechnology, are currently under study as potential sustained release (SR) therapeutics. There is growing interest in using aqueous gels prepared with hydrophilic polymers (hydrogels) and based on stimuli-responsive polymers for the treatment of numerous ocular disorders (Akulo et al., 2022). Because of their chemical structure, they are able to incorporate a wide variety of ophthalmic medications, allowing them to achieve their optimal therapeutic doses while also providing more clinically relevant time courses (weeks or months, as opposed to hours and days). This will inevitably result in a reduction in dose frequency, which will improve patient compliance and clinical outcomes. Glaucoma is a chronic disease that may respond well to gel technologies used as drug-delivery methods and as antifibrotic therapy during and after surgery (Fea et al., 2022). Sakaorat et al. (Petchyim et al., 2022) investigated bleb-related infections, including their symptoms, causes, treatments, and effects. Pain and redness were the primary symptoms that patients experienced when they had a bleb-related infection. Nearly 25% of people had experienced some kind of eye injury in the past. Patients who display symptoms and engage in undesired behavior that have the potential to result in bleb infection should be identified, and treatment and education should both be provided to these patients. The study is the first direct proof that glaucoma can be treated with noninvasive femtosecond laser trabeculotomy (FLT) (Mikula et al., 2022). The study (Mikula et al., 2021) examined the safety and efficacy of FLT in reducing IOP in a perfused anterior segment model. The findings suggested that FLT treatment can result in a considerable reduction in IOP in a perfusion model, which suggests that it could be a viable noninvasive treatment option for POAG. Ex-Press shunt implantation, canaloplasty, and viscocanalostomy, are alternative surgical techniques

that show promise in equivalence but need more research to evaluate discrepancy in outcome (Siesky et al., 2022) accurately. In addition to differences in treatment results, social disparities can also be seen to have an effect on clinical care in the form of decreased adherence, choice, and, access. Adherence to glaucoma drugs is a significant issue in the management of glaucoma patients, as up to fifty percent of patients fail to receive the desired treatment advantages. The study (Zaharia et al., 2022) overarching objective was to draw connections between the various approaches to gauging glaucoma patients' propensity to take their prescribed medications, as well as the interventions designed to improve adherence.

Summary

The damage caused by glaucoma is considered to be permanent and cannot be completely remedied. Nevertheless, the advancement of the disease can be decelerated by means of pharmaceutical interventions, laser therapy, or surgical procedures, which may aid in mitigating additional visual impairment. Various modalities have been used to detect structural and functional damage due to glaucoma, which includes fundus, GDx, scanning laser ophthalmoscopy, SAP, OCT, and OCTA. However, OCT is widely used by ophthalmologists for the structural analysis of glaucomatous damage. It has been revealed that the ONH, RNFL, and macular characteristics all have substantial diagnostic ability. LC analysis with OCT has great potential in glaucoma management if some of the current constraints are resolved, particularly those relating to image acquisition.

9 Technical studies: Review

Manual identification of retinal lesions through the scans of fundus/OCT/OCTA is a time-consuming and subjective task, thus resulting in intra-variations. So, automated algorithms have been used in clinical practice to assist the ophthalmologist. Research is ongoing to improve the accuracy and robustness of automated techniques, the following sections discuss the automated methods used for the identification and classification of major ocular diseases. We have divided the literature into three categories based on techniques, such as traditional image processing, ML and DL.

9.1 Traditional Image Processing Techniques

Optic Disc and Cup-based Methods: Ophthalmologists widely use fundus images for initial screening

of various retinal diseases such as DR, AMD, DME, and glaucoma. The bright circular region in the center of the human retina is characterized as an optic disc (OD) in fundus scan. Locating the OD accurately is a crucial stage in computer-assisted glaucoma and DR diagnosis. OD detection has been a challenge in fundus analysis if there are other bright spots on the retina or if the images were not taken in a very controlled setting. In the paper (Kose and Ikibacs, 2011), simple statistical methods were suggested for finding the OD and macula and determining the diameter of the OD and the distance between it and the macula. The weighted-distance method was used to make the healthy parts of a retinal image bigger. Qureshi et al. (Qureshi et al., 2012) propose an ensemble algorithm that can automatically detect the OD and macula in fundus images. The feature set was based on pyramidal decomposition, edge detection, entropy filter, hough transformation, and uniform sample grid. On the three publicly accessible databases, Diaretddb0, Diaretddb1, and DRIVE, experimental findings and analyses were presented, and the combined algorithm achieved an average Euclidean error of 29.64, 24.26, and 26.80, respectively. The study (Usman et al., 2014) proposed a method based on classic image processing techniques to localize the OD. To eliminate gaps and erroneous regions, a threshold is first applied to the red plane of the fundus picture, and then morphological techniques are performed. The linked component labeling algorithm was employed to assign labels to the objects of the binary image. Adaptive histogram equalization and Laplacian of Gaussian (LoG) kernel were applied to enhance the bright regions within the image. The threshold image is then subjected to morphological opening to eliminate the noisy regions. Quantitative evaluation of the proposed system was performed on publicly available datasets DRIVE, STARE, and DiaretDB and achieved an accuracy of 100%, 97.50%, and 95.85%, respectively. Approximate Nearest Neighbor Field (ANNF) maps are often in computer vision and graphics to solve problems, including noise removal, image completion, and retargeting. Ramakanth et al. (Ramakanth and Babu, 2014) extended the application of ANNF maps to include medical image analysis and more particularly, the detection of OD in fundus images. ANNF algorithm feature match was employed to determine the similarity between a reference image of an OD. This gives a list of the patches of image that are closest to the patches in the reference image. For OD detection, a probability map was made from the patch's distribution in the query image. Five publicly accessible databases (DIARETDB0, DIARETDB1, DRIVE, STARE, and MESSIDOR) were used to eval-

uate the suggested methodology. The study Kao et al. (2014) proposed a method that employed area which was free from vessels and adaptive Gaussian template for fovea center detection in retinal images. The center of the OD is localized by using the template matching method. Next, the disc-fovea axis was defined by scanning the vessel-free region. Finally, the fovea center was identified using the matching of the fovea template. The centers of the OD and fovea in the various image resolutions were identified using adaptive Gaussian templates. For the DIARETDB0, DIARETDB1, and MESSIDOR databases, the proposed method found the fovea with an accuracy of 93.1%, 92.1%, and 97.8%, respectively. The OD and OC were extracted from fundus images usbased on adaptive thresholding for glaucoma diagnosis (Issac et al., 2015). An automatic method (Hu et al., 2017) was proposed that combined color difference information and vessel bends information to determine the OC boundary from fundus images. Xiong et al. (Xiong and Li, 2016) proposed OD localization method that can accurately localize the OD even when the retinal image contains pathological abnormalities. Extracted features included were vessel direction, edges, intensity, and luminous region size. The proposed approach achieved an accuracy of 100% for the DRIVE, 95.8% for the STARE, 99.2% for the DIARETDB0, and 97.8% for the DIARETDB1 database. Wavelet feature extraction combined with optimized genetic feature selection to segment OD for glaucoma diagnosis through fundus images (Singh et al., 2016). Panda et al. (Panda et al., 2017) developed OD localization method incorporating three features; retinal vascular visual cues—global/local vessel symmetry, and vessel component count. The first OD center is determined by utilizing the skeletal image component with the highest concentration of major blood vessels. The proposed technique was effective for ocular diseased with different symptoms, such as bright lesions, hemorrhages, and twisted blood vessels. The study (Mahmood and Lee, 2022) proposed a technique based on color and blur analysis for accurate detection and localization of the OD. To improve the visibility of the OD, fundus image was transformed into Lab color space. The extended maximum transform and directional blur were used to extract OD candidates accurately. In order to isolate the OD from the rest of the candidates, a radial blur was applied. Zaaboub et al. (Zaaboub et al., 2022) proposed an algorithm for OD segmentation in fundus scans. In the first stage, the OD was located, which was accomplished by performing 1) a preprocessing step, 2) vessel removal, and 3) a geometric analysis that delineate OD position. An OD contour is accurately completed using

a candidate. Ten different public databases and one local database were employed to test the algorithm. RimOne and IDRID had an accuracy of 98.06% and 99.71%, respectively.

Blood Vessels Extraction Methods: Computer-aided pathology systems rely heavily on blood vessel detection in retinal images for early screening and diagnosis of ocular diseases such as retinal detachment, DR, and DME. Numerous studies (Ravichandran and Raja, 2014) (Liao et al., 2014) (Ali et al., 2017) (Ali et al., 2017) (Alhussein et al., 2020) were found in the literature that utilized the histograms and enhancement techniques for vessel segmentation. Ravichandran et al. (Ravichandran and Raja, 2014) developed an enhancement technique that incorporated histogram matching and Gabor filtering. The method first applied a region-based histogram equalizer to the retinal image, then used a 2D Gabor filter to further improve the appearance of the vessels. In the paper (Liao et al., 2014), a novel approach was proposed to the enhancement of retinal vessels. Initially, a multi-scale top-hat transformation was used to extract the best high-contrast and low-contrast picture features from an image. The optimal bright image features are then added to the image, and the optimal dim image features are removed, for a preliminary quality enhancement. As shown by the results findings on the DRIVE and STARE databases, the proposed technique efficiently boosted contrast and improved the finer features of the retinal vessels. Ali et al. (Ali et al., 2017) proposed a method to detect retinal vessels in fundus images by combining automatic thresholding and Gabor Wavelet (GW). The green channel was extracted and then used to generate gabor feature image by utilizing GW. The final vessel output is generated by combining two vessel-enhanced images, each of which has been converted to a binary image by automatic thresholding. The algorithm achieved an accuracy of 94.53% on the Drive dataset. A method that performed retinal blood vessel analysis using more traditional methods was proposed (Toptaş and Hanbay, 2021). The model extracted pixels-based features and grouped them into five groups, gradient, morphological, edge detection, statistical, and Hessian matrix. Every pixel is assigned an 18-D feature vector, and it is fed into the neural network. The system accuracy was calculated to be 96.18% for DRIVE and 94.56% for STARE. The normalized first and second-order derivatives of a Hessian matrix were used by study (Yang and Cheng, 2014) to segment medical images. The Hessian matrix's eigenvalues stand in for luminance data, while the eigenvector of the smallest

eigenvalue reveals the orientation of the lines. A novel Hessian matrix-based vessel enhancement measure was presented in the study (Jerman et al., 2016) and addressed the issues with existing Hessian methods. These included insufficient responses to vessels of variable intensities and scales, as well as vessel bifurcation. Using the eigenvalues produced by the Hessian matrix at two different scales, the study (Alhussein et al., 2020) developed an unsupervised segmentation method to extract the thick and thin vessels. CLAHE technique was employed to enhance the contrast of retinal images. For contextual region tuning of CLAHE, a better version of the PSO algorithm was used. A morphological filter and a wiener filter were employed to remove noise. In order to extract thick and thin vessels, the eigenvalues of the Hessian matrix were calculated at two different scales. Global otsu thresholding was performed to intensity-transformed images and enhanced images of thick vessels, while ISODATA local thresholding was applied to enhanced images of thin vessels. Area, eccentricity, and solidity were used as region parameters in a post-processing step. On the publicly available CHASE DB1 and DRIVE datasets, the proposed framework was evaluated, where it showed a sensitivity of 77.76 and 78.51, and an accuracy of 95.05 and 95.59, respectively. The study (Madathil and Padannayil, 2022) introduced a Morphological Closing-based Dynamic Mode Decomposition (MC-DMD) method for enhancing the retinal vessels, which is both effective and robust. The proposed algorithm uses the power of mathematical morphology to create the input channel for the DMD system, which separates the retinal images into their vessel and non-vessel features. The proposed method was accessed on three publicly available datasets: DRIVE, STARE, and HRF.

The other techniques for vessel enhancement in retinal images include, visual adaptation model (Wang et al., 2021d), Bi-orthogonal wavelet transform and bilateral filtering (Bala et al., 2021a), retinex theory and dark channel prior method (Zhang et al., 2022a), luminosity and contrast enhancement (Kumar and Bhandari, 2022), morphological operation (Ashanand and Kaur, 2022), graph-based method (Zhao et al., 2015), multiscale fractional anisotropic tensor (Alhasson et al., 2018), and statistical feature-based transformation (Mahapatra and Agrawal, ???).

Retinal Layers and Lesions Extraction Methods:

The automated identification of retinal boundaries is an area of significant research interest due to its ability to offer a reliable, measurable, and unbiased evaluation of retinal lesions. Several automated algorithms for reti-

nal layer segmentation have been suggested in scholarly literature. Those eight inner retinal boundaries were retrieved by Kromer et al. (R.Kromer et al., 2017). Before segmenting the layers, median filtering was performed for preprocessing, and curve regularization was then utilized. Duan et al. (Duan et al., 2018) presented a developed model that used groupwise curve alignment to extract the retinal layers in OCT volume. The seven sub-retinal layers were automatically segmented using a high-pass iterative filter. In addition, they introduced a new denoising method tailored specifically for the OCT image (Roychowdhury et al., 2013). Using gradient information and shortest path search, Yang et al. (Yang et al., 2010) devised a fast and accurate automated segmentation system to extract nine intra-retinal layers. Niu et al. (Niu et al., 2014) developed an algorithmic technique for the automated segmentation of the six retinal layers. This method utilizes correlation smoothness constraint and dual gradient information. The construction of the edge map was followed by the utilization of a convolution operator in order to obtain the gradient map. The removal of outliers was facilitated by the imposition of smoothness constraints on spatial correlation.

Several automated segmentation algorithms have been suggested in the literature for extracting retinal layers and subsequently measuring their thickness. Mayer et al. (Mayer et al., 2010) presented an algorithmic approach for the quantification of RNFL in images obtained through SD-OCT. The utilization of gradient and local smoothing techniques was implemented in order to minimize the energy function utilized for the segmentation of retinal layers. The study calculated the average thickness of the RNFL for individuals with normal vision (94.1 ± 11.7 μ m) and those diagnosed with glaucoma (65.3 ± 15.7 μ m). A study (Kafieh et al., 2015) generated a thickness map of the eleven retinal layers through SD-OCT images of normal individuals without any known ocular abnormalities. Segmentation of retinal layers was based on edge statistics rather than contextual information. The average thickness of the RNFL, GCL-IPL, and GCC in the macula was calculated using a graph-based approach proposed (Gao et al., 2014). It was estimated that the RNFL thickness of healthy people was 36.5 μ m while that of glaucoma patients was 26.7 μ m. Three different OCT devices were used to test and compare the Iowa Reference Algorithms from the Iowa Institute for Biomedical Imaging, which are used for automatic intra-retinal layer segmentation and image scaling (Terry et al., 2016). Twenty-five healthy volunteers were scanned twice for macular volume using a 3D-OCT 1000 (Topcon), Cirrus HD-OCT (Zeiss), and a non-commercial long-wavelength

(1040nm) OCT. Using the Iowa Reference Algorithms, the average thickness of 10 intra-retinal layers were calculated for the fovea, inner ring, and outer ring of the ETDRS field of view. The Iowa Reference Algorithms accurately segmented all 10 intra-retinal layers and showed more repeatability than the onboard software. With fixed-AEL scaling, the algorithm gave significantly different thickness values for the three OCT devices ($P < 0.05$). An automated approach was suggested to segment and estimate the thickness of the ILM, inner outer segment, and RPE layers in an OCT image, and an online platform was made available for this purpose (Ometto et al., 2019). Motamedi et al. (Motamedi et al., 2019) aimed to establish normative data for macular RNFL, GCL-IPL, and INL thickness; the obtained measurements for these parameters were 39.53 ± 3.57 μ m, 70.81 ± 4.87 μ m, and 35.93 ± 2.34 μ m, respectively. The present study (Abdellatif et al., 2019) aimed to investigate alterations in the thickness of the outer retinal layer in individuals of varying ages, utilizing images obtained through SD-OCT. The subjects included in the study were deemed to be within normal limits.

Babu et al. (Babu et al., 2012) proposed an algorithm for glaucoma diagnosis with an improved correlation coefficient. In order to measure CDR, the retinal nerve head vitreal boundary (RV) and the choroid nerve head boundary (RC) were separated. The RV and RC choroid boundaries were identified using multilevel thresholding and wavelet transform techniques. The accuracy was 92%, and the findings came extremely near to matching the values of the gold standard. Nithya et al. (Nithya and Venkateswaran, 2015) compared segmentation methods for OCT and fundus glaucoma diagnosis. Four normal and eight glaucoma images were included. Fundus and OCT images of the same patient were used to determine CDR. Cup and disc regions in a fundus image were segmented using Hill climbing, fuzzy c-means clustering, and region growth. RPE and RNFL segmentation was used to determine cup and disc diameter in OCT images. Fundus and OCT CDR results were compared to clinical standards. Fuzzy c-mean clustering had the lowest performance error in experiments. Zhang et al. (Zhang et al., 2015) proposed an automated model to segment and quantify the CME with macular hole (MH) in 3D OCT scans. The model consisted of three stages, denoising, flattening, and the segmentation of intra-retinal layers. Next, intra-retinal CME was segmented utilizing adaptive boosting and kernel graph cut. Following that, adaptive boosting and kernel graph cut were used for fine segmentation of intra-retinal CME. The model was evaluated on 3D OCT from 18 CME and MH subjects and achieved the

accuracy and false positive volume fraction of 84.6% and 1.7%, respectively. Sugruk et al. (Sugmk et al., 2014) presented a model for the detection of AMD and DME. The model extracted the RPE layer from the macular OCT scans in order to diagnose AMD. Whereas to diagnose DME, cysts from the macular pathology were extracted. For cases of AMD, they found a success rate of 100%, while for DME, they found a success rate of 86.6%. Chiu et al. (Chiu et al., 2015) proposed a kernel regression based classification model to identify retinal layer boundaries and fluids within the retina. Then classification estimates were used to refine the extracted retinal boundaries while employing graph theory and dynamic programming framework. The model was evaluated on 110 B-scans from 10 subjects with severe DME pathology and achieved a mean Dice coefficient of 0.78. Wang et al. (Wang et al., 2016) developed a model to identify between AMD, DME, and healthy macula scans. The Correlation-based Feature Subset (CFS) selection algorithm was used to filter the linear configuration pattern (LCP) based OCT images. Overall accuracy for the three classes was 99.3% for the best model based on the sequential minimum optimization (SMO) approach. Rashno et al. (Rashno et al., 2017) proposed a framework based on their proposed framework is based on neutrosophic transformation and graph-based shortest path search for the extraction of fluid-filled cyst segments from OCT scans. After undergoing a neutrophic transformation, an image was divided into three zones: true, indeterminate, and false. Noise in an image was represented by the indeterminate set, whereas the true set was obtained using their gamma-correction technique. The ILM, RPE, OPL, and ISM layers were extracted using a graph shortest path search. Using ILM and RPE, a target region of interest (ROI) was created, from which fluid-filled regions are automatically extracted using a cluster-based segmentation algorithm. Moreover, they were able to reach a sensitivity of 67.3% on the Duke Dataset-II, 88.8% on the Optima dataset, and 76.7% on their own dataset. Tehmina et al. (Khalil et al., 2018) developed a technique that segments retinal layers to calculate CDR for glaucoma diagnosis. Delineating ILM and RPE measured cup-diameter-calculation (CDC) and disc-diameter-calculation (DDC), respectively, and employed contour, interpolation, and thickness value estimation techniques.

9.2 Machine Learning Schemes

This section presents the techniques based on classical ML models, such as linear regression, logistic regres-

sion, random forest, support vector machine (SVM), and XGBoost, for the identification and segmentation of different significant biomarkers of DR, DME, AMD, and glaucoma.

Detection of Retinal Lesions through Fundus Scans:

DR is a serious threat to sight and must be diagnosed and treated early to prevent permanent vision loss. MAs are the earliest symptom of DR, and their diagnosis is crucial. The study proposed (Akram et al., 2013) a three-stage methodology to discover MAs by early utilizing filter banks. The technique began by identifying and removing any potential MA candidate regions from the retinal image. The system created a feature vector for each candidate region based on variables such as shape, color, intensity, and statistics to determine the MA region. In order to increase the accuracy of classification, a hybrid classifier incorporated the Gaussian mixture model (GMM), the SVM, and an extension of the multimodel mediod based modeling approach in an ensemble. The model was evaluated on publicly available datasets DIARETDB0 and DIARETDB1. Usman et al. (Akram et al., 2014a) introduced a method for identifying and categorizing NPDR lesions. The system that was proposed involved preprocessing, the extraction of candidate lesions, the creation of a feature set, and classification. Candidates for the various NPDR signs (MAs, HMs, and EXs) were extracted. A feature set was created for each lesion based on the characteristics of lesions. The real lesions are found and labeled with the use of a hybrid classifier, which was based on weighted mixture of multivariate m-Mediods and a GMM. Based on the types, number, and locations of lesions, the system categorized retinal images into different stages of NPDR. The proposed model was evaluated on four datasets: DRIVE, STARE, MESSIDOR, and DIARETDB, and achieved accuracy of 95%, 97.5%, 98.90, and 95.05%, respectively. Huda et al. (Huda et al., 2019) proposed a classification model for DR diagnosis based on decision trees, logistic regression, and SVM. Jebaseeli (Jebaseeli, 2021) developed a system that classified DR and analyzed the disease severity with high accuracy. Adaptive Histogram Equalization (AHE) technique was used for image enhancement. After that, Hop Field Neural Network technique simultaneously segmented the boundaries and determined width of the vessels in fundus scan. The model was tested using a local dataset in addition to publicly available datasets (DRIVE, STARE, MESSIDOR, HRF, and DRIONS). Retinal blood vessel analysis on fundus images can provide a variety of significant biomarkers of retinal disease. DR is one of the ocular diseases

that can be detected by analyzing the blood vessels in the retina. Deciphering cardiovascular illness from a retinal fundus image requires a careful examination of the vascular tree. Bifurcations and crosses of blood vessels must be located for an accurate study. Using COSFIRE filters, the study (Azzopardi and Petkov, 2013) presented a method for detecting automatically vascular bifurcations in segmented fundus images. The COSFIRE filter's output was determined by taking the geometric mean of the weighted responses of the blurred and shifted Gabor filters that were specifically chosen. The performance of algorithm was done on DRIVE and STARE datasets. Recall of 97.88% and precision of 96.94% were achieved on forty fundus scans from the DRIVE data set. Twenty manually segmented images from the STARE dataset had a recall of 97.32% and a precision of 96.04%. Manoj et al. (Manoj et al., 2013) proposed a technique that used feature based on orientation gradient vector fields, morphological transformation, and Gabor filter responses to extract the retinal vasculature in order to diagnose retinal disorders. A vector in 9-D feature space describes each pixel in the retinal image, and neural network classifiers are used to categorize those pixels using Feed Forward Backpropagation Neural network, Multi-Layer Perceptron, and Radial Basis Function. The method was evaluated on DRIVE, STARE, and MESSIDOR and achieved an accuracy of 96.23%, 95.83%, and 95.41%, respectively. Strisciuglio et al. (Strisciuglio et al., 2016) proposed a robust method based on a set of B-COSFIRE filters selective to segment blood vessels in fundus images. Features were chosen automatically for maximum flexibility, and they can be customized for a variety of other applications. Analyzed and compared the efficacy of several distinct selection approaches based on the principles of machine learning and information theory. Glaucoma affects the RNFL, which results in increased CDR; it is a clinically significant parameter for glaucoma diagnosis and screening. Computational analysis, such as the CDR, cup area, and rim area, is made possible by fundus imaging, greatly MESSIDOR assisting in identifying glaucoma. The fundus image provides the analysis of OC and OD; however, the edges of the OC are not very clear. Because of this, it is very hard to segment the OC accurately, and the performance of OD segmentation also needs to be improved. Usman et al. (Akram et al., 2015) presented a unique feature set-based diagnostic system for automated identification of glaucoma using fundus images. The system was comprised of modules, which are as follows: preprocessing, detection of the region of interest based on autonomously segmented OD, feature

extraction, and classification. Robust OD localization method (Usman et al., 2014) was employed. With the use of 2-D MESSIDORGabor wavelet and subsequent thresholding-based vessel segmentation, the vascular pattern is made more visible. Following ROI extraction, many features (CDR, Rim to disc ratio, mean intensity, standard deviation, energy, and gradient) were taken from it to create a detailed representation of the feature space. Local Fisher discriminant analysis (LFDA) was performed to do supervised enhancement of features. The retinal images were classified as normal or glaucoma using the m-Mediods model of normality. The performance of the proposed system was evaluated using publicly available (DRIVE, DiaretDB, Drions, HEI MED, HRF, MESSIDOR) and locally gathered fundus databases. An automated technique (Mvoulana et al., 2019) was proposed for glaucoma diagnosis from fundus scans. First, the method segmented the OD by combining a brightness criterion and a template-matching technique. Next, texture-based and model-based methods were employed to segment the OD and OC accurately. Finally, glaucoma screening is achieved through the calculation of the CDR, which allows for the differentiation between healthy and glaucomatous individuals. A publicly accessible DRISHTI-GS1 dataset was used to evaluate the proposed method and achieved 98% accuracy. The study (Mohamed et al., 2019) proposed an automatic glaucoma screening model based on superpixel classification. The preprocessing steps were noise removal and illumination correction, then input images were aggregated into superpixels by Simple Linear Iterative Clustering (SLIC). The statistical pixel-level (SPL) technique extracted image attributes from each superpixel based on histogram data and textural information. The extracted features are then fed into SVM to classify each superpixel into OD, OC, blood vessel, and background regions. On RIM-One dataset, the model was tested and achieved an accuracy and sensitivity of 98.6% and 92.3%, respectively. Rehman et al. (Rehman et al., 2019) employed region-based statistical and textural features to detect and localize OD in fundus images. Highly discriminative features were selected using the mutual information criterion, and four benchmark classifiers, SVM, RF, AdaBoost, and RusBoost, were compared. The RF classifier showed more competitive results than other classifiers and achieved an accuracy of 99.3%, 98.8%, and 99.3% on the DRIONS, MESSIDOR, and ONHSD datasets, respectively. DME is an ocular condition in which fluid rich in fat drains out of damaged blood vessels and is deposited near the macula, causing blurred central vision. The study (Akram et al., 2014b) proposed a

novel approach for macula detection while utilizing a rich feature set and a classifier based on the GMM. The method was evaluated on the DRIVE and STARE databases and achieved an accuracy of 100% and 95.4%, respectively. In ophthalmology, a transportable and cost-effective computer-aided diagnosis system can be achieved by the use of the d-Eye lens, which can be attached to a smartphone (Elloumi et al., 2018)(Elloumi et al., 2021). Mrad et al. (Mrad et al., 2022) proposed an automated technique for glaucoma screening that is specifically designed for fundus images captured by smartphones was provided (SCFIs). The first challenge was to design an algorithm that achieved a higher level of accuracy even with moderate-quality SCFIs. The second task is to make the detection process computationally cost and recourse effective so that the method can be used on a smartphone. To do so, a central concept was used to infer glaucoma from vessel displacement inside the OD, where the vascular tree may still be well described using SCFIs. So, the vessel tree is broken up into sections and divided into quadrants based on the ISNT. The centroid of the vessel distribution on each quadrant is then determined. After the feature vector was generated, it was fed into a classifier (SVM) to diagnose glaucoma accurately.

Detection of Retinal Lesions through OCT Scans: An automatic technique based on graph theory dynamic programming and SVM was presented in the study (Srinivasan et al., 2014a). Seven to 10 retinal layers were effectively extracted using the proposed method. Septiarini et al. (Septiarini et al., 2018) proposed an RNFL segmentation model by creating a co-occurrence matrix. The model employed 160 and 40 fundus images for training and testing, respectively, and achieved an accuracy of 94.52%. The study (Zang et al., 2019) performed the analysis of retinal layers and capillary plexuses from OCT and OCTA scans by segmenting the optic disc and retinal layers. A neural network and graph search technique was combined to segment the OD. The study (Hassan and Raja, 2016) proposed an automated algorithm for detecting ME while using directional gradients of the candidate OCT scan. Three features from computed gradients were extracted and used to train linear discriminant analysis to classify ME and healthy scans. They tested their proposed system on 30 OCT B-scans and got a sensitivity of 100% and a specificity of 86.67%. In the work (Abhishek et al., 2014), an automated segmentation approach was described for detecting intra-retinal layers in OCT images that are significant for edema detection. They found RPE layer and detected the

shape of the drusen, and finally, the technique employed a binary classification to distinguish between AMD and DME scans. Results from experiments showed that AMD and DME were classified with an accuracy of 87.5%. Srinivasan et al. (Srinivasan et al., 2014b) developed an algorithm for the detection of AMD and DME based on multiscale histograms of oriented gradient descriptors. Finally, supervised SVM was used for the classification task. The classifier was successful in identifying all cases of AMD and DME and 86.67% of normal patients. The quantitative classification of AMD and normal eyes through retinal OCT images was presented (Farsiu et al., 2014). The model semi-automatically segmented the RPE, drusen, and retina. A map of "normal" non-AMD thickness was created by registering and averaging maps of thickness from control participants. Five automated classifiers were generated based on a generalized linear model regression framework. The classifier achieved an area under the curve (AUC) greater than 0.99. Khalid et al. (Khalid et al., 2017) proposed a model for the diagnosis of retinal epithelial detachment (RE), CSR, and AMD based on multilayered SVM. The model was evaluated on 2819 OCT images (1437 healthy, 640 RE, and 742 CSCR) from 502 patients across two datasets, achieving an accuracy of 99.92%, a sensitivity of 100%, and a specificity of 99.86%. The study (Hassan et al., 2016a) presented proposes an automated framework based on SVM to classify ME and CSR from OCT images. A total of 30 labeled images (10 ME, 10 CSR, and 10 healthy) were utilized for training a model while using five features (two derived from cyst fluids inside the retinal layers and three features were extracted from thickness profiles of the sub-retinal layers). A total of 90 TD-OCT images (30 for ME, 30 for CSR, and 30 for healthy) from 73 patients were used to evaluate the algorithm. It correctly identified 88 of 90 cases (97.77% accuracy, 100% sensitivity, and 93.33% specificity). Hassan et al. (Hassan et al., 2016c) utilized coherent tensors to develop an automated method to segment and evaluate the subretinal layers in OCT scans. Then, the SVM classifier was employed to make a ME prediction based on the subretinal layers of the candidate images. Seventy-one OCT images were obtained locally from 64 patients, 15 and 49 were ME and healthy subjects, respectively. Overall, the model successfully distinguishes between ME patients and healthy subjects with an accuracy of 97.78%. The proposed model (Rathore et al., 2021) assists in predicting whether or not DR may be identified based on the number of exudates visible in retinal fundus images. Several procedures have been taken in order to detect exudates, including scaling, removal of blue

channels, performing feature extraction with Local Binary patterns (LBP), and classifying the images via SVM.

9.3 Deep Learning (DL) Schemes

DL computer models have recently made significant advances in various fields, such as computer vision, speech recognition, genomics, drug discovery, and ophthalmology. The DL algorithm can automatically learn complex structures from large data sets without explicit feature extraction. However, in order to achieve generalization large amount of data is required to train DL model. We have divided the DL literature into different categories, such as the segmentation model, segmentation-based classification model, and classification model. The segmentation section includes the studies which only extract the different biomarkers from fundus/OCT/OCTA scans for various ocular diseases and the segmentation-based classification model performed classification based on the identified biomarkers. Whereas the classification section includes those studies which performed the classification of scans without any segmentation performed.

9.3.1 Segmentation

Retinal Lesions & Optic Cup/Disc Segmentation from Fundus Scans Sevastopolsky et al. (Sevastopolsky, 2017) proposed a universal method for automatically segmenting the OD and OC, which was based on U-Net CNN. CLAHE was used as a preprocessing step to equalize the contrast. The model was evaluated on publicly available databases DRIONS-DB, DRISHTI-GS, and RIM-ONE v.3 and achieved IOU of 0.89, 0.75, and 0.69, respectively. A CNN model was developed and trained to automatically and simultaneously segment the OD, fovea, and blood vessels (Tan et al., 2017). Fundus images were normalized, then three channels were extracted and fed into the model. On Drive dataset, the model correctly classified 92.68% of the ground truths. The best single-image accuracy was 94.54%, and the worst was 88.85%. The study (Al-Bander et al., 2018) proposed a DL model for the segmenting OC and OD. The model was based on DenseNet, a fully-convolutional network with a symmetric U-shaped topology that enables pixel-wise classification. The CDR for glaucoma diagnosis is then estimated along two axes using the projected OD and OC boundaries. The model was evaluated on four publicly available datasets, ORIGA, DRIONS-DB, Drishti-GS, ONHSD, and RIM-ONE. The results showed model achieved better segmentation, and

it was suggested that the model could be used to detect various other retinal lesions. The majority of current ML segmentation techniques rely on manual segmentation of the disc. The annotation of pixel-level optic disc masks is a time-consuming task that invariably results in inter-subject variance. To address this issue, Xiong et al. (Xiong et al., 2022a) proposed an automatic Bayesian U-Net with weak labels and Hough transform-based annotations to segment OD from fundus images. The expectation-maximization approach was alternately applied to estimating the OD mask and updating the weights of the Bayesian U-Net in order to optimize the model. Another study (Lu et al., 2019) presented a weakly-supervised learning approach based on modified CNN to segment the OD in fundus images. Labels at the image level and bounding box labels were employed to guide segmentation. The enhanced constraint CNN method was combined with the GrabCut method to construct a more refined foreground segmentation map with image-level labels and use them as "GroundTruth" for the subsequent training step. A weak loss function was used to constrain the training network base output size of a modified U-net model. The model was evaluated on RIM-ONE and DRISHTI-GS databases. This DL network contains 22 layers, which had 11 inception modules. Li et al. (Li et al., 2018a) proposed DL algorithm for recognizing glaucomatous optic neuropathy (GON) from color fundus images. A total of 70000 fundus images were randomly acquired from LabelMe (lab, 2019 (accessed Nov 25, 2022)). The results showed model achieved an AUC of 0.986 with a specificity of 92.0% and a sensitivity of 95.6%. Sun et al. (Sun et al., 2018) proposed based on deep object detection networks to segment OD from retinal fundus images. To find the OD border by transforming the projected bounding box into a vertical and non-rotated ellipse. The method outperformed state-of-the-art algorithms in OD segmentation on the ORIGA dataset using Faster R-CNN as the object detector. The study (Sun et al., 2022) presented a Neural architecture search (NAS) in a two-level nested U-shaped structure. The segmentation model achieved average dice of 92.88% on the REFUGE dataset. The model was validated on Drishti-GS and GAMMA and obtained a dice of 92.32% and 92.11%, respectively. Sharath et al. (Shankaranarayana et al., 2019) proposed a DL framework to estimate monocular retinal depth from a fundus image. To handle the sparsity of labeled data, pretraining the deep network using a pseudo-depth reconstruction technique which was more effective than denoising methods. A fully convolutional guided network that used the depth map and the fundus image

to perform OD and OC segmentation. The model was evaluated on three datasets ORIGA, RIMONer3, and DRISHTI-GS. The study (Tian et al., 2020) used a multi-scale CNN to extract feature maps. For the segmentation task, GCN requires the feature map to be appended to graph nodes. The model was tested on the REFUGE dataset, Dice similarity coefficients (DSC) of the proposed technique for OD and OC were 0.97 and 0.95, respectively. A DL model DDSC-Net (densely connected depthwise separable convolution network) (Liu et al., 2021a) was proposed for OD and OC based on multi-category semantic segmentation. To achieve better segmentation results, the model utilized an image pyramid input and a depthwise separable convolutional layer. Model was evaluated on two publicly available datasets, Drishti-GS and REFUGE. The DDSC-Net outperformed GL-Net by 0.70 in disc coefficients on the Drishti-GS dataset and pOSAL by 0.79% on the REFUGE dataset. Wang et al. (Wang et al., 2019b) developed a coarse-to-fine DL architecture based on a classical CNN, the U-net model, to accurately segment the OD. The network used two distinct sets of inputs during training: color fundus images and their corresponding grayscale vessel density maps. The model fused the data using an overlap technique to locate a local image patch (disc candidate region), which was then used as input into the U-net model for further segmentation. On our dataset of 2978 test images, the model achieved an average of 0.89 for IoU and 0.93 for DSC. Surendiran et al. (Surendiran et al., 2022) developed modified recurrent neural networks (mRNN) with fully convolutional network (FCN) for the extraction and segmentation of OD and OC. FCN generated a feature map for the intra- and interslice contexts, whereas RNN paid more attention to the interslice context. A novel method JOINED proposed for multi-task learning for joint OD, OC, and fovea detection (He et al., 2022a). To make the most of the information provided by the distance from each image pixel to landmarks of interest, a distance prediction branch was built in addition to the segmentation and detection branches. The JOINED pipeline has two stages: the coarse stage and the fine stage. At the coarse stage, a joint segmentation and detection module performed OD/OC coarse segmentation and generated a heatmap, which showed the location of fovea. After that, ROI was cropped for further fine processing, and use the predictions from the coarse stage as extra information to improve performance and speed up convergence. The model was on publicly available GAMMA, PALM, and REFUGE datasets. Although many DL methods have shown promising results in the area of OD and OC

segmentation, it remains a difficult problem to segment the OC boundary while also increasing computing efficiency correctly. To address this issue, study (Wei et al., 2022) proposed a robust Multiscale Feature Extraction with Depthwise Separable Convolution (RMSDSC-Net) that tradeoff between performance and computational cost. The basic building blocks were the Multiscale Input (MSI), Dilated Convolution Block (DCB), Depthwise Separable Convolution Unit (DSCU), and External Residual Connection (ERC). MSI can help to mitigate data loss caused by the network's pooling layers when it comes to having detailed representations of features. The model builds DSCU and DCB modules to improve segmentation performance and computational efficiency by preserving higher-level semantic features while minimizing the loss of spatial information from tiny details in the image. Finally, ERC was set up between the encoding and decoding layers to reduce feature degradation as much as possible. The model achieved Dice Coefficients of (0.978, 0.919) and (0.965, 0.910) for OD and OC segmentation on the DRISHTI-GS and REFUGE databases, respectively. Garifull et al. (Garifullin et al., 2021) developed a model for segmenting DR lesions based on a Bayesian baseline. The model considered the parameters of a CNN as random variables and used stochastic variational dropout approximation to quantify uncertainty. The method achieved an AUC of 0.84 for HMs, 0.641 for EXs, 0.593 for MAs, and 0.484 for microaneurysms on IDRiD dataset. State-of-the-art models cannot achieve significant segmentation results because of a lack of sufficient pixel-level annotated data during training. To address this shortcoming, Lui et al. (Liu et al., 2019b) proposed a semi-supervised conditional GAN-based approach for joint OD and OC segmentation. The model comprised a segmentation net, a generator, and a discriminator, that learned to map between the fundus images and segmentation maps. To further enhance the segmentation performance, both labeled and unlabeled data were used. Extensive trials demonstrated that model attained improved results on ORIGA and REFUGE datasets for segmenting the optic disc and cup. Jiang et al. (Jiang et al., 2019) proposed a multi-label DL model(GL-NET) that combined the GANs. GL-Net had a generator and discriminator. In the generator, skip connections were used to facilitate the fusion of low and high-level feature information, which minimizes the downsampling factor and prevents excessive feature information loss. L1 distance and cross-entropy were used as loss functions to improve segmentation accuracy. The model was verified on DRISHTI-GS1 dataset. Another study (Son et al., 2019) presented

the OD and blood vessel segmentation model based on GAN. Results showed the model achieved better performance in blood vessel segmentation on DRIVE and STARE datasets. However, OD segmentation on DRIONS-DB, RIM-ONE, and Drishti-GS datasets did not provide statistically significant increases in AU-ROC. Table 4 summarized the various DL model for the segmentation of OD.

Blood Vessels Segmentation from Fundus Scans The paper (Wang et al., 2015) introduced a supervised approach for retinal blood vessel segmentation by combining CNN and Random Forest. The CNN served as a hierarchical feature extractor that can be trained, while the ensemble Random Forest performed the role of a classifier. The suggested method automatically learned features from the raw images and predicted the patterns using a combination of the benefits of feature learning and classical classifier. Two publicly available databases, DRIVE and STARE, of retinal images were used to evaluate the model and achieved an accuracy of 97.67% and 98.13%, respectively. To improve feature recognition in retinal images, a unique method was proposed (Fang et al., 2015), which first applied the DL method for vessel segmentation in order to produce the probability map of the image. The multi-scale Hessian response on the retinal image's probability map was then used to detect landmarks. Melinšćak et al. (Melinscak et al., 2015) proposed a CNN-based model for the classification of retinal vasculature. The network has four convolutional and max pooling layers and two fully connected layers. The ReLU activation function was used in convolutional layers, and the softmax activation function was employed in the last fully connected layer. The model achieved an average accuracy of 94.66% on DRIVE dataset. The study (Fu et al., 2016) proposed a DL model and utilized the CNNs to generate a vessel probability map. The model was a modification of a holistically nested edge detection (HED) network (Xie and Tu, 2015). Probability maps from output layers were combined to produce a single probability map. Conditional Random Fields (CRF) were utilized for the exact localisation of vascular boundaries. Mean field approximation of CRF distribution yields maximum posterior marginal inference. The method achieved an accuracy of 94.70% and 95.45% on the DRIVE and STARE datasets, respectively. Liskowski et al. (Liskowski and Krawiec, 2016) proposed a DL model for vessel segmentation. The preprocessing steps were based on global contrast normalization and zero-phase whitening. Data augmentation was performed to increase the number of images. Six distinct CNN models were constructed:

PLAIN, GCN, ZCA, AUGMENT, NO-POOL, and BALANCED. The segmentation models were verified on DRIVE, STARE, and CHASE databases. A supervised method (Jiang et al., 2018) was proposed based on a pre-trained fully CNN through transfer learning. The suggested method reduces the complex challenge of retinal vascular segmentation from full-size picture segmentation to regional vessel element detection. Unsupervised image post-processing techniques were applied to the proposed method to enhance the final result further. Using the DRIVE, STARE, CHASE DB1, and HRF databases, extensive testing had shown an accuracy of 95.93%, 96.53%, 95.91%, and 96.62, respectively. Hu et al. (Hu et al., 2018) proposed a model based on CNN and fully connected CRFs. There are essentially two phases to the segmentation procedure. First, a multiscale CNN architecture with an enhanced cross-entropy loss function was presented to generate the inter-image probability map. To acquire more specific knowledge of the retinal arteries, a multiscale network was built by merging the feature map of each intermediate layer. The proposed cross-entropy loss function concentrates on learning the difficult cases and pays less attention to losing small amounts of data on the easier samples. Second, the final binary segmentation result was achieved by applying CRFs, which used spatial context information by considering the interactions among all of the pixels in the fundus images. The DRIVE and STARE public datasets were used to test the efficacy of the proposed method and achieved an accuracy of 95.33% and 96.32%, respectively. The study (Wang et al., 2019a) presented a model based on Dense U-net and the patch-based learning strategy for retinal vessel segmentation. Training patches were obtained using a random extraction strategy, the Dense U-net was utilized as the training network, and a random transformation technique was employed to augment the training data. The segmented image can be recovered using an overlapping-patches sequential reconstruction technique. The DRIVE and STARE public datasets were used to test the effectiveness of the model, which achieved an accuracy of 95.11% and 95.38%, respectively. By balancing losses with stacked deep FCN, Park et al. (Park et al., 2020) proposed a novel conditional generative adversarial network termed M-GAN for performing retinal vascular segmentation. For enhanced segmentation, a M-generator with deep residual blocks was included, while an M-discriminator with a greater in-depth network facilitates more rapid adversity-based model training. In particular, to facilitate scale-invariance of vessel segmentations of varying sizes, a multi-kernel pooling block was included between the stacked layers. The

Table 4: Summarizing the different DL-based studies that segmented the OD.

Study	Techniques	Dataset	IOU	Dice	Accuracy
Sevastopolsky (2017)	CLAHE U-Net CNN	DRIONS-DB, DRISHTI-GS, RIM-ONE v.3	0.89, 0.75, 0.69	-	-
Tan et al. (2017)	CNN	DRIVE	-	-	92.68%
Al-Bander et al. (2018)	DenseNet	ORIGA, DRIONS-DB, DRISHTI-GS, ONHSD RIM-ONE	0.77,0.94, 0.90, 0.91, 0.90	-	93.0% 89.12% 99.69% 99.90% 99.69%
Sun et al. (2022)	CNN	REFUGE, Drishti-GS, GAMMA	-	0.92, 0.92, 0.92	-
Liu et al. (2021a)	Depth-wise separable CNN	Drishti-GS, REFUGE	-	0.70, 0.79	-
Wang et al. (2019b)	U-net	Local	0.89	0.93	-
Wei et al. (2022)		DRISHTI-GS, REFUGE	0.97, 0.91	-	-

M-generator utilizes down-sampling layers to collect relevant data for feature extraction and up-sampling layers to create segmented retinal blood vessel pictures from the collected data. The pre-processing step utilized automated color equalization (ACE) to improve the visibility of the retinal vessels, and post-processing with a Lanczos resampling approach to smooth the vessel branching that reduced false negatives. To verify the proposed method, DRIVE, STARE, HRF, and CHASE-DB1 datasets were used and achieved an accuracy of 97.06%, 98.76%, 97.61%, and 97.36%, respectively. The study (Boudegga et al., 2021) proposed U-shaped DL design with lightweight convolution blocks used to maintain good performance while decreasing computational complexity. In order to improve the quality of the retinal image and the information gleaned from the blood vessels, a series of preprocessing and data augmentation techniques was proposed. The proposed method was evaluated on the DRIVE and STARE databases. It was shown to produce a better compromise between the retinal blood vessel identification rate and the detection time, with an average accuracy of 97.80% and 98% in 0.59 s and 0.48 s per fundus image, respectively. Wang et al. (Wang et al., 2021a) proposed a model for fine retinal vascular segmentation by integrating Nest U-net and patch-learning. Training samples that included fine retinal vessels were generated efficiently with the help of a custom extraction approach, giving them a significant advantage in the segmentation of these specialized structures. The model sent high-

resolution feature maps directly from the encoder to the decoder network. The model was learned with k-fold cross-validation, predictions were made using testing samples, and the final retinal vasculature was reconstructed using a sequential approach. The proposed model was evaluated using the DRIVE and STARE datasets and achieved an accuracy of 95.12% and 96.41%, respectively.

According to the properties of the retinal vessels in fundus scans, a residual CNN-based retinal vessel segmentation model was presented (Xu et al., 2021). The encoder-decoder network structure was built by joining the low-level and high-level feature graphs, and dilated convolution was integrated into the pyramid pooling. In addition to this, an improved residual attention module and deep supervision module were also used. The results from data sets DRIVE and STARE demonstrate that algorithm can segment the entire retinal vessel, along with related vessel stems and terminals. The accuracy achieved on DRIVE and STARE datasets was 95.90% and 96.88%, and specificity was 98.85% and 97.85%, respectively. Deng et al. (Deng and Ye, 2022) proposed a model for vessel segmentation based on multi-scale attention with a residual mechanism D-Mnet (Deformable convolutional M-shaped Network) and an improved PCNN (Pulse-Coupled Neural Network) model. The model was based on the encoder-decoder network structure. In order to boost the efficiency of retinal blood vessel segmentation, the network integrates an enhanced PCNN model, bringing together the benefits

of supervised and unsupervised learning. Publicly available databases, DRIVE, STARE, CHASE-DB1, and HRF were used to conduct comparative verification, the model achieved an accuracy of 96.83%, 97.32%, 97.14%, and 96.68%, respectively. Kar et al. (Kar et al., 2022a) proposed a segmentation model based on a generative adversarial network (GAN) and several loss functions to detect retinal vessels accurately. CLAHE method was used in the preprocessing stage to improve the contrast of blood vessels. The GAN architecture combined a segmentation network (the generator) and a classification network (the discriminator). The inception module detects fine vessel segments by extracting multi-scale properties of vessel segments at various scales. The discriminator is made up of two layers of stacked self-attention networks and a layer of position-wise fully linked feed-forward networks that infer a binary output. The transformer's attention mechanism can effectively discriminate and store global and local information. The DRIVE, STARE, CHASE DB1, HRF, ARIA, IOSTAR, and RC-SLO databases were used to test the robustness and effectiveness of the proposed method. Chen et al. (Chen et al., 2022a) proposed Patches Convolution Attention-based Transformer UNet (PCAT-UNet), which was a U-shaped network with a convolution branch based on transformer. Skip connections were employed to fuse the deep and shallow features. The model captures the global dependency connection and the features of the underlying feature space, overcoming the difficulties of insufficient retinal microvessel feature extraction and low sensitivity caused by easily predicting pixels as background. PCAT-UNet was evaluated using three publicly accessible retinal vasculature datasets DRIVE, STARE, and CHASE DB1. Results for accuracy were 96.22%, 97.96%, and 98.12%, and results for sensitivity were 85.76%, 87.03%, and 84.93%, respectively. The study presented (Zhang et al., 2022d) framework that provided new edge-aware flows into U-Net encoder-decoder architecture to steer retinal vascular segmentation, which makes the segmentation more sensitive to the capillaries' fine edges. Using characteristics taken from the encoder path, edge-gated flow with gated convolution learns to highlight the vessel edges and then exports the resulting edge prediction. To further improve the segmentation results, the edge-downsampling flow extracted the edge features from the edge prediction output and re-feeds them into the decoder path. On the publicly available DRIVE, STARE, and CHASEDB1 datasets, the proposed technique outperforms the state-of-the-art U-Net baseline by 0.0056, 0.0026, and 0.0047, respectively. Most segmentation approaches

still have certain shortcomings in effective fine vessel detection, however, mainly as a result of information loss issues produced by many pooling operations and insufficient process issues of local context features by skip connections. In order to solve this problem, a novel retinal vascular segmentation network named ResDO-UNet (Liu et al., 2023b) was proposed based on the encoder-decoder architecture to offer an automatic and end-to-end detection strategy using fundus photographs. Together with a depth-wise over-parameterized convolutional layer (DO-conv), a residual DO-conv (ResDO-conv) network was proposed to serve as the network's backbone in order to obtain robust context features, which would improve feature extraction. Furthermore, a pooling fusion block (PFB) was developed to implement nonlinear fusion pooling, which used the benefits of max pooling and average pooling layers to mitigate the information loss that results from performing numerous pooling operations. Meanwhile, an attention fusion block (AFB) was employed as a solution to the problem of insufficient processing of local context information by skip connections. The model was evaluated on DRIVE, STARE, and CHASE-DB1 datasets. In the study (Qu et al., 2023), a vessel segmentation model (TP-Net) based on fundus images was proposed, which consisted of three modules, i.e., main-path, sub-path, and multi-scale feature aggregation module (MFAM). The main path's responsibility is to identify the retinal vascular trunk, while the branching path is to track vessel information accurately. Retinal vascular segmentation was improved by combining the predictions from the two pathways using MFAM. In the main-path, a three-layer lightweight backbone network was designed based on retinal vessel features. Then a global feature selection mechanism (GFSM) was developed for the automated selection of features that are significant for the segmentation task. An edge feature extraction approach and an edge loss function were proposed in sub-path, which improved the network's ability to capture edge information. Finally, MFAM combined the prediction by main and sub-paths, which can eliminate disturbances from the background while still keeping edge features, leading to improved vascular segmentation. The proposed TP-Net was tested using the DRIVE, STARE, and CHASE-DB1 datasets. A new lightweight segmentation model Wave-Net (Liu et al., 2023c), was proposed for accurate vascular segmentation in the fundus images. The skip connections of the original U-Net were replaced with a detail enhancement and denoising block (DED) to improve the precision segmentation. DED reduced the impact of the semantic information loss problem in thin vessels

and learned more about micro structures and features. In addition, it helped to reduce the impact of the semantic gap issue. Additionally, a multi-scale feature fusion block (MFF) was created for multi-scale vessel identification to fuse cross-scale contexts. The model was evaluated on DRIVE, CHASEDB1, and STARE datasets and achieved the F1 score of 0.8254, 0.8349, and 0.8140, respectively.

Table 5 summarises the studies that performed segmentation of blood vessels in fundus images. There are various other DL models, such as Bridge-Net (Zhang et al., 2022e), CSAUNet (Huang et al., 2022c), DilUnet (Huang et al., 2022c), Staircase-Net (Sethuraman and PALAKUZHAYIL GOPI, 2022), DCCMED-Net (Budak et al., 2020), CcNet (Feng et al., 2020), MD-Net (Shi et al., 2021), NFN+ (Wu et al., 2020), DF-Net (Yin et al., 2022) found in the literature for segmentation of retinal vessels in fundus images.

Retinal Lesions Segmentation from OCT Scans OCT has been utilized extensively for scanning the retina to detect various ocular diseases. Significant indicators for a wide variety of ocular disorders can be found in the retinal layers. Multi-scale, end-to-end CNN architecture was proposed to delineate choroidal borders (Sui et al., 2017). The method was successful when applied to data on various global and local scales. Pixel data was used to update the appropriate graph-edge weight immediately. Results from testing the system on 912 OCT images showed that it performed best when using learned graph-edge weights. Gopinath et al. (Gopinath et al., 2017) proposed a model that combined CNN with a Long Short Term Memory (LSTM) to extract the retinal layers through an OCT image. The model's pixel-wise mean absolute error was 1.30 ± 0.48 . Fang et al. (Fang et al., 2017) presented a framework (CNN-GS) that integrated the CNN and graph search techniques for automated layer-by-layer retinal delineation. In order to learn how to classify retinal images, CNN was used to extract features from a specific layer of the retina. In addition, the probability maps produced by CNN were employed using a graph search approach to identify the boundaries of the retina. The supervised model (Xiang et al., 2018) was developed for segmenting layers and neovascularization. For the neural network classifier, spatial features (3), gray-level features (7), and layered-like features (14) were extracted. Multiple-scale bright and dark layer detection filters were employed to enhance retinal layer pathologies. To refine the retinal layers, graph search algorithm was utilized, and the weights of nodes were computed based on extracted layers. To validate the model, 42 SD-OCT images of AMD patients were

used. Hu et al. (Hu et al., 2019) proposed a model that combined multiscale CNN (MCNN) and graph search to extract the retinal layer in OCT images. Initially, multiscale features of the retinal layer were extracted in order to generate probability maps. To lessen the likelihood of the network incorrectly identifying the background as a target, the model uses location information to differentiate between foreground and background pixels. Finally, an enhanced graph search technique was used to delineate the retinal layers using probability maps. Mariotoni et al. (Mariotoni et al., 2020) introduced an algorithm that was capable of determining the thickness of the RNFL without the need for segmentation. The algorithm was trained using conventional RNFL thickness values obtained from SD-OCT images. In the study (Wei and Peng, 2020), the priority of the mutex relationship among retinal layers was considered, and introduced new loss function as mutex dice loss (MDL). In addition to this, a novel FCN-based model was proposed that utilized the depth max pooling (DMP) to segment fluids and retinal layers in SD-OCT images. The Shortest Path (DL-SP) algorithm (Mishra et al., 2020) was proposed for automatically identifying the retinal layers responsible for drusen and reticular pseudodrusen (RPD) in OCT images. The U-net model was used to generate probability maps and then combined with pixel-to-pixel edge weights, which were measured using the gradient in the z-direction. The model was evaluated on 1000 images and achieved absolute mean differences for RPD and drusen of 0.75 ± 1.99 pixels (2.92 ± 7.74 μ m) and 1.53 ± 1.47 pixels (5.97 ± 5.74 μ m), respectively. A segmentation model DeepRetina (Li et al., 2020), was proposed to segment the retinal layers. Xception65 extracted feature maps and then fed them into atrous spatial pyramid pooling module to get multiscale information. The method was validated using 280 OCT volumes (40 B-scans per volume) and achieved IOU and sensitivity of 0.90 and 92.15%, respectively. The paper (Li et al., 2021) presented a novel two-stage approach that uses a graph convolutional network (GCN) to identify all nine retinal layers and the OD in OCT images. Multi-scale global reasoning module integrated into the U-shaped neural network between the encoder and the decoder to use the network's prior knowledge of anatomy. The method was validated on Duke SD-OCT dataset, dice score, and pixel accuracy of 0.820 ± 0.001 and 0.830 ± 0.002 , respectively. The work (Sousa et al., 2021) presented a method for the segmentation of the ILM, RPE, and BMO in OCT images of healthy and Intermediate AMD subjects. U-Net and DexiNed, two DL networks were used, and the results showed an average

Table 5: Summarizing the DL models for the segmentation of blood vessels in fundus images

Study	Techniques	Dataset	Accuracy	Specificity	Sensitivity
Wang et al. (2015)	CNN Random Forest	DRIVE, STARE	97.67%, 98.13%	97.33%, 97.91%	81.73%, 81.04%
Melinscak et al. (2015)	CNN	DRIVE	94.66%	-	-
Fu et al. (2016)	CNN CRF	DRIVE, STARE	94.70%, 95.45%	-	72.94%, 71.40%
Jiang et al. (2018)	AlexNet	DRIVE, STARE, CHASE	95.93%, 96.53%, 95.91%, 96.62%	98.32%, 97.98%, 97.70%, 98.26%	71.21%, 78.20%, 72.17%, 76.86%
Hu et al. (2018)	CNN CRFs	DRIVE, STARE	95.33%, 96.32%	77.72%, 75.43%	97.93%, 98.14%
Wang et al. (2019a)	Dense U-net, Patch-based learning	DRIVE, STARE	95.11%, 95.38%	97.36%, 97.22%	79.86%, 79.14%
Park et al. (2020)	GAN ACE Lanczos resampling	DRIVE, STARE, HRF, CHASE-DB1	97.06%, 98.76%, 97.61%, 97.36%	98.36%, 99.38%, - -	83.46%, 83.24%, - -
Boudegga et al. (2021)	U-net Patch-learning	DRIVE STARE	95.12%, 96.41%	98.69%, 99.45%	80.60%, 82.30%
Deng and Ye (2022)	D-Mnet PCNN	DRIVE, STARE, CHASE_DB1 , HRF	96.83%, 97.32%, 97.14%, 96.68%	-	-
Kar et al. (2022a)	GAN CLHAE	DRIVE, CHASE_DB1, HRF, ARIA	97.42%, 98.73%, 97.73%, 96.28%	-	-
Chen et al. (2022a)	PCAT-UNet	DRIVE, STARE, CHASE_DB1	96.22%, 97.96%, 98.12%	-	85.76%, 87.03%, 84.93%
Zhang et al. (2022d)	U-Net	DRIVE, STARE, CHASEDB1	97.01%, 96.91%, 98.11%	-	-

absolute error of 0.49, 0.57, and 0.66 for ILM, RPE, and BM, respectively. In the paper, ([He et al., 2021b](#)), a unified DL framework was introduced that directly performed modeling of the distribution of the surface positions. A single feed-forward operation generated surfaces that are topologically accurate, continuous, and smooth. An embedded residual recurrent network (ERR-Net) ([Hu et al., 2021](#)) was developed based on a graph search for coarse-to-fine retinal layer delineation. In addition to resolving the gradient issue introduced by depth, the ERR-Net also encapsulates the image’s global spatial structure. Graph search was used to refine the retinal boundaries. The model was evaluated on Duke, Open University of Miami , and AREDS2

dataset. Parra et al. ([Parra-Mora and da Silva Cruz, 2022](#)) introduced a novel FCN architecture, dubbed LOCTSeg, to segment different diagnostic markers in OCT images. LOCTSeg was a lightweight model designed to balance performance and efficiency. Two publicly available benchmarking datasets were used to assess the performance of the model, AROI (1136 images) and HCMS (1715 images). The evaluation showed that the model achieved increased Dice score by 3% on the AROI dataset and by 1% on the HCMS dataset. The study ([Viedma et al., 2022](#)) proposed Mask R-CNN for segmenting retinal layers from OCT images. A CNN model was used for feature extraction from images and generated feature maps which were

fed into the region proposal network (RPN). After that, bounding boxes (called anchors) were generated that were distributed over each feature map. The RPN then separates these anchors into two groups: foreground class (positive anchors), which are located in areas that reflect features relating to the objects, and background class (negative anchors), which are located outside of these objects. The study (Man et al., 2023) investigated different U-net models that combined with VGG and ResNet to segment the retinal layers, and compared their accuracy. Results showed that VGG16 and U-net (VGG16-Unet) performed better than the U-net and U-net++ model.

The study (Wilkins et al., 2012) presented a CNN model based on U-net autoencoder architecture to detect intraretinal fluid (IRF) in OCT image. The OCT images were collected from 2006 to 2016 at the Ophthalmology Department, University of Washington, 934 B-scans were used for training and 355 B-scans were used for the validation purposes. Karri et al. (Karri et al., 2017) proposed an algorithm for identified retinal pathologies in OCT images. A pre-trained CNN, GoogLeNet, was fine-tuned to increase its prediction capabilities, and salient responses were identified during prediction to comprehend the properties of the learned filters. Subjects with dry AMD, DME, and normal were considered during the study. Roy et al. (Roy et al., 2017) proposed a DL model (ReLayNet) to segment the retinal layers and fluid masses through OCT scans. The proposed model was evaluated on the Duke publicly available dataset. ReLayNet was able to provide more accurate estimates of layer thickness than graph-based comparing techniques. RelayNet extracted the ILM, NFL-IPL, INL, OPL, ONL-ISM, ISE, OS-RPE, and cumulative retinal fluids with dice coefficients of 0.99, 0.90, 0.94, 0.87, 0.84, 0.93, 0.92, 0.90, 0.99, and 0.77 respectively. Schlegl et al. (Schlegl et al., 2018) developed a semantic segmentation model to extract IRF and sub-retinal fluid (SRF) from 1200 OCT volumes acquired from Zeiss Cirrus and Heidelberg Spectralis OCT machines. The model extracted IRF and SRF with a mean accuracy of 94.0% and 92.0%, respectively. Agari et al. (Asgari et al., 2019) developed an encoder-decoder model for solving the multitask problem of drusen segmentation. To segment RPE and BM, instead of training a multiclass model, a single decoder was employed for each target class. To further enhance the regularization, links between each class-specific branch and the decoder were developed. To enhance OCT image segmentation performance, Y-Net (Farshad et al., 2022) was proposed, an architecture that fuses frequency domain characteristics with the image domain. Y-net performed better than

U-net, and obtained an increase in fluid segmentation dice score by 13% and our overall dice score by 1.9%. Hsu et al. (Hsu et al., 2022) proposed a DL model that segmented the IRF, SRF, and ellipsoid zone (EZ) in OCT images, in addition to this, also correlated the extracted features with visual acuity. The modified U-net model was trained on manually annotated 127 scans from 50 patients and validated on 38 scans from 16 patients. For IRF and SRF, the model obtained values of 0.80 and 0.89 for Srensen-Dice coefficients, respectively. The study (Philippi et al., 2023) employed a transformer-based technique to detect and isolate retinal lesions in SD-OCT scans automatically. The approach combined the data-efficient training of CNNs with the efficient long-range feature extraction and aggregation capabilities of Vision Transformers. Swin UNet TTransformers (Swin-UNETR) (Hatamizadeh et al., 2022) was used, which was a segmentation network tailored to the unique challenges of medical image analysis. A private dataset consisted of 3842 SD-OCT images was used to evaluate the method. Specialists at the Franziskus Eye Center in Muenster manually classified the images. The Unet3+ achieved highest mean dice score of 0.508, whereas Swin-UNETR-24 obtained the second-best score of 0.457. Wang et al. (Wang et al., 2022a) proposed a novel technique for segmenting 10 retinal layers in OCT images, including intraretinal fluid. A fan filter was utilized to minimize the impact of vessel shadows and fluid regions in an OCT image, hence improving the linear information pertaining to retinal borders. Random forest classifier was used to predicate the retinal boundaries. By combining the unique techniques of boundary redirection (SR) and similarity correction (SC), the model was able to perform boundary tracking and identify the retinal layers. On average, the proposed method utilized OCT images from 415 healthy subjects and 482 DME patients.

9.3.2 Segmentation driven classification methods

Techniques Based on Fundus Scans The study (Lim et al., 2015) proposed a model CNN-FE to extract feature-enhanced inputs that highlight disc pallor without a degree of vessel kinking and blood vessel obstruction in fundus image. Pixel-level probability maps constructed by CNN went through a process of robust refinement, which takes into account information already known about the retinal morphology. In addition, confidence was estimated on the validity of the segmentation by analyzing the probability maps. Finally, the extracted cup and disc border were utilized to estimate CDR. MESSIDOR and SEED-DB

Table 6: Summarizing the Segmentation Models based on DL Techniques for Retinal Lesions from OCT Scans

Study	Techniques	Images	Machine	Retinal lesion	Evaluation
Sui et al. (2017)	Mutliscale CNN	912 OCT B-scans Normal subjects:42 ME patients:31	Heidelberg Spectralis	Choroidal boundaries	-
Gopinath et al. (2017)	CNN LSTM	-	-	Retinal layers	Mean absolute error: 1.30 ± 0.48 .
Xiang et al. (2018)	Graph search-Multiscale CNN	42 AMD scans	Cirrus HD-OCT 4000	Retinal layers and neovascularization	
Mishra et al. (2020)	U-netProbability maps	1000 images Normal: 20 AMD: 25	Heidelberg Spectralis	Drusen and Reticular pseudo-drusen (RPD)	0.75 ± 1.99 5.97 ± 5.74
Li et al. (2020)	Xception65, Atrous spatial pyramid pooling	280 OCT volumes	Cirrus HD-OCT	Retinal layers	IOU: 0.90 Sensitivity: 0.92
Li et al. (2021)	Graph CNN	1.12 radial OCT B-scans2. Duke SD-OCT dataset	DRI OCT-1 Atlantis	Retinal layers	Dice score: 0.820 ± 0.001 Pixel accuracy: 0.830 ± 0.002 ,
Schlegl et al. (2018)	CNN	1200 OCT volumes	Zeiss Cirrus and Heidelberg Spectralis OCT	IRF and SRF	Mean accuracy IRF: 94% SRF: 92%
Philippi et al. (2023)	CLAHE Unet3+ Vision Transformers	3842 SD-OCT	Spectralis SD-OCT, Heidelberg Engineering.	IRF, SRF, and Pigment epithelium detachment (PED)	Mean dice: 0.50
Hsu et al. (2022)	U-net model	127 scans	-	IRF, SRF, and Ellipsoid zone (EZ)	IRF: 0.80 SRF: 0.89

datasets were used to evaluate the model. The overall screening performance of CNN-FE was higher ($AUC = 0.847$) than that of the reconstruction-based method ($AUC = 0.838$). A DL model for directly screening for glaucoma using fundus images based on image-relevant information ([Fu et al., 2018](#)). Global image stream, segmentation-guided network, local disc region, and disc polar transformation streams were defined as four deep streams on different levels. Finally, the probabilities of each stream’s output were combined to produce a final output. The model was evaluated on two glaucoma datasets (SCES and SINDI), and the results showed better performance than other state-of-the-art methods. An improved U-net CNN model was proposed to segment the OD and OC from the fundus image ([Joshua et al., 2019](#)). The DRISHTI-GS and RIM-ONE v.3 datasets were used to evaluate the model. Another DL model using Gradient-weighted Class Activation Mapping (Grad-CAM) ([Kim et al., 2019b](#)) was proposed for glaucoma diagnosis based

on OD localization. The model was tested on fundus images from Samsung Medical Center (SMC) and achieved accuracy, sensitivity, and specificity of 96%, 96%, and 100%, respectively. Sreng et al. ([Sreng et al., 2020](#)) proposed a model for glaucoma diagnosis through fundus images. DeepLabv3+ architecture and encoder module with multiple CNN were employed for segmentation. For glaucoma classification, the model was tested on RIM-ONE, ORIGA, DRISHTI-GS1 and ACRIMA datasets with an accuracy of 97.37%, 90.00%, 86.84%, and 99.53%, respectively. Tulsani et al. ([Tulsani et al., 2021](#)) presented a novel method for detecting glaucoma by employing segmentation of the OD and OC in fundus scan. For the segmentation task, a custom UNET++ model was developed by tuning the hyperparameters and a custom loss function. The employed loss function was useful for addressing the class imbalance that arises due to the small size of the ONH. Based on the identification of clinical features, the proposed method was 96% accurate at classifying

images as either glaucomatous or healthy. Training times were decreased than state-of-the-art models and achieved Intersection over Union (IOU) scores (0.9477 for OD and 0.9321 for OC) using the improved model. The model was evaluated on RIM-ONE, DRIONS-DB, and ORIGA, and it was able to achieve an accuracy of 91%, 92%, and 90%, respectively. Abdel et al. (Abdel-Hamid, 2022) proposed a deep convolutional (TWEEC) network that extracted anatomical information of OD and blood vessels. The spatial retinal images and wavelet subbands were fed into the model as inputs. TWEEC model achieved accuracy for the spatial and wavelet inputs of 98.78% and 96.34%, respectively. A novel multi-task strategy (Hervella et al., 2022) for identifying glaucoma while segmenting the optic disc and cup was proposed. The model achieved an increase in performance by utilizing pixel-level and image-level labels during training. Biomarkers like the CDR was extracted from the segmentation maps that were already predicted with the diagnosis. The model designed concurrent segmentation and classification that maximizes the use of shared parameters. In order to minimize the need for loss weighting hyperparameters, a multi-adaptive optimization technique was employed during training. CDR-based classification achieved an area under the curve of 94.18% on the REFUGE dataset. The study (Nawaz et al., 2022) developed a DL model for glaucoma diagnosis, the EfficientNet-B0 feature extractor was used to compute the deep features from the suspect samples. The features computed by EfficientNet-B0 are then fed into the EfficientDet-Bi-directional D0's Feature Pyramid Network (BiFPN) module, where they fused many times using a top-down and bottom-up approach. Finally, the anticipated class of glaucoma lesions inside that confined region was predicted. To demonstrate model generalizability, cross-dataset validation was performed on the High-Resolution Fundus (HRF) and RIMONE datasets. An OD localization and Glaucoma Diagnosis Network (ODGNet) was presented by study (Latif et al., 2022). Initially, a visual saliency map combined with shallow CNN localized OD from images. In the second step, pre-trained transfer learning models (AlexNet, ResNet, and VGGNet) diagnosed glaucoma. The model was evaluated on ORIGA, HRF, DRIONS-DB, DR-HAGIS, and RIM-ONE publicly available datasets. The results showed that ODGNet tested on ORIGA for glaucoma diagnosis achieved accuracy, specificity, sensitivity, and AUC of 95.75%, 94.90%, 94.75%, and 97.85%, respectively. Touahri et al. (Touahri et al., 2022) proposed a glaucoma diagnosis model through fundus images that first segment the OD and OC and then classify them into normal

or glaucomatous scans. To begin, the OD region was segmented in the fundus images to create a ROI. To get the fine-grained segmentation, a U-Net model was developed. The model was validated using the publicly available REFUGE dataset. Roshini et al. (Roshini and Alex, 2022) proposed MultiResUNet architecture for glaucoma diagnosis based on CDR estimation. The results showed that MultiResUNet achieved a mean accuracy of 97.2%. Context encoding network (CE-Net) (Wang and Huang, 2022) architecture was developed for segmentation of the OD in diabetic retinal images. The model consisted of three module, 1) an encoder for features extraction, 2) a context extractor, and 3) a decoder. The context extractor module consisted of a residual multi-kernel pooling (RMP) and improved dense atrous convolutional block. The model was validated on Indian Diabetic Retinopathy Image Dataset (IDRID). A model (Zhang et al., 2022b) proposed for DR diagnosis based on lesion detection through fundus images. Inception V3 model was adopted for classification, whereas the grading of DR was performed by identification of different lesions. The Kaggle DR dataset was used for the training and testing of model. Another DL model (Li et al., 2018b) was proposed for the detection of DR (PDR, DME). A total of 106,244 nonstereoscopic retinal images were used to test the model. For external validation, 35,201 images of 14,520 eyes from population-based cohorts of Malays, Caucasian Australians, and Indigenous Australians were used. When tested on the independent, multiethnic data set, the AUC, sensitivity, and specificity were all found to be 0.95, 92.5%, and 98.5%, respectively. A fully patch-based CNN model (Zago et al., 2020) was developed for DR diagnosis by performing the retinal lesion localization. The use of strides enhances lesion localization by a factor of 25. Only 28 fundus images (from DIARETDB1) annotated at the pixel level were utilized in the training process for the model and tested on Messidor dataset. The system achieved sensitivity and an AOUC of 94.0% and 0.912, respectively. The study (Qomariah et al., 2021) presented a unique DL-network (MResUNet) that adapts UNet by replacing its identity mapping residual units with modified residual units to segment microaneurysm for DR diagnosis. During training, the mean weighted loss function was employed to handle imbalanced pixels of background and microaneurysms. Based on experimental results, the model outperformed than autoencoder, FCN16, FCN8, and UNet in terms of sensitivity on the IDRID and DiaretDB1 datasets. The paper (Kumari et al., 2022) presented image-processing techniques to extract the four key features microaneurysms, blood vessels,

hemorrhages, and exudates from raw fundus images, and then employed a CNN for automatic identification of DR. When compared to other models, DenseNet-16 provides the best accuracy, when tested on DRIVE database. Jiwane et al. (Jiwane et al., 2022) developed a DL model (ResNet50) for the detection of DR based on soft exudate and hard exudate along with OD. The paper (Murugan and Roy, 2022) presented CNN model to train MA and non-MA patches, and a majority voting method was employed to identify MA patches. Retinopathy Online Challenge (ROC) data was used to assess the effectiveness of the provided technique. A three-class semantic segmentation model (Selçuk et al., 2022) was proposed to extract the exudates and hemorrhage. Also, a color space transformation was done, and the classic U-Net algorithm was employed so that high performance was achieved in images with low contrast. The results showed that the Dice and Jaccard similarity indices for the segmentation performance were calculated to be close to 0.95. In order to detect and grade DR through fundus images, the study (Parthiban and Kamarasan, 2022) introduced a Wavelet Neural Network (EN-CSOWNN) model trained with EfficientNet and Chicken Swarm Optimization. In order to identify diseased areas in an image, a customized U-Net-based segmentation model was employed. Additionally, feature vectors were derived using the EfficientNet model, and class labels were assigned using the wavelet neural network model. Ultimately, the CSO approach was used to optimize the model's classification performance by adjusting the model's initial parameters. The model was validated on MESSIDOR dataset an accuracy of 98.60%. Tomaz et al. (Bisneto et al., 2020) developed a DL model based on GAN to segment OD for glaucoma diagnosis through fundus images. ROIs segmented by the GAN were characterized using taxonomic indices. These indices were based on the diversity of species and the frequency of individuals, or the range of pixel values and the number of pixels with a given value, respectively. The model was evaluated on RIM-ONE and Drishti-GS public databases and achieved 77.9% accuracy. With modifications and changes, the model obtained 100% accuracy and a ROC curve of 1.

Techniques Based on OCT Scans A DL technique was presented to segment retina surfaces in OCT volume and diagnose AMD (Shah et al., 2017). The training data was used to cultivate a set of features and a transformation. Normal and diseased image surfaces were learned using the same CNN. A total of 40 OCT volumes were used to validate the model, 20 volumes from each group. The suggested method outperformed

graph-based optimum surface segmentation using convex priors (G-OSC). Shah et al. (Shah et al., 2018) developed a CNN model to detect intermediate AMD using segmented multiple retinal surfaces through OCT scans. In order to classify B-scan images into "healthy" and "intermediate AMD," a single CNN was trained to segment all three retinal layers in a single pass. The model was validated on 3000 B-scans acquired from 50 OCT volumes. Saha et al. (Saha et al., 2019) developed a DL method for the automated detection OCT biomarker and classification of early AMD. The model automatically detected and classified HFs, hyporeflective foci inside the drusen, and subretinal drusenoid deposits from OCT B-scans. A total of 19584 OCT B-scans with at least one eye diagnosed with early or intermediate AMD were included in the dataset, images were acquired from the Doheny Eye Centers. The model detected the subretinal drusenoid deposit with an accuracy of 86%. The accuracy of detecting HFs and hyporeflective foci was 89% and 88%, respectively. Fauw et al. (De Fauw et al., 2018) developed a DL model that segments retinal layers from 3D OCT scans and then employs the extracted information for the diagnosis of retinal diseases. The segmentation network was trained on 877 images, and the classification network was trained on 14,884 maps and achieved an accuracy of 96.4% on the validation set. Chen et al. (Chen et al., 2019) developed a DL method for screening early glaucoma that utilized features from fundus and EDI-OCT images. Both textual and structural elements from each modality were integrated. Once the OC was segmented from the fundus image using brightness compensation, CDR and textural features were obtained. Each pixel in an OCT image was labeled as being on the anterior LC surface or the background using a region-aware method and a residual U-Net architecture. After extracting features of LC deformation using an improved templated local binary pattern, the LC depth and width of the BMO's were calculated. A CNN model (Raja et al., 2020b) was proposed based on CDR estimation for glaucoma diagnosis. To estimate the CDR, first ILM and RPE layers were extracted using CNN, and the graph searched was to refine the layers. Afterward, missing areas were filled by linear interpolation. Finally, cup and disc borders were determined in order to calculate the CDR. The model used the Armed Forces Institute of Ophthalmology (AFIO) dataset and achieved average specificity, sensitivity, and accuracy of 94.07%, 94.6%, and 94.68%, respectively. Hassan et al. (Hassan et al., 2020) proposed a hybrid convolutional framework (RAG-FW) that extracted multiple retinal lesions (such as IRF, SRF, HE, drusen, and CA) from OCT scans and

utilized them for grading of retinopathy. RAG-FW was tested on 43,613 multi-vendor OCT scans and performed better than state-of-the-art solutions by getting 14.15% better at extracting retinal fluids from Duke-II, 2.02% better at classifying retinopathy from Zhang, and 1.24% better from BIOMISA datasets. Hina et al. (Raja et al., 2020d) proposed a hybrid convolutional network (RAG-NETv2) for glaucoma diagnosis and grading by utilizing extracted RNFL, GC-IPL regions. For segmentation, encoder-decoder architecture was employed, atrous convolution, skip connection, and pyramid pooling techniques allowed to retain fine details of retinal layers. Afterward, the thickness profiles of extracted regions were computed and fed as a feature vector to the SVM for grading of OCT scan. The model was trained and tested on the publicly available AFIO dataset, and achieved a mean DC score of 0.8697 for extracting the regions, the F1 score, and accuracy of 0.9577 and 91.17% for glaucoma diagnosing and grading, respectively. In the study (Smitha and Jidesh, 2022), a GAN-based model was proposed for the automated segmentation and classification of OCT-B images for the purpose of diagnosing AMD and DME. The handcrafted Gabor features were integrated into the method in order to improve retina layer segmentation, and non-local denoising was utilized in order to get rid of speckle noise. The model showed better results for OCT image segmentation and classification, with an F1-score of 0.79 and an accuracy of up to 92.42%. Deep ensemble learning model (Moradi et al., 2023) was proposed for early AMD diagnoses based on retinal layer segmentation in OCT images. In order to automatically annotate 11 retinal borders, the model combined a graph-cut method with a cubic spline. After the images had been refined, they were fed into a deep ensemble model that used a Bagged Tree with deep learning classifiers. Our boundary refinement-based segmentation model has a much lower overall error rate than OCT Explorer segmentation (1.7% vs 7.8%, p-value = 0.03).

9.3.3 Classification

Fundus Scans The study (Ahn et al., 2018) suggested that using DL algorithms in conjunction with fundus photography can be an effective method for differentiating between normal and glaucoma subjects, even in the early stages of the disease. From Kim's Eye Hospital, fundus images (1,542 images) were acquired from both healthy and glaucomatous eyes; out of a total 754 were used for training, 324 for validating, and 464 for testing. A logistic regression and CNN was developed; in addition to this GoogleNet Inception v3

model was also fine-tuned using the same datasets. The fundus image is a 3D array (240x240x3), but for the purpose of performing logistic regression, the images were flattened into a one-dimensional array. CNN model was consisted of two convolutional layers with 2020 and 4040 patch sizes, 1 stride, and 16 and 32 depths were utilized. Patch size 22 and stride 2 were used for max pooling. Fully connected layers have 32 and 64 hidden units. Convolutional and fully linked layers employed 0.5 dropout rate to avoid overfitting. The training accuracy of the logistic model was 82.9%, the validation accuracy was 79.5%, and the test accuracy was 77.2%. Transfer-learned On training data, the GoogleNet Inception v3 model obtained an accuracy and AUROC of 99.7% and 0.99, while on validation data, it reached 87.7% and 0.95, and on test data, it reached 84.5% and 0.93. The AUROC and accuracy of the CNN were 0.98 and 92.2% on the training data, 0.95 and 88% data, and on the validation data, 0.94 and 87% on the test data, respectively. The paper (Zhao et al., 2019) presented a semi-supervised model for glaucoma detection based on CDR estimation without segmentation of the OD and OC. The method directly regresses the CDR value based on the feature of the OHD using MFPPNet through fundus image. The proposed technique was tested on Direct-CSU and public ORIGA glaucoma datasets and improved average accuracy of 0.063% and the correlation of about 0.726 with measurements taken before human specialists manually segmented the optic disc/cup. On a dataset of 421 fundus images, estimated CDR values were tested for glaucoma screening and achieved an AUC of 0.905. ImageNet-trained models (VGG16, VGG19, InceptionV3, ResNet50, and Xception) were trained for automatic glaucoma assessment using fundus images (Diaz-Pinto et al., 2019). The Xception model achieved an average AUC of 0.9605 with a 95% confidence range. Gheisari et al. (Gheisari et al., 2021) proposed a CNN and RNN that extracted the spatial features in a fundus image and temporal features from a fundus video. Combined CNN and RNN were used to train with 1810 images and 295 videos. The average F-measure for CNN basic and combined model was 79.2% and 96.2%, respectively. Other studies (Raghavendra et al., 2018) (Gómez-Valverde et al., 2019) reported the DL model for glaucoma diagnosis without any explicit segmentation of biomarkers. The study (Gulshan et al., 2016) used DL to develop an algorithm for automated detection of DR and DME in retinal fundus images. Between May and December 2015, a panel of 54 US-based licensed ophthalmologists and ophthalmology senior residents graded a total of 128 and 175 retinal images for DR, DME,

Table 7: Summarizing the Segmentation Driven Classification Model based on DL Techniques

Study	Techniques	Modality	Dataset	Retinal lesion	Evaluation
Lim et al. (2015)	Pixel-level probability maps CNN	Fundus	MESSIDOR, SEED-DB	OD, OC CDR	AUC: 0.847
Joshua et al. (2019)	U-net	Fundus	DRISHTI-GS, RIM-ONE v.3	OD, OC, CDR	-
Kim et al. (2019b)	Gradient-weighted Class Activation Mapping	Fundus	Samsung Medical Center	OD	Accuracy: 96% Sensitivity: 96% Specificity: 100%,
Sreng et al. (2020)	DeepLabv3+	Fundus	RIM-ONE, ORIGA, DRISHTI-GS1, ACRIMA	-	Accuracy: 97.37%, 90.00%, 86.84%, 99.53%
Tulsani et al. (2021)	UNET++ model	Fundus	RIM-ONE, DRIONS-DB, ORIGA	OD, OC	Accuracy: 91%, 92%, 90%.
Abdel-Hamid (2022)	Wavelet Transformation CNN	Fundus	RIM-ONE v.2	OD, Blood vessels	Accuracy: 98.78%
Hervella et al. (2022)	Segmentation maps CNN	Fundus	REFUGE	OD, OC, CDR	AUC: 0.94
Saha et al. (2019)	CNN	OCT	Local dataset	HF's Hyporeflective foci, Subretinal drusenoid	Accuracy: 89%, 88%, 86%
Hassan et al. (2020)	Hybrid convolutional framework (RAG-FW)	OCT	Duke-II, Zhang, BIOMISA	IRF, SRF, HE, drusen, and CA	-
Raja et al. (2020b)	RAG-NET	OCT	BIOMISA	ILM and RPE	Accuracy: 94.68% Specificity: 94.07% Sensitivity: 94.6%

respectively. For EyePACS-1, the model had an AUC of 0.991 (95% CI, 0.988-0.993). Another automated DL model ([Gargeya and Leng, 2017](#)) was developed for the detection of DR. Seventy-five thousand and one hundred thirty-three publicly available fundus images from diabetic patients were used to train and test the model respectively. Whereas validation was performed on MESSIDOR 2 and E-Ophtha databases. Tests performed on the MESSIDOR 2 and E-Ophtha databases yielded an AUC of 0.94 and 0.95, respectively. Wang et al. ([Wan et al., 2018](#)) proposed a DR classification model, with transfer learning of AlexNet, VggNet, GoogleNet, and ResNet. The model was tested on a publicly available Kaggle dataset and achieved a classi-

fication accuracy of 95.68%. Qummar et al. ([Qummar et al., 2019](#)) proposed DL ensemble approach for DR detection and employed five CNN models, Resnet50, Inceptionv3, Xception, Dense121, and Dense169. The results showed that the model detected all the stages of DR when tested on Kaggle dataset. A DL method was proposed for feature extraction from fundus images and SVM-based classification of DR ([Qomariah et al., 2019](#)). The paper employed a CNN method for DR classification of fundus images. Pre-trained CNN models, AlexNet, VGG-16, and SqueezeNet) resulted in a 93.46%, 91.82%, and 94.49% accuracy in classification, respectively. The study ([Doshi et al., 2020](#)) proposed and investigated the usage of multiple down-scaling

techniques prior to submitting image data to a DL network for classification. Multi-Channel Inception V3 architecture with a unique self-crafted preprocessing phase was employed. Jordi et al. (de La Torre et al., 2020) presented a DL interpretable classifier for DR detection through fundus scans, it also performed grading. The classifier was able to provide an explanation for the classification findings by giving a score to each point in both the hidden space and the input space. These scores, generated by pixel-wise score propagation model, represented how significantly each pixel aided in the overall classification. Four different transfer learning algorithms (VGG16, ResNet50, InceptionV3, and DenseNet121) were used to detect DR from fundus images (Sheikh and Qidwai, 2020). DenseNet121 model yielded the best results for making predictions. Karki et al. (Karki and Kulkarni, 2021) developed a DL model based on EfficientNet for the classification of the DR. In addition to this, model performed grading of images, into mild, moderate, severe, or PDR. A quadratic kappa score of 0.924377 was attained by the best model on the APTOS test dataset after the models were trained using various datasets. The work (Deepa et al., 2022) presented a CNN ensemble (MPDCNN) model for accurate fundus image-based DR identification and grading. In the first phase, each input image was split into four patches and fed into one of two pre-trained CNN models (InceptionV3 and Xception). Prior knowledge is derived from the pertinent characteristics that are located in the shallow-dense layers of CNN models. The model was taught the crucial details from DR images by combining features from shallow and dense layers. In the second step, combined probability vectors from four patches were utilized to train the network classifier. DR classification accuracy was enhanced by using the ensemble method with multi-stage DL model and achieved an accuracy of 96.2% with fivefold cross-validation. A hybrid method (Butt et al., 2022) was proposed for finding and classifying DR based on fundus images. Model employed transfer learning, based on GoogleNet and ResNet-18 architectures, to find features that can be put together to make a hybrid feature vector. A number of classifiers were used to classify fundus images into binary and multiclass based on the extracted feature vector. The model was trained and tested on APTOS, Kaggle, and The Aravind Eye Hospital in India datasets. For binary classification, the proposed a maximum accuracy of 97.8%, and for multiclass classification, it had an accuracy of 89.29%. The paper (Muthukannan et al., 2022) developed a DL model (CNN-MDD) to detect early-stage AMD. Maximum entropy transformation

was applied, and then images were fed into CNN which optimized using a flower pollination optimization algorithm (FPOA) for feature extraction. A Multiclass SVM classifier was employed to identify the disease from the CNN's output. The model was tested on Ocular Disease Intelligent Recognition (ODIR) dataset and had specificity, precision, accuracy, and recall of 95.21%, 98.30%, 95.27%, and 93.3%, respectively. The study (Bhimavarapu and Battineni, 2023) presented the DL with improved activation function for DR diagnosis from fundus images that reduced loss and processing time. Models was trained and evaluated using the DIARETDB0, DRIVE, CHASE, and Kaggle datasets. On the Kaggle dataset, the ResNet-152 model achieved the highest accuracy of 99.41%. A lightweight CNN (Lu et al., 2023) used transfer learning to classify the DR and DME simultaneously. The model's average accuracy, precision, recall, and specificity after five rounds of cross-validation were 96.66%, 96.85%, 99.32%, and 96.63%. In the article (Adak et al., 2023), significant parameters of fundus images were captured using transformer-based learning models for a more nuanced understanding of DR severity. To determine the severity of DR from fundus photographs, transformers were employed and used four models: the Vision Transformer (ViT), Data-Efficient Image Transformers (DeiT), Bidirectional Encoder representation for image Transformer (BEiT), and Class-Attention in Image Transformers (CaiT). The model was tested on used the publicly available APTOS-2019 dataset. The work presented a CNN ensemble model for accurate fundus image-based DR identification and grading. The other studies (Rakhlin, 2018) (Fellah et al., 2023) (Moin et al., 2023) (Swarnalatha et al., 2023) (Elmoufidi and Ammoun, 2023) proposed DL model for DR classification through fundus images.

OCT Scans A CNN model (An et al., 2019) was developed for glaucoma diagnosis through fundus and OCT images. The parameters OD, RNFL deviation map, macular GCC thickness map, and RNFL thickness map were all calculated by commercial software and were used to train the model. Another study feature-based and feature agnostic techniques (Maetschke et al., 2019) for glaucoma diagnosis. A feature method based on 22 parameters (calculated by the OCT machine) and a traditional machine learning classifier was used. An unsegmented OCT volume was classified as normal or glaucomatous using a feature-agnostic framework built on 3D CNN for glaucoma diagnosis. To acquire depth information, they used 3D convolution, which allowed them to locate the significant area for diagnosis. The features were derived from raw data by

using Class Activation Maps. The method failed to detect glaucoma in OCT images from patients over the age of 65 or those with advanced disease. In order to digitally stain the neuronal and connective tissues of ONH, a DL framework called DRUNET (Devalla et al., 2018) was presented, which was a U-Net-derived fully convolutional neural network and takes advantage of skip connections. The peripapillary sclera and LC were both successfully separated by the algorithm. The model could extract both global (spatial) and local (texture) characteristics of ONH tissues. A shortcoming of the proposed architecture is that it was only trained on 100 OCT images obtained from healthy and glaucoma participants.

Muhammad et al. (Muhammad et al., 2017) proposed DL model based on AlexNet and utilized transfer learning. The OCT software's measurements of features like RNFL and GCIPL thickness were fed into the CNN. CNN's feature extraction was utilized to train a random forest classifier. Depending on the parameters used, the model's accuracy was anywhere from 63.7% to 93.1%. Kermany et al. (Kermany et al., 2018b) proposed a DL model to diagnose DME, CNV, DRUSEN and normative retinal OCT. They used 108,312 OCT images from 4,686 patients for training and 1,000 scans from 633 subjects for testing and achieved accuracy, sensitivity, and specificity ratings of 96.6%, 97.8%, and 97.4%, respectively. Feng et al. (Li et al., 2019a) proposed a deep classification model for choroidal neovascularization (CNV), DME, and DRUSEN through OCT images. To identify retinal OCT images, the proposed approach used an ensemble of four classification model instances, all of which were based on an enhanced ResNet50. The dataset consisted of 21,357 retinal OCT scans that were gathered from 2,796 adult patients at Shanghai Zhongshan Hospital and Shanghai First People's Hospital between 2014 and 2019. The model classification accuracy for the B-scan was 0.973 (95% 0.971–0.975), the CI, 0.971–0.975), sensitivity was 0.963 (95% and the 95% CI, 0.983–0.987). Butola et al. (Butola et al., 2020) proposed a CNN model (LightOCT) to classify OCT images into classes normal, AMD, and DME. LightOCT had a two-convolutional-layer and a fully-connected-layer, and achieved accuracy greater than 96%. A DL model (Jin et al., 2022) was proposed based on feature-level fusion (FLF) method that combined the OCT and OCTA images for the assessment of CNV in AMD. The model was tested on two external datasets and achieved an accuracy of 95.5% and an AUC of 0.9796 on multimodal data.

A novel uncertainty guided semi-supervised model (Sedai et al., 2019) was proposed based on student-

teacher methodology. Limited labeled samples and a large number of unlabeled images were used for training. First, using Bayesian deep learning, a teacher segmentation model was trained using the labeled data. In order to generate soft segmentation labels and an uncertainty map for the unlabeled collection, the trained model was employed. After the data were softly segmented, the uncertainty of the teacher model was assessed, and the pixel-wise confidence of the segmentation quality was used to update the student model. Normal OCT scans were reconstructed using an adversarial network that was trained with little supervision (Wang et al., 2021c). The network then reconstructed the abnormal (disease) images at the inference stage, using the difference between the input and reconstructed scans to identify lesion pathologies. Das et al. (Das et al., 2020b) proposed an unsupervised framework using the GAN to perform fast and reliable super-resolution without the requirement of aligned low and high-resolution pairs. Adversarial learning identified mapping priors to obtain the spatial, color, and texture information in the high-resolution scans. Automated AMD diagnosis using the generated images yields an improved classification accuracy of 96.54%. Das et al. (Das et al., 2020a) proposed a semisupervised GAN-based classifier for automated diagnosis using limited labeled data. The two main components of the framework were the generator and the discriminator. The adversarial learning between them aids in the development of a generalizable classifier for the prediction of degenerative retinal illnesses like AMD and DME.

Research trends shifted towards the analysis of OCT volume for detecting various retinal diseases; the study (Rasti et al., 2018) proposed a model for the classification of abnormal macula through 3D-OCT. The technique evaluated intraretinal layers and lesions without the use of denoising, segmentation, or retinal alignment operations. A two-stage plan was used to separate abnormal cases from the control group based on adaptive feature learning and diagnostic scoring. Initially, the cumulative characteristics of 3-D volumes were extracted using a wavelet-based CNN model for generating B-scan CNN codes in the spatial-frequency domain. The second step involved using the derived features to score the existence of anomalies in the 3D OCT. The technique was tested on two independent retinal SD-OCT datasets using the five-fold cross-validation (CV) method. The first group is composed of 30 normal participants and 30 patients with DME 3-D OCT scans acquired with a Topcon instrument. The second set of data was from the Heidelberg device and included 45 subjects, each class (AMD, DME, and nor-

mal) contained 15 subjects. The results showed that in the two-class classification problem (dataset1), the suggested method achieved an average precision of 99.33%. When used for the three-class classification problem (dataset2), the model achieved an average precision of 98.67%. The study (Hassan et al., 2018a) introduced a multilayered CNN structure tensor Delaunay triangulation that extracted nine retinal and choroidal layers and the macular fluids. The retrieved retinal information was used for the automated diagnosis of maculopathy and the reliable reconstruction of the 3D macula of the retina. The model was validated on 41,921 OCT images collected from different vendors and achieved mean accuracy of 95.27% for extracting retinal layers. Whereas, for extracting fluid, the reported mean dice coefficient was 0.90, and the overall accuracy for maculopathy diagnosis was 96.07%. Mantel et al. (Mantel et al., 2021) proposed a DL model to identify and localize AMD biomarkers such as IRF, SRF, and pigment epithelium detachment (PED). Cubic volumes of SD-OCT were collected from 117 AMD eyes, then manual annotation of the retinal lesions was performed. A 3D-FCN (Li et al., 2019b) based on U-Net was proposed to segment the retinal fluid OCT images. The model was evaluated on the local dataset (75 volumes), achieved Kappa coefficient of 98.47%, accuracy rate of 99.56%, and F1 score of retinal fluid was 95.50%. In the paper (Mukherjee et al., 2022), a 3D deep neural network was proposed that segmented the retinal layers ensuring accuracy and smoothness. The model was made up of two separate but complementary networks: (1) 3D UNet that performed multi-class voxel labeling of retinal layer surfaces, and (2) 3D convolutional-autoencoder, which limits the 3D UNet's output and compels it to estimate a smooth contour.

10 Advanced Deep Learning Schemes

This section presents a brief introduction to advance DL techniques and state-of-the-art methods for the identification and classification of retinal lesions.

10.1 Meta-Learning & Multi-task Learning

Meta-learning is a subfield of DL that focuses on the problem of learning how to learn or learning from previous learning experiences. The goal of meta-learning is to enable a model to quickly adapt to new tasks using only a small amount of data by leveraging the knowledge gained from previously seen tasks. There are several different approaches to meta-learning, each with its own set of advantages and disadvantages.

- One common approach is to use a neural network as the model and train it on a variety of tasks in a way that the parameters of the network are updated so that they can be used to adapt to new tasks quickly. This is done by defining a loss function for the meta-learning process that tries to minimize the difference between the parameters of the model after adapting to a new task and the parameters of the model after adapting to similar tasks in the past.
- Metric-based meta-learning, which learns a distance metric in the space of task representations, such that new tasks can be quickly adapted to by finding the most similar tasks to the new task in the learned metric space.
- Model-based meta-learning methods, which learn a model of the task-generating process and can use this model to adapt to new tasks quickly.
- Optimization-based meta-learning methods, which learn an optimization algorithm that can quickly adapt to new tasks by using the gradients of the loss function with respect to the model parameters.

All of these methods have been successfully applied to a variety of different problems, such as few-shot and one-shot learning, where a model must quickly adapt to new tasks with limited data, reinforcement learning, and other areas. Overall, the main idea behind meta-learning is to train a model on a variety of tasks such that it can quickly adapt to new tasks using the knowledge gained from the previous tasks. This allows the model to improve its learning efficiency and generalization performance. The meta-learning strategy involves training the model's parameters explicitly so that good generalization performance can be achieved on a new task using a short number of gradient steps and a small amount of training data (Finn et al., 2017). For automated diagnosis of DR in fundus images, an anomaly characterization algorithm (Matta et al., 2023) was developed. A few-shot learning solution in which CNN trained for common conditions was combined with an unsupervised probabilistic model for detecting rare conditions. CNNs often assume that images with the same anomalies were similar, even though they were trained to look for differences. The algorithm achieved an average AUC of 0.938.

10.2 Few-shot learning

Few-shot learning (FSL) model is able to learn and recognize new classes with only a small number of examples. The goal is to train models that can generalize well to new classes, even when only a small number of

examples are available for these classes. There are two main approaches for few-shot learning:

- Meta-learning: This approach involves training a model on a large number of similar tasks so that it can learn to adapt quickly to new tasks. The model learns a general way of learning rather than memorizing the specific training examples.
- Transfer learning: This approach involves using a pre-trained model on a large dataset and fine-tuning it on the few-shot task. The idea is that the model has already learned useful features from the large dataset that can be useful for the few-shot task.

FSL is often used in tasks such as image classification, where there is a small number of examples per class. Some other examples of real-world applications that use few-shot learning are medical imaging, rare species identification, and speech recognition. Recently, some new techniques have been proposed for few-shot learning, such as few-shot learning with attention mechanisms, memory-augmented neural networks, and metric-based learning. These methods have shown promising results in various few-shot learning benchmarks. Yoo et al. (Yoo et al., 2021) proposed a model based on FSL using GAN to diagnose rare ocular diseases in OCT images. Before training the classifier, GAN model was built to turn normal OCT images into pathological OCT images for disease. Inception-v3 was trained using a training dataset, and then the final model was tested on a separate test dataset. The study (Mai et al., 2021) modeled the problems caused by a lack of labeled data as a Student-Teacher learning with a knowledge distillation (KD). Kim et al. (Kim et al., 2017) proposed a model for glaucoma diagnosis in fundus images using FSL. The study (Murugappan et al., 2022) proposed model DRNet, based on FSL and attention, that performed grading and detection of DR. To build the attention mechanism to preserve visual representations, the network makes use of aggregated transformations and class gradient activations. The model was evaluated on APTOS2019 dataset and achieved 99.73 % accuracy, 99.82% sensitivity for DR detection, 98.18% accuracy, 97.41% sensitivity for DR grading. Gulati et al. (Gulati et al., 2022) used FSL on the iris dataset to find out hemorrhages or Microaneurysms disease in images.

10.3 Incremental learning

Incremental learning model continually updates its knowledge from newly acquired data, without being retrained from scratch. This allows the model to continuously learn and improve its performance over

time, making it suitable for scenarios where the data is constantly changing. The model parameters update incrementally instead of retraining the entire model on all the data again. This helps to reduce computational resources required to train the model, as well as allow the model to learn from new data continuously. The approach typically involves dividing the incoming data into mini-batches and using these mini-batches to update the model parameters using gradient descent or a similar optimization technique. It can be used in various tasks such as classification, regression, and clustering. It is especially useful in scenarios where the data is too large to fit into memory or where the data is streaming and needs to be processed in real-time. To improve classification accuracy, the study (Meng and Shin'ichi, 2020) presented model "Attribute Driven Incremental Network" (ADINet) that combined class label prediction with attribute prediction inside an incremental learning framework. Knowledge distillation (KD) was used for image classification to preserve the information of base classes. For improved accuracy in attribute prediction, weights were assigned to each image attribute based on their relative importance. They came up with the concept of attribute distillation (AD) loss to preserve the data of base class attributes despite the advent of new classes. There is only a small performance hit when repeating this incremental learning process numerous times. Hassan et al. (Hassan et al., 2021) introduced a novel incremental cross-domain adaption technique that can be used by any deep classification model to gradually learn pathological abnormalities in OCT and fundus imaging with only a small number of training examples. By using a Bayesian multiobjective function, the proposed technique not only ensures that the candidate classification network retains its prior learned knowledge during incremental training but also that it understands the relationships between previously learned pathologies and recently introduced disease categories so the model can effectively recognize them during the inference stage. The model achieved an overall accuracy and F1 score of 98.26% and 0.98, respectively, when tested on six public datasets. In the study (He et al., 2021a), an incremental learning-based model was proposed for the DR lesion segmentation that distills the knowledge of the previous model in order to enhance the current model. A probability-map alignment scheme was proposed to combine the previous map and the current map. The scheme dealt with the special class background in the context of segmentation. Using the scheme, it was easy to calculate the optimized value for the model-based weight. The idea of "knowledge distillation" was used

to move the information from the probability map to the current model.

10.4 Contrastive learning

Contrastive learning (CL) is a self-supervised learning method that aims to learn a feature representation of data that separates positive pairs from negative pairs (Tian et al., 2019). The idea is to maximize the similarity between positive pairs while minimizing the similarity between negative pairs. This is typically done by designing a contrastive loss function and optimizing it using gradient descent (Tan et al., 2022). The learned representation can then be used for downstream tasks, such as classification or clustering, without the need for labeled data. It has been applied to various domains, including computer vision and natural language processing, and has shown promising results. Numerous DL-based methods have been proposed, and they perform better than human analysis at diagnosing retinal disorders. Cross-entropy is widely employed as a loss function in conventional DL model training. But it has recently been found that this loss function has certain drawbacks, such as a poor margin that might cause erroneous findings, sensitivity to noisy data, and hyperparameter variability. To fix these problems, contrastive learning has been gaining popularity. Islam et al. (Islam et al., 2022) proposed a supervised CL model for detecting DR from fundus images. For image enhancement, CLAHE was used, and Xception model was employed as the encoder for representation learning. The SCL of the model was interpreted by projecting a 128-D embedding space into a 2-D plane using the t-SNE method. Two publicly available datasets, APTOS and Messidor-2 were used for training and testing of the model. For DR (Binary classification), the model achieved an AUC of 98.50% and an accuracy of 98.36% and on the APTOS 2019 dataset. Whereas for five-stage grading, it gained AUC of 93.81% and an accuracy of 84.36%. Tian et al. (Tian et al., 2019) developed CL-driven methodologies to constrain the model's knowledge to learn the difference between new anchor examples and previously acquired positive and negative examples. With the goal of identifying retinal biomarkers in OCT images, a novel contrastive uncertainty network (CUNet) (Liu et al., 2022b) was developed. To improve the network's capacity for distinguishing between distinct classes of retinal biomarkers, CUNet employed a proposed CL strategy to strengthen the feature representation of biomarkers. To further enhance the network's sensitivity to the fuzzy boundaries of retinal biomarkers, bounding box uncertainty was proposed

and integrated with the conventional bounding box regression. In the study (Kaplan and Lensu, 2022), a variational autoencoder (VAE)-based technique was developed for the generation of OCT images of the retina using CL. In the second step, disease-specific OCT images were generated by applying VAEs to the learned embeddings. It was found that the diseases were effectively partitioned in the embedding space, and the suggested method successfully produced high-quality images with high-detail spatial resolution. Alam et al. (Alam et al., 2022) proposed a CL-based framework with neural style transfer (NST) augmentation to generate models with improved representations for detecting DR in fundus scans. The EyePACS dataset was used to train and evaluate the model, and clinical data from the University of Illinois, Chicago (UIC) was used for testing. To improve a U-Net embedding capacity to segment retinal vessels in fundus image, a model (Xu et al., 2022) was presented that uses a local-region and cross-dataset CL strategy without introducing complex network structures. The main goal was to distinguish the characteristics of pixels that are easily confused with their neighbors within the same local region. The model took full advantage of the global contextual information of the entire dataset that improves the features by employing a memory bank method. The model was evaluated on DRIVE and CHASE-DB1 datasets. In order to provide lesion-aware scanner-independent screening and grading of retinopathy, the study (Hassan et al., 2023) introduced a novel self-supervised segmentation-driven classification pipeline that used a proposed angular contrastive distillation approach to extract retinal lesions. To further improve the proposed framework's diagnostic capabilities, a novel co-attention mechanism was incorporated. The mechanism allowed the underlying network to concentrate on retinal abnormalities and effectively grade retinal diseases without requiring ground truth labels. The model was tested on seven publicly available datasets acquired using four different scanners, where it achieved a 9.22% improvement in mean IOU for extracting retinal lesions and a 10.71% improvement in F1 score as compared to state-of-the-art solutions for grading retinopathy. In order to identify and segregate the biomarkers in OCT scans using only image-level annotations, a weakly supervised network called TSSK-NET (Liu et al., 2023a) was proposed. The method is a Teacher-Student network with Self-supervised CL and Knowledge distillation-based anomaly localization. Initially, a unique pre-training technique based on supervised CL was proposed to teach the model morphology of normal OCT images. Second, a module for fine-tuning was

built, and a novel hybrid network was proposed. The model employed supervised CL for learning features and cross-entropy loss for learning classes. To further enhance performance, it was proposed to combine these two losses in order to preserve the various morphologies and improve the encoding representation of features. Finally, a knowledge distillation-based anomaly segmentation method was utilized that was effectively integrated with the prior model to relieve the difficulty of insufficient supervision. In the study (Holland et al., 2023), the AMD progression through OCT images was analyzed in a self-supervised feature space. CL was used to pretrain an encoder, which then projects images from longitudinal time series to positions in feature space. This enables the construction of disease trajectories that were subsequently denoised, and divided into clusters. These clusters were associated with OCT biomarkers and were discovered in two datasets encompassing time series of 7,912 patients scanned over a period of eight years.

10.5 Domain Adaptation

Domain adaptation is an advanced DL technique that enables models trained on one domain (source domain) to generalize well to another domain (target domain) with different distributions (Liu et al., 2019a). This is especially useful in scenarios where annotated data is scarce in the target domain. The main idea behind domain adaptation is to align the feature representation of the source and target domains so that the model trained on the source domain can effectively generalize to the target domain. This can be achieved by various methods, including fine-tuning the model using a small amount of labeled target data, adversarial training, and feature reconstruction. The goal is to reduce the domain shift, or the difference between the source and target domains so that the model can perform well on both domains. In order to facilitate unsupervised domain adaptation to segment retinal vessels in fundus images, Zhuang et al. (Zhuang et al., 2019) derived the asymmetrical maximum classifier discrepancy (AMCD) strategy from maximum classifier discrepancy. The model was trained using labeled data and then tested with unlabeled data from the target domain. The three classifiers were trained in an asymmetrical fashion, with one main classifier using only the source examples and the other two assist classifiers being utilized to maximize the discrepancy on target samples. The model was validated on DRIVE, STARE, CHASE-DB1, and IOSTAR eye vessel segmentation datasets. Lui et al. (Liu et al., 2019a) proposed an unsupervised domain

adaptation model Collaborative Feature Ensembling Adaptation (CFEA) that collaborated adaptation through both adversarial learning and ensembling weights. By ensembling weights during training, the model not only achieved domain-invariance but also maintained an exponential moving average of the previous predictions, leading to improved prediction for the unlabeled data. Multiple adversarial losses enable the extraction of domain-invariant features to confound the domain classifier and simultaneously benefit the ensembling of smoothing weights, all without performing annotation of any sample from the target domain. Song et al. (Song et al., 2020) proposed a domain-adaptive multi-instance learning with attention technique for DR grading. Labeled examples are generated through cross-domain to eliminate irrelevant instances. A multi-instance learning with attention technique was created to collect the spatial information of highly suspicious lesions and performed DR grading. The model achieved an average accuracy of 76.40% and an AUC value of 0.749 when tested on the Messidor dataset. Wang et al. (Wang et al., 2021b) developed an unsupervised domain adaption model based on faster-RCNNs for lesion detection in multi-device retinal OCT images. Both the shift at the image level and the shift at the instance level were minimized together to reduce the domain shift. In order to synchronize the changes across all of the levels, the model used a combination of a domain classifier and a Wasserstein distance critic. Using OCT image data from two separate devices, the model achieved an average accuracy improvement of more than 8% compared to the technique without domain adaptation and surpassed the performance of other comparable domain adaptation methods. Another study (Yang et al., 2020) proposed an unsupervised domain adaptation framework for lesion detection in OCT images. To compel the network to learn device-independent features, the model developed global and local adversarial discriminators. A non-parameter adaptive feature norm was then presented for the global adversarial discriminator in order to stabilize classification in the target domain. The study proposed a Collaborative Adversarial Domain Adaptation (CADA) model (Liu et al., 2022a) based on domain adaptation with multi-scale inputs and multiple domain adaptors employed in feature and output space. The information loss caused by the network's pooling layers used for feature extraction can be mitigated with multi-scale inputs. CADA is an interactive paradigm that enables collaborative adaptation through adversarial learning and weight ensembling. Model accomplished domain invariance and

model generalizability by using adversarial learning at multi-scale outputs from distinct network layers and retaining an exponential moving average (EMA) of the historical weights during training. Multiple adversarial losses in the encoder and decoder layers direct the extraction of domain-invariant features without annotating a single sample from the target domain. The model outperformed on REFUGE, Drishti-GS, and Rim-One-r3 datasets. An innovative approach (Madadi et al., 2022) for glaucoma diagnosis based on learned representations that included both domain-invariant and domain-specific in order to extract generic and domain-specific information. Low-rank coding was employed for aligning source and target distributions, as well as progressive weighting was used for the correct transfer of source domain information and mitigation of negative knowledge transfer to the target domain. The model was evaluated on OHTS, ACRIMA and RIM-ONE. Zhang et al. (Zhang et al., 2022c) proposed an unsupervised domain-adaptive segmentation (CAE-BMAL) model to extract the OD and OC. Initially, a convolutional autoencoder was used to boost the source domain, allowing the model to generalize better. Then, to mitigate the effects of the complex environment on segmentation, a boundary discrimination branch based on adversarial learning was introduced. The model was validated on three datasets, Drishti-GS, RIM-ONE-r3, and REFUGE. The study (Cao et al., 2022a) proposed a unified weakly-supervised domain adaptation framework for the DR diagnosis. The model comprised three parts: domain adaptation, progressive discriminator for individual instances, and multi-instance learning with attention. The method utilized multi-instance learning and an attention mechanism to model the connection between patches and images in the target domain. Additionally, it used a combined learning approach that takes into account data from both the source and the target domains. Results on the Messidor dataset showed that the model had an average accuracy and AUC of 94.90% and 0.76 for binary-class and 95.80%, 0.74 for multi-class classification, respectively. The model achieved 88.70% accuracy on Eyepacs dataset. Chen et al. (Chen et al., 2022d) proposed a segmentation-guided domain-adaptation model for adapting images from various OCT machines into a single image domain. It eliminates the time-consuming processes of manually labeling new datasets and retraining the existing network. The study (Hou et al., 2023) deals with image quality enhancement of fundus images in a completely unsupervised manner, neither paired nor high-quality photos were used.

10.6 Attention-based Models

The study (Fang et al., 2019) proposed a novel lesion-aware DL model (LACNN) for retinal OCT image classification. At first, the OCT image was used to create a soft attention map using the lesion detection network. A classification network is then used to assign relative importance to the various convolutional layers based on the attention map. An improved U-Net model (Liu et al., 2021c) based on an attention mechanism was developed to identify the fluid region. By bringing together high-level and low-level information, skip connections improved the accuracy of the segmentation outcomes. The loss function is a combination of the weighted binary cross-entropy loss, the dice loss, and the regression loss (to prevent the problem of converging fluid areas). Another study (Liu et al., 2021b) presented a one-stage attention-based method for retinal OCT image segmentation and classification. Mishra et al. (Mishra et al., 2021) proposed a model for the classification of macular OCT images using Multilevel perturbed spatial attention to extract context-aware diagnostic features. The model classified AMD, DME, and CNV. Preprocessing techniques like region of interest extraction, denoising, and retinal flattening were not required with the proposed end-to-end trainable architecture. Liu et al. (Liu et al., 2020) proposed an enhanced nested U-Net architecture (MDAN-UNet) for end-to-end segmentation of OCT images. The model was evaluated on two publicly available benchmark datasets, Duke DME and the RETOUCH datasets. The study (Sun et al., 2020) presented a model to classify OCT volume for diagnosing macular diseases. The model consisted of three modules: feature extractor from B-scan, 2D map generation, and volume-level classifier. The model was trained and used to construct a 2D map for OCT volume, whereas volume-level classifiers (SVM) classified 2D feature maps. The results of a five-fold cross-validation of the model showed an average of 98.17% accuracy, 99.26% sensitivity, and 95.65% specificity. The model was trained and tested on a publicly available dataset (Kermany et al., 2018a). In terms of accuracy, the model achieved 97.79% on the training data and 95.6% on the testing data. Rendering en face OCT of arbitrary retinal layers was made possible by real-time segmentation in combination with high-speed OCT volume acquisition, which can be used to improve the success rate of high-quality scans and give surgeons immediate feedback during image-guided procedures. In the study (Borkovkina et al., 2020), researchers used three tiers of optimization to successfully segment the eight retinal layers in real time using OCT. First, a

simplified neural network architecture; second, a novel neural network compression approach using TensorRT; and third, dedicated GPU hardware to speed up calculations. The U-NetRT compressed network offered 21 times faster inference than regular U-Net inference with no loss of accuracy. Kumar et al. (Kumar et al., 2022) developed a model that incorporated Attention and Transfer Learning to classify the CNV, DME, drusen from the OCT images. An innovative end-to-end multiscale attention-gated network (MAGNet) was proposed (Cazañas-Gordón and da Silva Cruz, 2022) for detecting and segmenting retinal layers and macular cystoid edema in OCT images. In order to deal with class imbalance, the MAGNet utilizes a weighting loss methodology and a FCN model that uses attention gates at different scales to perform segmentation. All B-scans were center-cropped along their longest axis to reduce their dimensions and create 496-by-496-pixel squares as part of the preprocessing phase. The model used Duke and HCMS datasets for training and testing and achieved the mean dice score of 0.92 ± 0.03 . Li et al. (Li et al., 2023) a multiscale attention-guided fusion network (MAGF-Net) was proposed for vessel segmentation in fundus images. A multiscale attention (MSA) block was proposed for the construction of the backbone network in order to capture multiscale contextual variables. To obtain global multiscale contextual information, a feature enhancement (FE) block was designed and integrated into the bottleneck layer. Attention-guided fusion (AGF) blocks were created to combine characteristics from various network levels in order to maximize the usefulness of both channel information from deep layers and spatial information from shallow layers. For further data retention throughout the downsampling process, a hybrid feature pooling (HFP) block was utilized. The model was validated on three public datasets: the CHASE-DB1, the DRIVE, and the STARE. The model achieved F1 and accuracy of 0.8329 and 96.77% on DRIVE, 0.8307 and 95.78% on STARE, and 0.8364 and 96.49% on CHASE-DB1, respectively. A multi-scale residual attention network (MRANet) (Yi et al., 2023) based on U-Net was developed to segment retinal vessels in fundus scans. Initially, a multi-level feature fusion (MLF block) block was introduced to collect blood vessel information more effectively. Then, variable weights of each fused feature were learned through the use of attention blocks, which can preserve more useful feature information while lowering interference from redundant features. Next, a multi-scale residual connection block (MSR block) was created to extract features more effectively. Finally, network overfitting was mitigated by incorporating a DropBlock layer

within the network. The model achieved an accuracy rate of 96.98% and an AUC performance value of 0.98 on the DRIVE dataset, and 97.55% and 0.98 on the CHASE DB1 dataset, respectively.

11 Datasets

This section provides information about the datasets of fundus and OCT images. There are various datasets, private and publicly accessible, are present in the literature for both modalities. Here we are only describing the publicly available datasets. The publicly available dataset was originally created to serve as a testing dataset against which various detection algorithms could be evaluated.

11.1 Fundus Datasets

There are various fundus-based datasets that are publicly available, which are used to detect various retinal abnormalities. Table 8 summarizes the features of publicly available fundus datasets. **DRIVE** (DRIVE, 2004) dataset consists of 40 fundus images and segmented blood vessels.

DIARETDB0 dataset (DiaRetDb0, 2007) contains 30 CFPs, 20 of which are considered normal and 10 of which exhibit DR (hard and soft EXs, MAs, HMs, and neovascularization). There are a total of 89 CFPs in the DIARETDB1 DiaRetDb1 (2007) database; 84 show at least mild NPDR signs of the DR, while five are considered normal and show no signs of the DR.

STARE (Structured Analysis of the Retina) (STARE, 2000) dataset consists of 400 raw fundus images with labels of 13 categories and also segmentation annotation of blood vessels, arteries, and optic nerve for 40, 10, and 80 images, respectively.

DRIONS-DB (RIONS-DB, 2009) consisting of 110 unlabeled images with two different segmentation of the OD for each image. The Messidor project Messidor (2017) objective was to conduct a comparative evaluation of various segmentation algorithms developed for the purpose of detecting lesions in fundus images. More specifically, there are 1200 fundus images in this dataset, each of which has been labeled with a medical diagnosis. The medical experts have presented two diagnoses for each image, retinopathy grade and risk of DME. It has been determined to classify DR into six levels of severity, four levels of exudation, and three levels of hemorrhage and to specify the number

of microaneurysms for each image.

RIGA (RIGA, 2018) is a dataset including 750 retinal fundus images for glaucoma analysis. The dataset includes the OC and OD ground truth for each image; however, the diagnosis of glaucoma is not provided. ORIGASO (Zhang et al., 2010) consists of 482 and 168 fundus images of healthy and glaucoma, respectively, as well as the segmentation of the disc and cup. This dataset was accessible to the public and downloadable in 2010, but it does not appear to be accessible to the public now.

RIMONE (RIMONE, 2011) first made available to the public in 2011. To test the CDR, 159 stereo fundus images were given in 2015, with two ground truth segmentations of OD and OC. These photos represented healthy individuals and glaucoma patients. The dataset was recently revised and improved for a deep learning context in 2020. The new data set includes 313 and 172 images from healthy and glaucoma patients, respectively.

Drishti-GS (Drishti-GS, 2014) is a dataset including OD and OC segmentation for glaucoma assessment. It is comprised of 101 monocular fundus images (31 normal, 70 glaucoma images), divided into training and test sets, with four segmentation of the OD and OC for the training set.

ACRIMA (Diaz-Pinto et al., 2019) has 705 fundus photos with labels (309 normal and 396 glaucomatous images). Two glaucoma specialists were involved for the annotations, and no other clinical evidence was considered while providing labels for the images.

G1020 (Bajwa et al., 2020) is a huge dataset of retinal fundus images for glaucoma diagnosis, containing 1020 images (724 healthy and 296 glaucoma). There was segmentation of the OD and OC as well as labeling of the images.

REFUGE (REFUGE, 2020) dataset was released, which includes 1200 fundus images annotated with clinical glaucoma diagnoses and ground truth segmentation of the OC and OD.

PAPILA (Kovalyk et al., 2022) dataset includes data from 244 patients (333 health, 155 glaucoma images). Each file contains organized data on a single patient's clinical history, as well as segmentation of the OD and OC in both eyes.

Kaggle Diabetic Retinopathy (Kaggle-DR) (Kaggle-DR, 2015) a total of 88,702 CFPs are available in the dataset, split between 35,126 training samples and 53,576 test samples. EyePACS contributed the images, which were taken using a wide range of devices in a variety of settings at numerous primary care clinics in California and abroad. Images of both the left and right eyes were taken at the same resolution for each individual. Clinicians used the Early Treatment DR Study (ETDRS) scale to assess the severity of DR in each image.

GAMMA (GAMMA, 2021) dataset includes 3D OCT and 2D fundus images from 300 patients. Each image in the dataset was annotated with glaucoma grade, macular fovea coordinates, and an optic disc/cup segmentation mask from the fundus image.

11.2 OCT Datasets

The publicly available OCT datasets are the Zhang Kermany et al. (2018b), Duke-1 Farsiu et al. (2014), Duke-2 Chiu et al. (2015), Duke-3 Srinivasan et al. (2014b), Rabbani Rasti et al. (2017), BIOMISA (Hasan et al., 2018c), and AFIO (Raja et al., 2020a). The table 9 provides an overview of the OCT datasets that are publicly available.

Zhang dataset (Kermany et al., 2018b) dataset is one of the most extensive OCT datasets that are freely accessible to the public. The images were acquired from Spectralis OCT, Heidelberg Engineering, Germany at Beijing Tongren Eye Center, the Shanghai First People's Hospital, the California Retinal Research Foundation, Medical Center Ophthalmology Associates, and the Shiley Eye Institute of the University of California San Diego between 1 July 2013 and 1 March 2017. It has a total of 108,309 OCT images and was primarily developed with the intention of screening for DME, DRUSEN, CNV, and other normal images. Among the total of 109,309 scans analyzed, 51,140 of them exhibit a normal retina, while 11,348 scans indicate the presence of DME symptoms, 8,616 shows DRUSEN, and 37,205 depicts CNV symptoms.

Duke-1 (Farsiu et al., 2014) is consisted of 38400 BScans from 269 AMD patients and 115 normal subjects. Images were collected from the BiopTigen system. Total retina (TR, between the ILM and the inner aspect of Bruch's membrane) mean, and standard deviation maps for individual subjects are also provided in the dataset. In addition to this, the dataset contains the subject-specific mean and standard de-

Table 8: Summarizing the feature of publicly available fundus dataset. The abbreviations are Class Label: Classification Label, N: healthy images, GLA: glaucoma images, MiDR: Mild DR, MDR: Moderate, PDR: Proliferative DR, SER: Severe DR, HEXs: hard exudates, and SOEXs: soft exudates

Dataset	Images	Categories	Diseases	Class Label	Segmentation label
DRIVE DRIVE (2004)	40	-	DR	-	Blood vessels
DIARETDB0 DiaRetDb0 (2007)	130	N:20, DR:110	DR	Yes	MAs, HMs, HEXs, SOEXs
DIARETDB1 DiaRetDb1 (2007)	89	N:5, PDR:84	DR	Yes	MAs, HMs, HEXs, SOEXs
Drions-DB RIONS-DB (2009)	110	-	-	No	ONH
MessidorMessidor (2017)	1200	-	DR, DME	Yes	-
RIGARIGA (2018)	750	-	Glaucoma	Yes	OC, OD
RIMONE RIMONE (2011)	485	N:313, GLA: 172	Glaucoma	Yes	OC, OD
STARESTARE (2000)	400	-	AMD, PDR,CNV	Yes	Blood vessels, artery, optic nerve
Drishti-GS Drishti-GS (2014)	101	N:31, GLA: 70	Glaucoma	Yes	OC, OD
(Kaggle-DR) Kaggle-DR (2015)	35126	N: 25810, MiDR: 2443, MDR: 5292, PDR: 708, SER: 873	DR	Yes	-
ACRIMA Diaz-Pinto et al. (2019)	705	N:309, GLA: 396	Glaucoma	Yes	-
G1020 Bajwa et al. (2020)	1020	N:724, GLA: 296	Glaucoma	Yes	OC, OD
REFUGE REFUGE (2020)	1200	N:1080, GLA: 120	Glaucoma	Yes	OC, OD
PAPILA Kovalyk et al. (2022)	488	N: 333, GLA: 155	Glaucoma	Yes	OC, OD
GAMMA GAMMA (2021)	300	-	Glaucoma	Yes	OC, OD, fovea

viation thickness maps of the RPE and drusen complex.

Duke-2 dataset (Chiu et al., 2015) dataset was created by the Vision and Image Processing (VIP) group at Duke University and is currently accessible to the public. The Duke-II was designed to address DME pathologies of varying severity levels, ranging from mild to moderate to severe. The dataset comprised 610 OCT scans obtained from a cohort of ten subjects diagnosed with DME.

Duke-3 dataset (Srinivasan et al., 2014b) was also created by researchers in Duke University’s VIP lab. Fifteen controls, fifteen participants with dry AMD, and fifteen with DME all underwent volumetric Spectralis SD-OCT scans.

Rabbani dataset (Rasti et al., 2017) consisted of 4,141 OCT images (including 50 normal OCTs, 48 OCTs of dry AMD, and 50 OCTs of DME) that were acquired at Noor Eye Hospital in Tehran. In this data set, the lateral and azimuthal resolutions were not uniform across patients, although the axial resolution is 3.5 m with a scan dimension of 8.9 7.4 mm². Therefore, the number of A-scans varies between 512 and 768 scans, and the number of B-scans per volume varies between 19, 25, 31, and 61.

BIOMISA dataset (Hassan et al., 2018c) was created by the lab at the National University of Science and Technology, Pakistan, for the purpose of investigating retinal layers, lesions, and identifying normal and abnormal retinal conditions like DME, CSR, AMD, and Glaucoma. There are a total of 5,324 scans from 99 people in the dataset, broken down as follows: 657 scans of dry AMD, 2,195 scans of DME, 407 scans of wet AMD, 1,161 scans of CSR, and 904

scans of normal eyes.

AFIO (Raja et al., 2020a) was created by the lab at the National University of Science and Technology, Pakistan; it contains OCT and fundus images. The images were captured using the TOPCON 3D OCT-1000 camera attached to an OCT machine. There are a total of 50 images in the dataset, including both normal and glaucomatous conditions. Each OCT image has an accompanying annotated fundus image. Glaucoma experts provided labels for the CDR measured from fundus images. The optic nerve head (ONH) is the focal point of OCT scans. An ophthalmologist manually annotated the ILM and the RPE.

12 Discussion and Future directions

Researchers are increasingly investigating the genetic and genomic factors that contribute to the development and progression of eye diseases. Advances in genomics and personalized medicine may lead to new diagnostic and therapeutic approaches that can target specific genetic mutations or risk factors. Nanotechnology-based formulations are also gaining popularity. The usage of aqueous gels made from hydrogels is also getting attention for the treatment of a wide range of ocular disorders. The next generation of healthcare professionals needs to be trained to address SDOH in clinical care to improve clinical outcomes.

We have reviewed the most commonly used imaging technologies, which include CFP, FA, FAF, OCT, and OCTA, for detecting different ocular disorders. FA (Fluorescein Angiography) is an invasive technique that employs an intravenous dye injection to capture dynamic images of retinal circulation, blood flow, and leakage. FAF (Fundus Autofluorescence) detects natural autofluorescence emitted by molecules in the

Table 9: A detailed summary of the publicly available OCT datasets, Zhang (Kermany et al., 2018b), Duke-1 (Farsi et al., 2014), Duke-2 (Chiu et al., 2015), Duke-3 (Srinivasan et al., 2014b), Rabbani (Rasti et al., 2017), BIOMISA (Hassan et al., 2018c), and AFIO (Raja et al., 2020a)

Dataset	Scanner	Label	Total Scans	Subjects	Drusen	DME	Normal	CNV	CSR	Glaucoma
Zhang	Spectralis	Yes	109,309	-	8,866	11,598	51,390	37,455	-	-
Duke-1	Bioptigen	No	38,400	384	26,900	-	11,500	-	-	-
Duke-2	Spectralis	No	610	10	-	610	-	-	-	-
Duke-3	Spectralis	No	3,231	45	723	1,101	1,407	-	-	-
Rabbani	Spectralis	No	4,142	148	969	862	2,311	-	-	-
BIOMISA	Topcon	No	5,324	99	657	2,195	904	407	1,161	-
AFIO	Topcon	Yes	50	26	-	-	18	-	-	32

retinal pigment epithelium (RPE) to assess metabolic health and RPE integrity. These imaging modalities are valuable for diagnosing and monitoring a range of retinal diseases, including vascular disorders and RPE-related conditions. CFP is a non-invasive that takes pictures of the inside of the eye, including the retina, optic disc, and blood vessels. Fundus imaging provides a wide-angle view of the retina, making it useful for general screening and documenting retinal diseases. Fundus scans are very good at detecting significant changes in the retina, but they may not be able to see small changes. However, OCT is a non-invasive imaging technique that provides 3D structural analysis of the retina. OCT scans have higher resolution than fundus photographs, which means that we can analyze more minor changes in the retina. OCT's higher spatial resolution enables earlier detection of eye diseases when treatment is more likely to be efficacious. OCT technique can be used to diagnose and monitor a variety of eye diseases, such as DR, AMD, DME, and glaucoma. OCTA is also gaining popularity, it provides visualization of retinal and choroidal blood flow and microvascular networks by combining OCT with motion contrast technique. It allows for depth-resolved imaging, enabling the assessment of both superficial and deep retinal vasculature, perfusion patterns, identification of vascular abnormalities, and evaluation of capillary networks without the need for invasive dye injection or contrast agents. OCTA does not require the use of dye injection, making it more comfortable for patients and reducing the potential risks associated with invasive procedures. OCTA imaging can be repeated over time, allowing for a longitudinal analysis of changes in retinal blood flow. It also offers the potential for quantitative analysis, enabling the measurement of parameters such as vessel density and blood flow velocity. OCTA is often used to diagnose and monitor eye diseases such as diabetic retinopathy and macular edema. It's important to note that while OCTA has these advantages, it does not replace the structural information provided by OCT.

Both imaging modalities have their unique strengths and applications, and they are often used together to provide a comprehensive assessment of retinal health. The choice between OCT and OCTA depends on the specific clinical question and the information needed for diagnosis and management. Fundus photography is currently widely employed by an ophthalmologist. Still, it is less commonly used than OCT and OCTA because it produces 2D scans that don't provide as much detailed information about the retina. FA is also still widely used, but it is less commonly used than OCT and OCTA because it is more invasive. FAF is not as widely used as the other techniques because it does not provide as much information about the retina and blood vessels. The choice of imaging modality depends on the specific clinical question, the suspected condition, and the expertise of the health-care professional. In many cases, multiple imaging modalities may be used in combination to provide a more comprehensive assessment of the retina and its associated structures. However, the limited availability of ophthalmologists and constrained accessibility to retinal image-capturing systems in developing nations hinder the timely identification of glaucoma. Current trends indicate a shift towards mobile-assisted screening systems for the detection of ocular diseases, as they offer greater cost-effectiveness and durability.

The identification and quantification of various biomarkers are required for the diagnosis and progression tracking of ocular diseases. Manual segmentation can offer high accuracy when performed by experienced specialists. They can precisely outline the boundaries of retinal lesions and differentiate them from normal tissues. However, manual segmentation is subjective and can vary among different observers. Automated detection algorithms, on the other hand, can provide consistent and reproducible results, reducing inter-observer variability. Manual segmentation can be time-consuming and labor-intensive, especially for large datasets or complex cases. Automated detection algorithms can process images rapidly, providing

efficient and time-saving solutions for screening or large-scale analysis. Automated methods also allow for the potential integration of telemedicine and remote screening programs, improving access to care. The integration of manual segmentation into routine clinical practice can be challenging due to the time and expertise required. Automated detection algorithms can be integrated into existing imaging systems, facilitating their implementation in clinical workflows and making them more accessible for wider usage. However, automated methods may have some false positives or false negatives, their performance has been improving with advancements in AI. Numerous automated studies have been published exploring the utility of fundus photography and OCT in diagnosing and monitoring various ocular conditions. It was witnessed that a substantial number of published studies focusing on fundus studies compared to OCT studies. Figure 15 presents the number of studies found in the literature concerning both OCT and fundus imaging for detecting ocular diseases, highlighting the comprehensive research conducted in these complementary imaging modalities. There is a large number of studies presented in the literature that identified the significant biomarkers and performed diagnosis of ocular disorders with high accuracy. The main areas of concern in fundus images analysis are inconsistent image quality, blurry or otherwise unclear backgrounds, and pixels that seem like blood vessels. Fundus image analysis is expanding into new research areas, including multimodal imaging fusion, combining genetic and clinical data, longitudinal studies, and incorporating other medical imaging modalities. These areas provide opportunities for further advancements and exploration. While research advancements are promising, the translation of fundus image analysis algorithms into clinical practice and widespread adoption may still be limited. Integration with existing healthcare systems and addressing regulatory and ethical considerations are crucial for practical implementation. OCT analysis is complex, as the images can be affected by various artifacts, such as motion artifacts caused by patient movement during the scan, shadowing artifacts due to tissue irregularities or structures in the path of the OCT beam, speckle noise, and axial or lateral resolution limitations. Correcting or mitigating these artifacts requires advanced algorithms and techniques.

In this comprehensive review, we thoroughly examined the utilization of digital image processing, classic machine learning, and deep learning techniques in the segmentation of retinal lesions and the classification of ocular diseases. Figure 16 illustrates the distribution of different techniques employed in retinal analysis, specif-

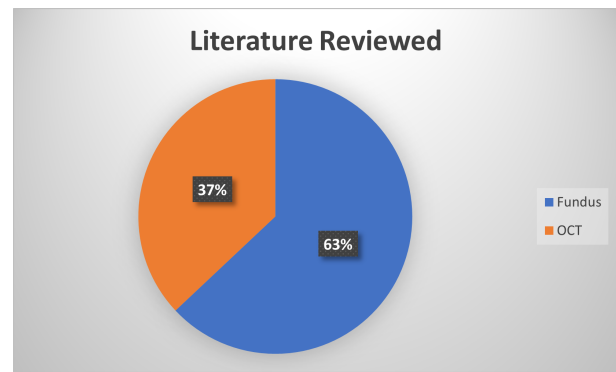


Fig. 15: Distribution of fundus and OCT studies reviewed in this survey. Fundus-related studies have a higher publication frequency compared to studies based on OCT analysis.

ically digital image processing (DIP), classic machine learning (CML), and DL methods. It visually represents the shift in the prominence of these techniques over time, with DL techniques gaining increasing popularity in recent years. We explored the advancements in each approach, highlighting their strengths and limitations. One of the limitations of image processing techniques is that they require manual parameter tuning, which can be time-consuming and subjective. The selection of appropriate parameters may vary across datasets and researchers, leading to potential inconsistencies in the analysis. Image processing methods may not adapt well to variations in image quality, such as variations in contrast, illumination, or noise characteristics. These techniques often rely on predefined rules or assumptions that may not be universally applicable. Image processing techniques may struggle to handle complex cases, such as overlapping or intertwined structures, subtle abnormalities, or cases with severe ocular pathologies. So, ML-based techniques have gained popularity, but they have limitations in terms of manual feature engineering, which can be time-consuming and may not capture all relevant information in complex domains like retinal analysis. Furthermore, CML models may struggle with generalization to unseen or diverse data, leading to decreased performance in real-world scenarios. Additionally, CML algorithms are sensitive to the choice of hyperparameters and can be prone to overfitting if the model complexity is not properly controlled. In recent years, deep learning (DL) has emerged as a dominant force in the field of retinal analysis, surpassing other machine learning (ML) techniques in popularity and performance. One major advantage is DL's ability to automatically learn hierarchical representations from raw data, eliminating the need for manual feature engineering. Additionally, DL models can be trained end-to-end, allowing them to learn the entire task directly from

input to output, without relying on intermediate steps or handcrafted rules. This streamlines the training and inference processes, making DL models more efficient. Furthermore, DL models have demonstrated superior scalability and performance for the segmentation and classification of retinal lesions. With ongoing advancements in the field of retinal analysis, DL is poised to revolutionize the future of diagnosis, treatment, and monitoring of retinal diseases, offering transformative potential for improved patient care and outcomes. Areas of focus include multi-modality fusion for a comprehensive understanding of retinal pathologies, real-time applications for timely diagnosis, transfer learning and domain adaptation for improved generalization, integration with electronic health records for personalized medicine, uncertainty estimation for risk assessment, and collaborative/federated learning for robust and secure analysis. These advancements have the potential to revolutionize retinal analysis, leading to better diagnosis, personalized treatment, and improved patient outcomes.

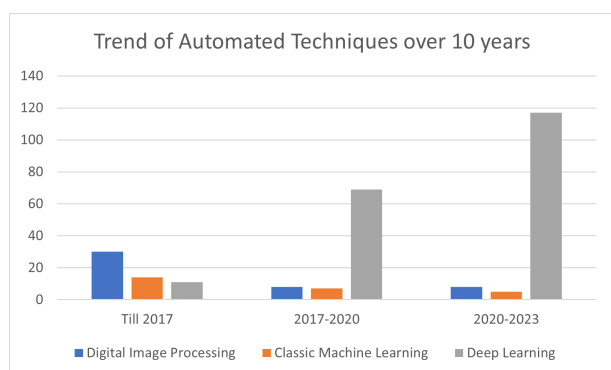


Fig. 16: The chart illustrates the transformative trend in automated techniques over the last decade, showcasing the shift from traditional image processing methods to the adoption and prominence of deep learning approaches. It highlights the increasing reliance on deep learning algorithms for tasks such as the identification, quantification, and classification of biomarkers for various retinal diseases.

Early detection and appropriate treatment are crucial for preserving vision and halting the progression of diseases. This review highlights the current trends in both clinical and technical domains regarding the detection of significant biomarkers for retinal diseases such as diabetic retinopathy (DR), diabetic macular edema (DME), age-related macular degeneration (AMD), and glaucoma. Imaging techniques utilized for the identification, diagnosis, and management of

these diseases were also reviewed. Fundus imaging, optical coherence tomography (OCT), OCT angiography (OCTA), fundus autofluorescence (FAF), and fluorescein angiography (FA) are the most widely employed imaging techniques. Fundus imaging is commonly used for screening, while OCT modalities are preferred for diagnosis and monitoring disease progression. Angiography is gaining popularity in clinical practice for generating 3D angiograms to visualize retinal and choroidal vasculature pathologies. Each technique has its advantages and disadvantages, and the choice depends on the specific eye disease and the healthcare professional's judgment. Portable devices are also gaining attention due to the limited ophthalmologist-to-patient ratio, particularly in rural and developing areas. Research is now focused on enhancing the performance and robustness of these portable devices. Exciting directions in the field include adaptive optics, genetics and genomics, and telemedicine. Deep learning (DL) has emerged as a powerful approach, surpassing traditional methods by automatically learning complex features from data, resulting in improved accuracy and robust analysis of retinal images. However, it is important to note that digital image processing techniques are still relevant and can complement advanced analysis approaches like machine learning (ML) or DL by serving as a preprocessing step or providing feature extraction. Combining different techniques can leverage their strengths and mitigate limitations, leading to a more accurate and robust fundus and OCT image analysis.

Acknowledgements

This work has been funded by Khalifa University, Ref: CIRA-2021-052, and ASPIRE, Ref: AARE-2020

Statements and Declarations

All the authors declare that there are no competing interests related to this article.

References

- (2019 (accessed Nov 25, 2022)) A crowdsourcing platform for labeling fundus images. <https://www.labelme.org/>.
- (2019 (accessed Nov 5, 2020)) The structure of the human eye. <https://www.anatomynote.com/human-anatomy/ophthalmology-eye-anatomy/the-structure-of-the-human-eye/>.

- (2020 (accessed December 24, 2020)) Blindness and visual impairment. <https://www.who.int/westernpacific/health-topics/blindness-and-vision-loss>
- (2022 (accessed Jan 25, 2022)) Fundus photography overview. <https://www.opsweb.org/page/fundusphotography>.
- (2022 (accessed Jan 25, 2023)) Fundus photography: What you need to know. <https://eyesoneyecare.com/resources/fundus-photography/>.
- ((accessed Dec 12, 2020)) Glaucoma. <https://www.mayoclinic.org/diseases-conditions/glaucoma/symptoms-causes/syc-20372839>.
- Abdel-Hamid L (2022) Tweec: Computer-aided glaucoma diagnosis from retinal images using deep learning techniques. *International Journal of Imaging Systems and Technology* 32(1):387–401
- Abdellatif MK, Elzankalony YAM, Ebeid AAA, Ebeid WM (2019) Outer retinal layers' thickness changes in relation to age and choroidal thickness in normal eyes. *Journal of Ophthalmology* 2019:1–8, DOI 10.1155/2019/1698967
- Abdullah F, Imtiaz R, Madni HA, Khan HA, Khan TM, Khan MA, Naqvi SS (2021) A review on glaucoma disease detection using computerized techniques. *IEEE Access* 9:37,311–37,333
- Abhishek AM, Berendschot TT, Rao SV, Dabir S (2014) Segmentation and analysis of retinal layers (ilm & rpe) in optical coherence tomography images with edema. In: 2014 IEEE Conference on Biomedical Engineering and Sciences (IECBES), IEEE, pp 204–209
- Aboobakar IF, Wiggs JL (2022) The genetics of glaucoma: Disease associations, personalised risk assessment and therapeutic opportunities-a review. *Clinical & Experimental Ophthalmology* 50(2):143–162
- Abraham JR, Wykoff CC, Arepalli S, Lunasco L, Hannah JY, Hu M, Reese J, Srivastava SK, Brown DM, Ehlers JP (2021) Aqueous cytokine expression and higher order oct biomarkers: Assessment of the anatomic-biologic bridge in the imagine dme study. *American Journal of Ophthalmology* 222:328–339
- Abramoff MD, Garvin MK, Sonka M (2010) Retinal imaging and image analysis. *IEEE Reviews in Biomedical Engineering* 3:169–208, DOI 10.1109/RBME.2010.2084567
- Adak C, Karkera T, Chattopadhyay S, Saqib M (2023) Detecting severity of diabetic retinopathy from fundus images using ensembled transformers. *arXiv preprint arXiv:230100973*
- Adam Z, Freddy N, LOldenburg O, Marks ML, Boppart BA (2007) Optical coherence tomography: a review of clinical development from bench to bedside. *J Biomed Opt* 12(5):051,403, DOI 10.1117/1.2793736
- Ahn JM, Kim S, Ahn KS, Cho SH, Lee KB, Kim US (2018) A deep learning model for the detection of both advanced and early glaucoma using fundus photography. *PloS one* 13(11):e0207,982
- Akram MU, Khalid S, Khan SA (2013) Identification and classification of microaneurysms for early detection of diabetic retinopathy. *Pattern recognition* 46(1):107–116
- Akram MU, Khalid S, Tariq A, Khan SA, Azam F (2014a) Detection and classification of retinal lesions for grading of diabetic retinopathy. *Computers in biology and medicine* 45:161–171
- Akram MU, Tariq A, Khan SA, Javed MY (2014b) Automated detection of exudates and macula for grading of diabetic macular edema. *Computer methods and programs in biomedicine* 114(2):141–152
- Akram MU, Tariq A, Khalid S, Javed MY, Abbas S, Yasin UU (2015) Glaucoma detection using novel optic disc localization, hybrid feature set and classification techniques. *Australasian physical & engineering sciences in medicine* 38(4):643–655
- Aksoy F, Altan C, Yilmaz B, Yilmaz I, Tunç U, Kesim C, Kocamaz M, Pasaoglu I (2020) A comparative evaluation of segmental analysis of macular layers in patients with early glaucoma, ocular hypertension, and healthy eyes. *Journal Français d'Ophthalmologie* 43(9):869–878
- Akulo KA, Adali T, Moyo MTG, Bodamyali T (2022) Intravitreal injectable hydrogels for sustained drug delivery in glaucoma treatment and therapy. *Polymers* 14(12):2359
- Al-Bander B, Williams BM, Al-Nuaimy W, Al-Tae MA, Pratt H, Zheng Y (2018) Dense fully convolutional segmentation of the optic disc and cup in colour fundus for glaucoma diagnosis. *Symmetry* 10(4):87
- Al Mamun A, Mimi AA, Zaeem M, Wu Y, Monalisa I, Akter A, Munir F, Xiao J (2021) Role of pyroptosis in diabetic retinopathy and its therapeutic implications. *European journal of pharmacology* 904:174,166
- Alam MN, Yamashita R, Ramesh V, Prabhune T, Lim JI, Chan RVP, Hallak J, Leng T, Rubin D (2022) Contrastive learning-based pretraining improves representation and transferability of diabetic retinopathy classification models. *arXiv preprint arXiv:220811563*
- Alhasson HF, Alharbi SS, Obara B (2018) 2d and 3d vascular structures enhancement via multiscale fractional anisotropy tensor. In: *Proceedings of the European Conference on Computer Vision (ECCV) Workshops*, pp 0–0

- Alhussein M, Aurangzeb K, Haider SI (2020) An unsupervised retinal vessel segmentation using hes-sian and intensity based approach. *IEEE Access* 8:165,056–165,070
- Ali A, Hussain A, Zaki WMDW (2017) Vessel extrac-tion in retinal images using automatic threshold-ing and gabor wavelet. In: 2017 39th Annual In-ternational Conference of the IEEE Engineering in Medicine and Biology Society (EMBC), IEEE, pp 365–368
- Amini Z, Rabbani H (2016) Classification of medical image modeling methods: A review. *Current Medical Imaging* 12(2):130–148
- An G, Omodaka K, Hashimoto K, Tsuda S, Shiga Y, Takada N, Kikawa T, Yokota H, Akiba M, Nakazawa T (2019) Glaucoma diagnosis with machine learn-ing based on optical coherence tomography and color fundus images. *Journal of Healthcare Engineering* 2019:1–9, DOI 10.1155/2019/4061313
- Andrade JCF, Kanadani FN, Furlanetto RL, Lopes FS, Ritch R, Prata TS (2022) Elucidation of the role of the lamina cribrosa in glaucoma using opti-cal coherence tomography. *Survey of Ophthalmology* 67(1):197–216
- Araki T, Ishikawa H, Iwahashi C, Niki M, Mitamura Y, Sugimoto M, Kondo M, Kinoshita T, Nishi T, Ueda T, et al. (2019) Central serous chorioretinopathy with and without steroids: A multicenter survey. *PloS One* 14(2):e0213,110
- Asefa NG, Kamali Z, Pereira S, Vaez A, Jansonius N, Bergen AA, Snieder H (2022) Bioinformatic priori-tization and functional annotation of gwas-based can-didate genes for primary open-angle glaucoma. *Genes* 13(6):1055
- Asgari R, Orlando JJ, Waldstein S, Schlanitz F, Baratsits M, Schmidt-Erfurth U, Bogunović H (2019) Mul-ticlass segmentation as multitask learning for drusen segmentation in retinal optical coherence tomogra-phy. In: International Conference on Medical Im-age Computing and Computer-Assisted Intervention, Springer, pp 192–200
- Ashanand, Kaur M (2022) Efficient retinal image en-hancement using morphological operations. *Biomed-ical Engineering: Applications, Basis and Communi-cations* p 2250033
- Aspberg J, Heijl A, Bengtsson B (2021) Screening for open-angle glaucoma and its effect on blindness. *American Journal of Ophthalmology* 228:106–116
- Asrani S, Bacharach J, Holland E, McKee H, Sheng H, Lewis RA, Kopczynski CC, Heah T (2020) Fixed-dose combination of netarsudil and latanoprost in oc-ular hypertension and open-angle glaucoma: pooled efficacy/safety analysis of phase 3 mercury-1 and-2. *Advances in therapy* 37(4):1620–1631
- Azzopardi G, Petkov N (2013) Automatic detection of vascular bifurcations in segmented retinal images us-ing trainable cosfire filters. *Pattern Recognition Let-ters* 34(8):922–933
- Babu TG, Devi SS, Venkatesh R (2012) Automatic de-tection of glaucoma using optical coherence tomogra-phy image. *Journal of Applied Sciences* 12(20):2128–2138, DOI 10.3923/jas.2012.2128.2138
- Badar M, Haris M, Fatima A (2020) Application of deep learning for retinal image analysis: A review. *Com-puter Science Review* 35:100,203
- Baghaie A, Yu Z, D’Souza RM (2015) State-of-the-art in retinal optical coherence tomography image anal-ysis. *Quantitative imaging in medicine and surgery* 5(4):603
- Bajwa MN, Singh GAP, Neumeier W, Malik MI, Den-gel A, Ahmed S (2020) G1020: A benchmark retinal fundus image dataset for computer-aided glaucoma detection. In: 2020 International Joint Conference on Neural Networks (IJCNN), IEEE, pp 1–7
- Bala A, Maik V, et al. (2021a) Contrast and lumi-nance enhancement technique for fundus images us-ing bi-orthogonal wavelet transform and bilateral fil-ter. *ECS Journal of Solid State Science and Technol-ogy* 10(7):071,010
- Bala MP, Rajalakshmi P, Sindhuja AM, Naganandhini S (2021b) A review on recent development for diag-nosis of glaucoma. *Annals of the Romanian Society for Cell Biology* pp 2723–2736
- Bastelica P, Labbé A, El Maftouhi A, Hamard P, Paques M, Baudouin C (2022) Role of the lamina cribrosa in the pathogenesis of glaucoma. a review of the literature. *Journal Francais D’ophthalmologie* pp S0181–5512
- Bhandari S, Vitale S, Agrón E, Clemons TE, Chew EY, Study ARED, Group R (2022) Cataract surgery and the risk of developing late age-related macular de-generation: the age-related eye disease study 2 report number 27. *Ophthalmology* 129(4):414–420
- Bhimavarapu U, Battineni G (2023) Deep learning for the detection and classification of diabetic retinopa-thy with an improved activation function. In: Health-care, Multidisciplinary Digital Publishing Institute, vol 11, p 97
- Bhisitkul R, Klier S, Tsuruda P, Xie B, Masaki L, Bautista J, Khan A, Dananberg J (2022) Ubx1325, a novel senolytic treatment for patients with ad-vanced dme or wet amd: 24-week results of a phase 1 study. *Investigative Ophthalmology & Visual Science* 63(7):4287–4287
- Bindewald-Wittich A, Dolar-Szczasny J, Kuenzel SH, von der Emde L, Pfau M, Rejdak R, Schmitz-

- Valckenberg S, Ach T, Dreyhaupt J, Holz FG (2023) Blue-light fundus autofluorescence imaging of pigment epithelial detachments. *Eye* 37(6):1191–1201
- Bisneto TRV, de Carvalho Filho AO, Magalhães DMV (2020) Generative adversarial network and texture features applied to automatic glaucoma detection. *Applied Soft Computing* 90:106,165
- Boned-Murillo A, Albertos-Arranz H, Diaz-Barreda MD, Sánchez-Cano A, Ferreras A, Cuenca N, Pinilla I, et al. (2022) Optical coherence tomography angiography in diabetic patients: A systematic review. *Biomedicines* 10(1):88
- Borkovkina S, Camino A, Janponsri W, Sarunic MV, Jian Y (2020) Real-time retinal layer segmentation of oct volumes with gpu accelerated inferencing using a compressed, low-latency neural network. *Biomedical optics express* 11(7):3968–3984
- Boudegga H, Elloumi Y, Akil M, Bedoui MH, Kachouri R, Abdallah AB (2021) Fast and efficient retinal blood vessel segmentation method based on deep learning network. *Computerized Medical Imaging and Graphics* 90:101,902
- Bowd C, Zangwill LM, Weinreb RN, Medeiros FA, Belghith A (2017) Estimating optical coherence tomography structural measurement floors to improve detection of progression in advanced glaucoma. *American journal of ophthalmology* 175:37–44
- Boyd K (Sep 2020 (accessed Nov 9, 2020)) Who is at risk for glaucoma? <https://www.aaio.org/eye-health/diseases/glaucoma-risk>.
- Brubaker JW, Teymoorian S, Lewis RA, Usner D, McKee HJ, Ramirez N, Kopczynski CC, Heah T (2020) One year of netarsudil and latanoprost fixed-dose combination for elevated intraocular pressure: phase 3, randomized mercury-1 study. *Ophthalmology Glaucoma* 3(5):327–338
- Bu Y, Shih KC, Tong L (2022) The ocular surface and diabetes, the other 21st century epidemic. *Experimental Eye Research* p 109099
- Budak Ü, Cömert Z, Çibuk M, Şengür A (2020) Dccmed-net: Densely connected and concatenated multi encoder-decoder cnns for retinal vessel extraction from fundus images. *Medical Hypotheses* 134:109,426
- Butola A, Prasad DK, Ahmad A, Dubey V, Qaiser D, Srivastava A, Senthilkumaran P, Ahluwalia BS, Mehta DS (2020) Deep learning architecture “lightoct” for diagnostic decision support using optical coherence tomography images of biological samples. *Biomedical Optics Express* 11(9):5017–5031
- Butt MM, Iskandar DA, Abdelhamid SE, Latif G, Alghazo R (2022) Diabetic retinopathy detection from fundus images of the eye using hybrid deep learning features. *Diagnostics* 12(7):1607
- Campbell J, Zhang M, Hwang T, Bailey S, Wilson D, Jia Y, Huang D (2017) Detailed vascular anatomy of the human retina by projection-resolved optical coherence tomography angiography. *Scientific reports* 7(1):42,201
- Cao D, Leong B, Messinger JD, Kar D, Ach T, Yannuzzi LA, Freund KB, Curcio CA (2021) Hyperreflective foci, optical coherence tomography progression indicators in age-related macular degeneration, include transdifferentiated retinal pigment epithelium. *Investigative ophthalmology & visual science* 62(10):34–34
- Cao P, Hou Q, Song R, Wang H, Zaiane O (2022a) Collaborative learning of weakly-supervised domain adaptation for diabetic retinopathy grading on retinal images. *Computers in Biology and Medicine* 144:105,341
- Cao X, Lu M, Xie RR, Song LN, Yang WL, Xin Z, Yang GR, Yang JK (2022b) A high tsh level is associated with diabetic macular edema: a cross-sectional study of patients with type 2 diabetes mellitus. *Endocrine Connections* 11(7)
- Cazañas-Gordón A, da Silva Cruz LA (2022) Multiscale attention gated network (magnet) for retinal layer and macular cystoid edema segmentation. *IEEE Access* 10:85,905–85,917
- Chauhan MZ, Rather PA, Samarah SM, Elhusseiny AM, Sallam AB (2022) Current and novel therapeutic approaches for treatment of diabetic macular edema. *Cells* 11(12):1950
- Chen D, Yang W, Wang L, Tan S, Lin J, Bu W (2022a) Pcat-unet: Unet-like network fused convolution and transformer for retinal vessel segmentation. *Plos one* 17(1):e0262,689
- Chen H, Wang M, Xia L, Dong J, Xu G, Wang Z, Feng L, Zhou Y (2022b) New evidence of central nervous system damage in diabetes mellitus: Impairment of fine visual discrimination. *Diabetes*
- Chen J, Luo SF, Yuan X, Wang M, Yu HJ, Zhang Z, Yang YY (2022c) Diabetic kidney disease-predisposing proinflammatory and profibrotic genes identified by weighted gene co-expression network analysis (wgcn). *Journal of Cellular Biochemistry* 123(2):481–492
- Chen S, Ma D, Lee S, Yu TT, Xu G, Lu D, Popuri K, Ju MJ, Sarunic MV, Beg MF (2022d) Segmentation-guided domain adaptation and data harmonization of multi-device retinal optical coherence tomography using cycle-consistent generative adversarial networks. *arXiv preprint arXiv:220814635*
- Chen TC (2009) Spectral domain optical coherence tomography in glaucoma: qualitative and quantitative analysis of the optic nerve head and retinal nerve

- fiber layer (an aos thesis). Transactions of the American Ophthalmological Society 107:254
- Chen Z, Zheng X, Shen H, Zeng Z, Liu Q, Li Z (2019) Combination of enhanced depth imaging optical coherence tomography and fundus images for glaucoma screening. *Journal of Medical Systems* 43(6), DOI 10.1007/s10916-019-1303-8
- Chin MH (2016) Creating the business case for achieving health equity. *Journal of General Internal Medicine* 31(7):792–796
- Chiu SJ, Allingham MJ, Mettu PS, Cousins SW, Izatt JA, Farsiu S (2015) Kernel regression based segmentation of optical coherence tomography images with diabetic macular edema. *Biomedical optics express* 6(4):1172–1194
- Cho YK, Lee SM, Kang YJ, Kang YM, Jeon IC, Park DH (2022) The age-related macular degeneration (amd)-preventing mechanism of natural products. *Processes* 10(4):678
- Choquet H, Khawaja AP, Jiang C, Yin J, Melles RB, Glymour MM, Hysi PG, Jorgenson E (2022) Association between myopic refractive error and primary open-angle glaucoma: A 2-sample mendelian randomization study. *JAMA ophthalmology*
- Chou R, Selph S, Blazina I, Bougatsos C, Jungbauer R, Fu R, Grusing S, Jonas DE, Tehrani S (2022) Screening for glaucoma in adults: updated evidence report and systematic review for the us preventive services task force. *JAMA* 327(20):1998–2012
- Chua SY, Warwick A, Peto T, Balaskas K, Moore AT, Reisman C, Desai P, Lotery AJ, Dhillon B, Khaw PT, et al. (2022) Association of ambient air pollution with age-related macular degeneration and retinal thickness in uk biobank. *British Journal of Ophthalmology* 106(5):705–711
- Cohn AC, Wu Z, Jobling AI, Fletcher EL, Guymer RH (2021) Subthreshold nano-second laser treatment and age-related macular degeneration. *Journal of clinical medicine* 10(3):484
- Crick RP, Khaw PT (2003) *Textbook Of Clinical Ophthalmology, A: A Practical Guide To Disorders Of The Eyes And Their Management*. World Scientific Publishing Company
- Csaky K, Curcio CA, Mullins RF, Rosenfeld PJ, Fujimoto J, Rohrer B, Ribero R, Malek G, Waheed N, Guymer R, et al. (2022) New approaches to the treatment of age-related macular degeneration (amd). *Experimental Eye Research* p 109134
- Cui QN, Stein LM, Fortin SM, Hayes MR (2022) The role of glia in the physiology and pharmacology of glucagon-like peptide-1: implications for obesity, diabetes, neurodegeneration and glaucoma. *British Journal of Pharmacology* 179(4):715–726
- Czerpak C, Ling YTT, Jefferys JL, Quigley HA, Nguyen TD (2021) The curvature and collagen network of the human lamina cribrosa in glaucoma and control eyes. *Investigative Ophthalmology & Visual Science* 62(8):1656–1656
- Czerpak CA, Kashaf MS, Zimmerman BK, Quigley HA, Nguyen TD (2022) The strain response to intraocular pressure decrease in the lamina cribrosa of glaucoma patients. *Ophthalmology Glaucoma*
- Das S, Malathy C (2018) Survey on diagnosis of diseases from retinal images. In: *Journal of Physics: Conference Series*, IOP Publishing, vol 1000, p 012053
- Das T, Aurora A, Chhablani J, Giridhar A, Kumar A, Raman R, Nagpal M, Narayanan R, Natarajan S, Ramasamay K, et al. (2016) Evidence-based review of diabetic macular edema management: Consensus statement on indian treatment guidelines. *Indian Journal of Ophthalmology* 64(1):14
- Das V, Dandapat S, Bora PK (2020a) A data-efficient approach for automated classification of oct images using generative adversarial network. *IEEE Sensors Letters* 4(1):1–4
- Das V, Dandapat S, Bora PK (2020b) Unsupervised super-resolution of oct images using generative adversarial network for improved age-related macular degeneration diagnosis. *IEEE Sensors Journal* 20(15):8746–8756
- De Fauw J, Ledsam JR, Romera-Paredes B, Nikolov S, Tomasev N, Blackwell S, Askham H, Glorot X, O'Donoghue B, Visentin D, et al. (2018) Clinically applicable deep learning for diagnosis and referral in retinal disease. *Nature medicine* 24(9):1342–1350
- Deepa V, Kumar CS, Cherian T (2022) Ensemble of multi-stage deep convolutional neural networks for automated grading of diabetic retinopathy using image patches. *Journal of King Saud University-Computer and Information Sciences* 34(8):6255–6265
- Delori FC, Dorey CK, Staurenghi G, Arend O, Goger DG, Weiter JJ (1995) In vivo fluorescence of the ocular fundus exhibits retinal pigment epithelium lipofuscin characteristics. *Investigative ophthalmology & visual science* 36(3):718–729
- Deng X, Ye J (2022) A retinal blood vessel segmentation based on improved d-mnet and pulse-coupled neural network. *Biomedical Signal Processing and Control* 73:103,467
- Devalla SK, Renukanand PK, Sreedhar BK, Subramanian G, Zhang L, Perera S, Mari J, Chin KS, Tun TA, Strouthidis NG, Aung T, Thiéry AH, Girard MJA (2018) DRUNET: a dilated-residual u-net deep learning network to segment optic nerve head tissues in optical coherence tomography images. *Biomedical Optics Express* 9(7):3244, DOI 10.1364/boe.9.003244

- DiaRetDb0 (2007) Diaretddb0: Standard diabetic retinopathy database calibration level 0. <https://www.medicmind.tech/retinal-image-databases>
- DiaRetDb1 (2007) Diaretddb1: Standard diabetic retinopathy database calibration level 1. . <https://www.medicmind.tech/retinal-image-databases>
- Diaz V (2021 (accessed May 22, 2022)) The 4 stages of diabetic retinopathy. <https://www.healthline.com/health/diabetes/diabetic-retinopathy-stages#stages>
- Diaz-Pinto A, Morales S, Naranjo V, Köhler T, Mossi JM, Navea A (2019) Cnns for automatic glaucoma assessment using fundus images: an extensive validation. *Biomedical engineering online* 18(1):1–19
- Dieter C, Lemos NE, Corrêa NRDF, Assmann TS, Crispim D (2021) The impact of lncrnas in diabetes mellitus: a systematic review and in silico analyses. *Frontiers in endocrinology* 12:602,597
- Domalpally A, Xing B, Pak JW, Agron E, Ferris III FL, Clemons TE, Chew EY (2022) Extramacular drusen and progression of age-related macular degeneration (amd); age-related eye disease study 2 report 30. *Ophthalmology Retina*
- Doshi N, Oza U, Kumar P (2020) Diabetic retinopathy classification using downscaling algorithms and deep learning. In: 2020 7th International Conference on Signal Processing and Integrated Networks (SPIN), IEEE, pp 950–955
- Drishti-GS (2014) Drishti-gs database. <http://cvit.iiit.ac.in/projects/mip/drishti-gs/mip-dataset2/Home.php>.
- DRIVE (2004) Drive: Digital retinal images for vessel extraction. <https://drive.grand-challenge.org/>
- Duan W, Zheng Y, Ding Y, Hou S, Tang Y, Xu Y, Qin M, Wu J, Shen D, Bi H (2018) A generative model for OCT retinal layer segmentation by group-wise curve alignment. *IEEE Access* 6:25,130–25,141, DOI 10.1109/access.2018.2825397
- Elloumi Y, Akil M, Kehtarnavaz N (2018) A mobile computer aided system for optic nerve head detection. *Computer methods and programs in biomedicine* 162:139–148
- Elloumi Y, Mbarek MB, Boukadida R, Akil M, Bedoui MH (2021) Fast and accurate mobile-aided screening system of moderate diabetic retinopathy. In: Thirteenth International Conference on Machine Vision, SPIE, vol 11605, pp 232–240
- Elmoufidi A, Ammoun H (2023) Diabetic retinopathy prevention using efficientnetb3 architecture and fundus photography. *SN Computer Science* 4(1):1–9
- Elsharkawy M, Elrazzaz M, Sharafeldeen A, Alhalabi M, Khalifa F, Soliman A, Elnakib A, Mahmoud A, Ghazal M, El-Daydamony E, et al. (2022) The role of different retinal imaging modalities in predicting progression of diabetic retinopathy: A survey. *Sensors* 22(9):3490
- Eton EA, Newman-Casey PA (2022) A call for health equity in diabetic care to improve eye health. *JAMA ophthalmology*
- Fang L, Cunefare D, Wang C, Guymer RH, Li S, Farsiu S (2017) Automatic segmentation of nine retinal layer boundaries in OCT images of non-exudative AMD patients using deep learning and graph search. *Biomedical Optics Express* 8(5):2732, DOI 10.1364/boe.8.002732
- Fang L, Wang C, Li S, Rabbani H, Chen X, Liu Z (2019) Attention to lesion: Lesion-aware convolutional neural network for retinal optical coherence tomography image classification. *IEEE transactions on medical imaging* 38(8):1959–1970
- Fang T, Su R, Xie L, Gu Q, Li Q, Liang P, Wang T (2015) Retinal vessel landmark detection using deep learning and hessian matrix. In: 2015 8th International Congress on Image and Signal Processing (CISP), IEEE, pp 387–392
- Farshad A, Yeganeh Y, Gehlbach P, Navab N (2022) Y-net: A spatio-spectral dual-encoder network for medical image segmentation. In: Medical Image Computing and Computer Assisted Intervention—MICCAI 2022: 25th International Conference, Singapore, September 18–22, 2022, Proceedings, Part II, Springer, pp 582–592
- Farsiu S, Chiu SJ, O’Connell RV, Folgar FA, Yuan E, Izatt JA, Toth CA, Group AREDSASDOCTS, et al. (2014) Quantitative classification of eyes with and without intermediate age-related macular degeneration using optical coherence tomography. *Ophthalmology* 121(1):162–172
- Fea AM, Novarese C, Caselgrandi P, Boscia G (2022) Glaucoma treatment and hydrogel: Current insights and state of the art. *Gels* 8(8):510
- Fea AM, Ricardi F, Novarese C, Cimatorosi F, Vallino V, Boscia G (2023) Precision medicine in glaucoma: Artificial intelligence, biomarkers, genetics and redox state. *International Journal of Molecular Sciences* 24(3):2814
- Fellah KM, Tigane S, Kahloul L (2023) Diabetic retinopathy detection using deep learning. In: International Symposium on Modelling and Implementation of Complex Systems, Springer, pp 234–246
- Feng S, Zhuo Z, Pan D, Tian Q (2020) Ccnet: A cross-connected convolutional network for segmenting retinal vessels using multi-scale features. *Neurocomputing* 392:268–276

- Finn C, Abbeel P, Levine S (2017) Model-agnostic meta-learning for fast adaptation of deep networks. In: International conference on machine learning, PMLR, pp 1126–1135
- Fu H, Xu Y, Wong DWK, Liu J (2016) Retinal vessel segmentation via deep learning network and fully-connected conditional random fields. In: 2016 IEEE 13th international symposium on biomedical imaging (ISBI), IEEE, pp 698–701
- Fu H, Cheng J, Xu Y, Zhang C, Wong DWK, Liu J, Cao X (2018) Disc-aware ensemble network for glaucoma screening from fundus image. *IEEE transactions on medical imaging* 37(11):2493–2501
- Funk RO, Hodge DO, Kohli D, Roddy GW (2022) Multiple systemic vascular risk factors are associated with low-tension glaucoma. *Journal of Glaucoma* 31(1):15–22
- GAMMA (2021) Gamma:glaucoma grading from multi-modality images. <https://gamma.grand-challenge.org/>
- Gao E, Shi F, Zhu W, Chen B, Chen H, Chen X (2014) Comparison of retinal thickness measurements of normal eyes between topcon algorithm and a graph based algorithm. In: Proceedings of the Ophthalmic Medical Image Analysis First International Workshop, University of Iowa, DOI 10.17077/omia.1012
- Gargeya R, Leng T (2017) Automated identification of diabetic retinopathy using deep learning. *Ophthalmology* 124(7):962–969
- Garifullin A, Lensu L, Uusitalo H (2021) Deep bayesian baseline for segmenting diabetic retinopathy lesions: Advances and challenges. *Computers in Biology and Medicine* 136:104,725
- Gheisari S, Shariflou S, Phu J, Kennedy PJ, Agar A, Kalloniatis M, Golzan SM (2021) A combined convolutional and recurrent neural network for enhanced glaucoma detection. *Scientific reports* 11(1):1–11
- Gilbert C, Jackson ML, Kyari F (2019) World report on vision
- Glidai Y, Lucy KA, Schuman JS, Alexopoulos P, Wang B, Wu M, Liu M, Geest JPV, Kollech HG, Lee T, et al. (2022) Microstructural deformations within the depth of the lamina cribrosa in response to acute in vivo intraocular pressure modulation. *Investigative Ophthalmology & Visual Science* 63(5):25–25
- Gómez-Valverde JJ, Antón A, Fatti G, Liefers B, Heranz A, Santos A, Sánchez CI, Ledesma-Carbayo MJ (2019) Automatic glaucoma classification using color fundus images based on convolutional neural networks and transfer learning. *Biomedical optics express* 10(2):892–913
- González-Cela-Casamayor MA, López-Cano JJ, Bravo-Osuna I, Andrés-Guerrero V, Vicario-de-la Torre M, Guzmán-Navarro M, Benítez-del Castillo JM, Herrero-Vanrell R, Molina-Martínez IT (2022) Novel osmoprotective dopc-dmpc liposomes loaded with antihypertensive drugs as potential strategy for glaucoma treatment. *Pharmaceutics* 14(7):1405
- Gopinath K, Rangrej SB, Sivaswamy J (2017) A deep learning framework for segmentation of retinal layers from oct images. In: 2017 4th IAPR Asian Conference on Pattern Recognition (ACPR), IEEE, pp 888–893
- Gordon JA, Farooqi AS, Rabut E, Huffman GR, Schug J, Kelly JD, Dodge GR (2022) Evaluating whole-genome expression differences in idiopathic and diabetic adhesive capsulitis. *Journal of Shoulder and Elbow Surgery* 31(1):e1–e13
- Guan C, Ling YTT, Pease M, Quillen S, Johnson TV, Nguyen TD, Quigley HA (2022) Structure of astrocytes, axons, and lamina cribrosa beams in human glaucoma. *Investigative Ophthalmology & Visual Science* 63(7):2726–A0090
- Gulati P, Dhiman N, Singh T, Chauhan A (2022) Detection of haemorrhages and microaneurysms iris disease using few shot learning. In: AIP Conference Proceedings, AIP Publishing LLC, vol 2481, p 020025
- Gulshan V, Peng L, Coram M, Stumpe MC, Wu D, Narayanaswamy A, Venugopalan S, Widner K, Madams T, Cuadros J, et al. (2016) Development and validation of a deep learning algorithm for detection of diabetic retinopathy in retinal fundus photographs. *Jama* 316(22):2402–2410
- Gupta S, Karandikar A (2015) A survey on methods of automatic detection of diabetic retinopathy. *International Journal of Research in IT, Management and Engineering* 5(1)
- Haire-Joshu D, Hill-Briggs F (2019) The next generation of diabetes translation: a path to health equity. *Annual review of public health* 40:391–410
- Hamel AR, Rouhana JM, Yan W, Monavarfeshani A, Jiang X, Liang Q, Mehta PA, Wang J, Shrivastava A, Duchinski K, et al. (2022) Integrating genetic regulation and single-cell expression with gwas prioritizes causal genes and cell types for glaucoma. *medRxiv*
- Hammel N, Belghith A, Weinreb RN, Medeiros FA, Mendoza N, Zangwill LM (2017) Comparing the rates of retinal nerve fiber layer and ganglion cell–inner plexiform layer loss in healthy eyes and in glaucoma eyes. *American journal of ophthalmology* 178:38–50
- Hansen GL, Kofoed PK, Munch IC, Sillesen H, Jensen LP, Iversen HK, Larsen M (2013) Retinal angiographic blood flow is reduced in the ocular ischaemic syndrome. *Dan Med* 60:A4716
- Hassan B, Raja G (2016) Fully automated assessment of macular edema using optical coherence tomography (oct) images. In: 2016 International Conference

- on Intelligent Systems Engineering (ICISE), IEEE, pp 5–9
- Hassan B, Raja G, Hassan T, Akram MU (2016a) Structure tensor based automated detection of macular edema and central serous retinopathy using optical coherence tomography images. *JOSA A* 33(4):455–463
- Hassan T, Akram MU, Hassan B, Nasim A, Bazaz SA (2015) Review of OCT and fundus images for detection of Macular Edema. *IEEE International Conference on Imaging Systems and Techniques (IST)*, pp 1–4
- Hassan T, Akram MU, Hassan B, Syed AM, Bazaz SA (2016b) Automated segmentation of subretinal layers for the detection of macular edema. *Applied Optics*, Vol 55, Issue 3, pp 454–461
- Hassan T, Akram MU, Hassan B, Syed AM, Bazaz SA (2016c) Automated segmentation of subretinal layers for the detection of macular edema. *Applied optics* 55(3):454–461
- Hassan T, Akram MU, Akhtar M, Khan SA, Yasin U (2018a) Multilayered deep structure tensor delaunay triangulation and morphing based automated diagnosis and 3d presentation of human macula. *Journal of medical systems* 42(11):1–17
- Hassan T, Akram MU, Akhtar M, Shoab Ahmad Khan UY (2018b) Multilayered deep structure tensor delaunay triangulation and morphing based automated diagnosis and 3D presentation of human macula. *Journal of medical systems*, Vol 42, Issue 11, pp 1–17
- Hassan T, Akram MU, Masood MF, Yasin U (2018c) Biomisa retinal image database for macular and ocular syndromes. In: *Image Analysis and Recognition: 15th International Conference, ICIAR 2018, Póvoa de Varzim, Portugal, June 27–29, 2018, Proceedings* 15, Springer, pp 695–705
- Hassan T, Akram MU, Werghi N, Nazir MN (2020) Rag-fw: A hybrid convolutional framework for the automated extraction of retinal lesions and lesion-influenced grading of human retinal pathology. *IEEE journal of biomedical and health informatics* 25(1):108–120
- Hassan T, Hassan B, Akram MU, Hashmi S, Taguri AH, Werghi N (2021) Incremental cross-domain adaptation for robust retinopathy screening via bayesian deep learning. *IEEE Transactions on Instrumentation and Measurement* 70:1–14
- Hassan T, Li Z, Akram MU, Hussain I, Khalaf K, Werghi N (2023) Angular contrastive distillation driven self-supervised scanner independent screening and grading of retinopathy. *Information Fusion* 92:404–419
- Hatamizadeh A, Nath V, Tang Y, Yang D, Roth HR, Xu D (2022) Swin unetr: Swin transformers for semantic segmentation of brain tumors in mri images. In: *Brainlesion: Glioma, Multiple Sclerosis, Stroke and Traumatic Brain Injuries: 7th International Workshop, BrainLes 2021, Held in Conjunction with MICCAI 2021, Virtual Event, September 27, 2021, Revised Selected Papers, Part I, Springer*, pp 272–284
- He H, Lin L, Cai Z, Tang X (2022a) Joined: Prior guided multi-task learning for joint optic disc/cup segmentation and fovea detection. *arXiv preprint arXiv:220300461*
- He M, Rong R, Ji D, Xia X (2022b) From bench to bed: The current genome editing therapies for glaucoma. *Frontiers in Cell and Developmental Biology* 10:879,957
- He W, Wang X, Wang L, Huang Y, Yang Z, Yao X, Zhao X, Ju L, Wu L, Wu L, et al. (2021a) Incremental learning for exudate and hemorrhage segmentation on fundus images. *Information Fusion* 73:157–164
- He Y, Carass A, Liu Y, Jedynek BM, Solomon SD, Saidha S, Calabresi PA, Prince JL (2021b) Structured layer surface segmentation for retina oct using fully convolutional regression networks. *Medical image analysis* 68:101,856
- Heesterbeek TJ, Lorés-Motta L, Hoyng CB, Lechanteur YT, den Hollander AI (2020) Risk factors for progression of age-related macular degeneration. *Ophthalmic and Physiological Optics* 40(2):140–170
- Hervella ÁS, Rouco J, Novo J, Ortega M (2022) End-to-end multi-task learning for simultaneous optic disc and cup segmentation and glaucoma classification in eye fundus images. *Applied Soft Computing* 116:108,347
- Hickam JB, Frayser R (1965) A photographic method for measuring the mean retinal circulation time using fluorescein. *Investigative Ophthalmology & Visual Science* 4(5):876–884
- Hill JO, Galloway JM, Goley A, Marrero DG, Minners R, Montgomery B, Peterson GE, Ratner RE, Sanchez E, Aroda VR (2013) Scientific statement: socioecological determinants of prediabetes and type 2 diabetes. *Diabetes care* 36(8):2430–2439
- Hill-Briggs F, Adler NE, Berkowitz SA, Chin MH, Gary-Webb TL, Navas-Acien A, Thornton PL, Haire-Joshu D (2021) Social determinants of health and diabetes: a scientific review. *Diabetes care* 44(1):258–279
- Holland R, Leingang O, Holmes C, Anders P, Paetzold JC, Kaye R, Riedl S, Bogunović H, Schmidt-Erfurth U, Fritsche L, et al. (2023) Clustering disease trajectories in contrastive feature space for biomarker

- discovery in age-related macular degeneration. arXiv preprint arXiv:230104525
- Hou Q, Cao P, Wang J, Liu X, Yang J, Zaiane OR (2023) Self-supervised domain adaptation for breaking the limits of low-quality fundus image quality enhancement. arXiv preprint arXiv:230106943
- Hsu HY, Chou YB, Jheng YC, Kao ZK, Huang HY, Chen HR, Hwang DK, Chen SJ, Chiou SH, Wu YT (2022) Automatic segmentation of retinal fluid and photoreceptor layer from optical coherence tomography images of diabetic macular edema patients using deep learning and associations with visual acuity. *Biomedicines* 10(6):1269
- Hu CC, Ho JD, Lin HC (2010) Neovascular age-related macular degeneration and the risk of stroke: a 5-year population-based follow-up study. *Stroke* 41(4):613–617
- Hu K, Zhang Z, Niu X, Zhang Y, Cao C, Xiao F, Gao X (2018) Retinal vessel segmentation of color fundus images using multiscale convolutional neural network with an improved cross-entropy loss function. *Neurocomputing* 309:179–191
- Hu K, Shen B, Zhang Y, Cao C, Xiao F, Gao X (2019) Automatic segmentation of retinal layer boundaries in oct images using multiscale convolutional neural network and graph search. *Neurocomputing* 365:302–313
- Hu K, Liu D, Chen Z, Li X, Zhang Y, Gao X (2021) Embedded residual recurrent network and graph search for the segmentation of retinal layer boundaries in optical coherence tomography. *IEEE Transactions on Instrumentation and Measurement* 70:1–17
- Hu M, Zhu C, Li X, Xu Y (2017) Optic cup segmentation from fundus images for glaucoma diagnosis. *Bioengineered* 8(1):21–28
- Huang C, Qi P, Cui H, Lu Q, Gao X (2022a) Circfat1 regulates retinal pigment epithelial cell pyroptosis and autophagy via mediating m6a reader protein ythdf2 expression in diabetic retinopathy. *Experimental Eye Research* 222:109,152
- Huang D (2009) Oct terminology—demystified! *Ophthalmology Management* 13(4)
- Huang D, Swanson EA, Lin CP, Schuman JS, W G S, Chang W, Hee MR, Flotte T, Gregory K, Fujimoto JG (1991) Optical coherence tomography. *Science* 254(5035):1178–1181
- Huang H, Jansonius NM, Chen H, Los LI (2022b) Hyperreflective dots on oct as a predictor of treatment outcome in diabetic macular edema: A systematic review. *Ophthalmology Retina*
- Huang Z, Sun M, Liu Y, Wu J (2022c) Csaunet: A cascade self-attention u-shaped network for precise fundus vessel segmentation. *Biomedical Signal Processing and Control* 75:103,613
- Huda SA, Ila IJ, Sarder S, Shamsujjoha M, Ali MNY (2019) An improved approach for detection of diabetic retinopathy using feature importance and machine learning algorithms. In: 2019 7th International Conference on Smart Computing & Communications (ICSCC), IEEE, pp 1–5
- Iannucci V, Manni P, Mecarelli G, Giammaria S, Giovannetti F, Lambiase A, Bruscolini A (2023) Childhood uveitic glaucoma: Complex management in a fragile population. *Applied Sciences* 13(4):2205
- Igarashi R, Ochiai S, Sakaue Y, Suetake A, Iikawa R, Togano T, Miyamoto F, Miyamoto D, Fukuchi T (2017) Optical coherence tomography angiography of the peripapillary capillaries in primary open-angle and normal-tension glaucoma. *PLoS One* 12(9):e0184,301
- Ikram MK, Mitchell P, Klein R, Sharrett AR, Couper DJ, Wong TY (2012) Age-related macular degeneration and long-term risk of stroke subtypes. *Stroke* 43(6):1681–1683
- Im JH, Jin YP, Chow R, Yan P (2022) Prevalence of diabetic macular edema based on optical coherence tomography in people with diabetes: A systematic review and meta-analysis. *Survey of Ophthalmology*
- Islam MR, Abdulrazak LF, Nahiduzzaman M, Goni MOF, Anower MS, Ahsan M, Haider J, Kowalski M (2022) Applying supervised contrastive learning for the detection of diabetic retinopathy and its severity levels from fundus images. *Computers in Biology and Medicine* p 105602
- Issac A, Sarathi MP, Dutta MK (2015) An adaptive threshold based image processing technique for improved glaucoma detection and classification. *Computer methods and programs in biomedicine* 122(2):229–244
- Jebaseeli J (2021) The prediction of diabetic retinopathy using machine learning techniques. *Journal of Engineering Research*
- Jerman T, Pernuš F, Likar B, Špiclin Ž (2016) Enhancement of vascular structures in 3d and 2d angiographic images. *IEEE transactions on medical imaging* 35(9):2107–2118
- Jiang J, Chen Y, Zhang H, Yuan W, Zhao T, Wang N, Fan G, Zheng D, Wang Z (2022) Association between metformin use and the risk of age-related macular degeneration in patients with type 2 diabetes: a retrospective study. *BMJ open* 12(4):e054,420
- Jiang Y, Tan N, Peng T (2019) Optic disc and cup segmentation based on deep convolutional generative adversarial networks. *IEEE Access* 7:64,483–64,493
- Jiang Z, Zhang H, Wang Y, Ko SB (2018) Retinal blood vessel segmentation using fully convolutional network

- with transfer learning. *Computerized Medical Imaging and Graphics* 68:1–15
- Jimenez-Carmona S, Alemany-Marquez P, Alvarez-Ramos P, Mayoral E, Aguilar-Diosdado M (2022) Validation of an automated screening system for diabetic retinopathy operating under real clinical conditions. *Journal of Clinical Medicine* 11(1):14
- Jiménez-Gómez Y, Alba-Molina D, Blanco-Blanco M, Pérez-Fajardo L, Reyes-Ortega F, Ortega-Llamas L, Villalba-González M, Fernández-Choquet de Isla I, Pugliese F, Stoikow I, et al. (2022) Novel treatments for age-related macular degeneration: A review of clinical advances in sustained drug delivery systems. *Pharmaceutics* 14(7):1473
- Jin K, Yan Y, Chen M, Wang J, Pan X, Liu X, Liu M, Lou L, Wang Y, Ye J (2022) Multimodal deep learning with feature level fusion for identification of choroidal neovascularization activity in age-related macular degeneration. *Acta Ophthalmologica* 100(2):e512–e520
- Jiwane V, DattaGupta A, Chauhan A, Patil V (2022) Detecting diabetic retinopathy using deep learning technique with resnet-50. In: *ICDSMLA 2020*, Springer, pp 45–55
- de Jong EK, Geerlings MJ, den Hollander AI (2020) Age-related macular degeneration. *Genetics and genomics of eye disease* pp 155–180
- Joshua AO, Nelwamondo FV, Mabuza-Hocquet G (2019) Segmentation of optic cup and disc for diagnosis of glaucoma on retinal fundus images. In: *2019 Southern African Universities Power Engineering Conference/Robotics and Mechatronics/Pattern Recognition Association of South Africa (SAUPEC/RobMech/PRASA)*, IEEE, pp 183–187
- Kafieh R, Rabbani H, Kermani S (2013) A review of algorithms for segmentation of optical coherence tomography from retina. *Journal of medical signals and sensors* 3(1):45
- Kafieh R, Rabbani H, Hajizadeh F, Abramoff MD, Sonka M (2015) Thickness mapping of eleven retinal layers segmented using the diffusion maps method in normal eyes. *Journal of Ophthalmology* 2015:1–14, DOI 10.1155/2015/259123
- Kaggle-DR (2015) Kaggle: Diabetic retinopathy detection. <https://www.kaggle.com/competitions/diabetic-retinopathy-detection/data>
- Kao EF, Lin PC, Chou MC, Jaw TS, Liu GC (2014) Automated detection of fovea in fundus images based on vessel-free zone and adaptive gaussian template. *Computer methods and programs in biomedicine* 117(2):92–103
- Kaplan S, Lensu L (2022) Contrastive learning for generating optical coherence tomography images of the retina. In: *Simulation and Synthesis in Medical Imaging: 7th International Workshop, SASHIMI 2022, Held in Conjunction with MICCAI 2022, Singapore, September 18, 2022, Proceedings*, Springer, pp 112–121
- Kar MK, Neog DR, Nath MK (2022a) Retinal vessel segmentation using multi-scale residual convolutional neural network (msr-net) combined with generative adversarial networks. *Circuits, Systems, and Signal Processing* pp 1–30
- Kar SS, Sevgi DD, Dong V, Srivastava SK, Madabhushi A, Ehlers JP (2021) Multi-compartment spatially-derived radiomics from optical coherence tomography predict anti-vegf treatment durability in macular edema secondary to retinal vascular disease: preliminary findings. *IEEE Journal of Translational Engineering in Health and Medicine* 9:1–13
- Kar SS, Abraham J, Wykoff CC, Sevgi DD, Lunasco L, Brown DM, Srivastava SK, Madabhushi A, Ehlers JP (2022b) Computational imaging biomarker correlation with intraocular cytokine expression in diabetic macular edema: Radiomics insights from the imagine study. *Ophthalmology Science* 2(2):100,123
- Karaconji T, Zagora S, Grigg JR (2022) Approach to childhood glaucoma: A review. *Clinical & Experimental Ophthalmology* 50(2):232–246
- Karki SS, Kulkarni P (2021) Diabetic retinopathy classification using a combination of efficientnets. In: *2021 International Conference on Emerging Smart Computing and Informatics (ESCI)*, IEEE, pp 68–72
- Karri SPK, Chakraborty D, Chatterjee J (2017) Transfer learning based classification of optical coherence tomography images with diabetic macular edema and dry age-related macular degeneration. *Biomedical optics express* 8(2):579–592
- Karvonen E, Stoor K, Luodonpää M, Hägg P, Lintonen T, Liinamaa J, Tuulonen A, Saarela V (2020) Diagnostic performance of modern imaging instruments in glaucoma screening. *British Journal of Ophthalmology* 104(10):1399–1405
- Keane PA, Sadda SR (2014) Retinal imaging in the twenty-first century: state of the art and future directions. *Ophthalmology* 121(12):2489–2500
- Keenan TD, Chen Q, Agrón E, Tham YC, Goh JHL, Lei X, Ng YP, Liu Y, Xu X, Cheng CY, et al. (2022) Deep learning automated diagnosis and quantitative classification of cataract type and severity. *Ophthalmology*
- Kermany D, Zhang K, Goldbaum M (2018a) Large dataset of labeled optical coherence tomography (oct) and chest x-ray images. *Mendeley Data* 3:10–17,632

- Kermany DS, Goldbaum M, Cai W, Valentim CC, Liang H, Baxter SL, McKeown A, Yang G, Wu X, Yan F, et al. (2018b) Identifying medical diagnoses and treatable diseases by image-based deep learning. *Cell* 172(5):1122–1131
- Khalid S, Akram MU, Hassan T, Nasim A, Jameel A (2017) Fully automated robust system to detect retinal edema, central serous chorioretinopathy, and age related macular degeneration from optical coherence tomography images. *BioMed research international* 2017
- Khalil T, Khalid S, Syed AM (2014) Review of machine learning techniques for glaucoma detection and prediction. In: 2014 Science and Information Conference, pp 438–442, DOI 10.1109/SAI.2014.6918224
- Khalil T, Akram MU, Raja H, Jameel A, Basit I (2018) Detection of glaucoma using cup to disc ratio from spectral domain optical coherence tomography images. *IEEE Access* 6:4560–4576, DOI 10.1109/access.2018.2791427
- Khalili MR, Bremner F, Tabrizi R, Bashi A (2023) Optical coherence tomography angiography (oct angiography) in anterior ischemic optic neuropathy (aion): A systematic review and meta-analysis. *European Journal of Ophthalmology* 33(1):530–545
- Khan KB, Khaliq AA, Jalil A, Iftikhar MA, Ullah N, Aziz MW, Ullah K, Shahid M (2019) A review of retinal blood vessels extraction techniques: challenges, taxonomy, and future trends. *Pattern Analysis and Applications* 22(3):767–802
- Kim GN, Kim JA, Kim MJ, Lee EJ, Hwang JM, Kim TW (2020) Comparison of lamina cribrosa morphology in normal tension glaucoma and autosomal-dominant optic atrophy. *Investigative Ophthalmology & Visual Science* 61(5):9–9
- Kim JA, Kim TW, Lee EJ, Girard MJ, Mari JM (2019a) Lamina cribrosa morphology in glaucomatous eyes with hemifield defect in a korean population. *Ophthalmology* 126(5):692–701
- Kim JA, Lee SH, Son DH, Kim TW, Lee EJ, Girard MJ, Mari JM (2022) Morphologic changes in the lamina cribrosa upon intraocular pressure lowering in patients with normal tension glaucoma. *Investigative Ophthalmology & Visual Science* 63(2):23–23
- Kim M, Zuallaert J, De Neve W (2017) Few-shot learning using a small-sized dataset of high-resolution fundus images for glaucoma diagnosis. In: Proceedings of the 2nd international workshop on multimedia for personal health and health care, pp 89–92
- Kim M, Han JC, Hyun SH, Janssens O, Van Hoecke S, Kee C, De Neve W (2019b) Medinoid: computer-aided diagnosis and localization of glaucoma using deep learning. *Applied Sciences* 9(15):3064
- Kjærsgaard M, Grauslund J, Vestergaard AH, Subhi Y (2022) Relationship between diabetic retinopathy and primary open-angle glaucoma: A systematic review and meta-analysis. *Ophthalmic Research*
- Klein R, Klein BE, Moss SE (1984) Visual impairment in diabetes. *Ophthalmology* 91(1):1–9
- Kolli A, Sekimitsu S, Wang J, Segre A, Friedman D, Elze T, Pasquale LR, Wiggs J, Zebardast N (2022) Background polygenic risk modulates the association between glaucoma and cardiopulmonary diseases and measures: an analysis from the uk biobank. *British Journal of Ophthalmology*
- Kose C, Ikibacs C (2011) Statistical techniques for detection of optic disc and macula and parameters measurement in retinal fundus images. *Journal of Medical and Biological Engineering* 31(6):395–404
- Kovalyk O, Morales-Sánchez J, Verdú-Monedero R, Sellés-Navarro I, Palazón-Cabanes A, Sancho-Gómez JL (2022) Papila: Dataset with fundus images and clinical data of both eyes of the same patient for glaucoma assessment. *Scientific Data* 9(1):291
- Kuang TM, Zhang C, Zangwill LM, Weinreb RN, Medeiros FA (2015) Estimating lead time gained by optical coherence tomography in detecting glaucoma before development of visual field defects. *Ophthalmology* 122(10):2002–2009
- Kulshrestha A, Singh N, Moharana B, Gupta PC, Ram J, Singh R (2022) Axial myopia, a protective factor for diabetic retinopathy-role of vascular endothelial growth factor. *Scientific Reports* 12(1):1–6
- Kumar R, Bhandari AK (2022) Luminosity and contrast enhancement of retinal vessel images using weighted average histogram. *Biomedical Signal Processing and Control* 71:103,089
- Kumar R, Gupta M, et al. (2022) Optical coherence tomography image based eye disease detection using deep convolutional neural network. *Health Information Science and Systems* 10(1):1–16
- Kumari CU, Hemanth A, Anand V, Kumar DS, Sanjeev RN, Harshitha TSS (2022) Deep learning based detection of diabetic retinopathy using retinal fundus images. In: 2022 Third International Conference on Intelligent Computing Instrumentation and Control Technologies (ICICICT), IEEE, pp 1312–1316
- Kwan CC, Fawzi AA (2019) Imaging and biomarkers in diabetic macular edema and diabetic retinopathy. *Current diabetes reports* 19(10):1–10
- de La Torre J, Valls A, Puig D (2020) A deep learning interpretable classifier for diabetic retinopathy disease grading. *Neurocomputing* 396:465–476
- Lakshminarayanan V, Kheradfallah H, Sarkar A, Jothi Balaji J (2021) Automated detection and diagnosis of diabetic retinopathy: A comprehensive sur-

- vey. *Journal of Imaging* 7(9):165
- Latif J, Tu S, Xiao C, Ur Rehman S, Imran A, Latif Y (2022) Odgnet: a deep learning model for automated optic disc localization and glaucoma classification using fundus images. *SN Applied Sciences* 4(4):1–11
- Lei L, Bai YH, Jiang HY, He T, Li M, Wang JP (2021) A bioinformatics analysis of the contribution of m6a methylation to the occurrence of diabetes mellitus. *Endocrine Connections* 10(10):1253–1265
- Li F, Chen H, Liu Z, Zhang Xd, Jiang Ms, Wu Zz, Zhou Kq (2019a) Deep learning-based automated detection of retinal diseases using optical coherence tomography images. *Biomedical optics express* 10(12):6204–6226
- Li J, Jin P, Zhu J, Zou H, Xu X, Tang M, Zhou M, Gan Y, He J, Ling Y, et al. (2021) Multi-scale gcn-assisted two-stage network for joint segmentation of retinal layers and discs in peripapillary oct images. *Biomedical Optics Express* 12(4):2204–2220
- Li J, Gao G, Liu Y, Yang L (2023) Magf-net: A multi-scale attention-guided fusion network for retinal vessel segmentation. *Measurement* 206:112,316
- Li L, Fang F, Feng X, Zhuang P, Huang H, Liu P, Liu L, Xu AZ, Qi LS, Cong L, et al. (2022a) Single-cell transcriptome analysis of regenerating rgcs reveals potent glaucoma neural repair genes. *Neuron*
- Li MX, Yu SQ, Zhang W, Zhou H, Xu X, Qian TW, Wan YJ (2019b) Segmentation of retinal fluid based on deep learning: application of three-dimensional fully convolutional neural networks in optical coherence tomography images. *International journal of ophthalmology* 12(6):1012
- Li Q, Li S, He Z, Guan H, Chen R, Xu Y, Wang T, Qi S, Mei J, Wang W (2020) Deepretina: layer segmentation of retina in oct images using deep learning. *Translational Vision Science & Technology* 9(2):61–61
- Li Z, He Y, Keel S, Meng W, Chang RT, He M (2018a) Efficacy of a deep learning system for detecting glaucomatous optic neuropathy based on color fundus photographs. *Ophthalmology* 125(8):1199–1206
- Li Z, Keel S, Liu C, He Y, Meng W, Scheetz J, Lee PY, Shaw J, Ting D, Wong TY, et al. (2018b) An automated grading system for detection of vision-threatening referable diabetic retinopathy on the basis of color fundus photographs. *Diabetes care* 41(12):2509–2516
- Li Z, Deng X, Lu T, Zhou L, Xiao J, Lan Y, Jin C (2022b) Hyperreflective material serves as a potential biomarker of dyslipidemia in diabetic macular edema. *Photodiagnosis and Photodynamic Therapy* p 102903
- Liao M, Zhao Yq, Wang Xh, Dai Ps (2014) Retinal vessel enhancement based on multi-scale top-hat transformation and histogram fitting stretching. *Optics & Laser Technology* 58:56–62
- Lim G, Cheng Y, Hsu W, Lee ML (2015) Integrated optic disc and cup segmentation with deep learning. In: 2015 IEEE 27th International Conference on Tools with Artificial Intelligence (ICTAI), IEEE, pp 162–169
- Lim G, Bellemo V, Xie Y, Lee XQ, Yip MY, Ting DS (2020) Different fundus imaging modalities and technical factors in ai screening for diabetic retinopathy: a review. *Eye and Vision* 7:1–13
- Liskowski P, Krawiec K (2016) Segmenting retinal blood vessels with deep neural networks. *IEEE transactions on medical imaging* 35(11):2369–2380
- Liu B, Pan D, Song H (2021a) Joint optic disc and cup segmentation based on densely connected depthwise separable convolution deep network. *BMC Medical Imaging* 21(1):1–12
- Liu P, Kong B, Li Z, Zhang S, Fang R (2019a) Cfea: collaborative feature ensembling adaptation for domain adaptation in unsupervised optic disc and cup segmentation. In: *International Conference on Medical Image Computing and Computer-Assisted Intervention*, Springer, pp 521–529
- Liu P, Tran CT, Kong B, Fang R (2022a) Cada: Multi-scale collaborative adversarial domain adaptation for unsupervised optic disc and cup segmentation. *Neurocomputing* 469:209–220
- Liu S, Hong J, Lu X, Jia X, Lin Z, Zhou Y, Liu Y, Zhang H (2019b) Joint optic disc and cup segmentation using semi-supervised conditional gans. *Computers in biology and medicine* 115:103,485
- Liu S, Wang D, Chen F, Zhang X (2019c) Hyperreflective foci in oct image as a biomarker of poor prognosis in diabetic macular edema patients treating with conbercept in china. *BMC ophthalmology* 19(1):1–6
- Liu W, Sun Y, Ji Q (2020) Mdan-unet: multi-scale and dual attention enhanced nested u-net architecture for segmentation of optical coherence tomography images. *Algorithms* 13(3):60
- Liu X, Bai Y, Jiang M (2021b) One-stage attention-based network for image classification and segmentation on optical coherence tomography image. In: 2021 IEEE International Conference on Systems, Man, and Cybernetics (SMC), IEEE, pp 3025–3029
- Liu X, Wang S, Zhang Y, Liu D, Hu W (2021c) Automatic fluid segmentation in retinal optical coherence tomography images using attention based deep learning. *Neurocomputing* 452:576–591
- Liu X, Zhou K, Yao J, Wang M, Zhang Y (2022b) Contrastive uncertainty based biomarkers detection in

- retinal optical coherence tomography images. *Physics in Medicine & Biology* 67(24):245,012
- Liu X, Liu Q, Zhang Y, Wang M, Tang J (2023a) Tssk-net: Weakly supervised biomarker localization and segmentation with image-level annotation in retinal oct images. *Computers in Biology and Medicine* 153:106,467
- Liu Y, Shen J, Yang L, Bian G, Yu H (2023b) Resdo-net: A deep residual network for accurate retinal vessel segmentation from fundus images. *Biomedical Signal Processing and Control* 79:104,087
- Liu Y, Shen J, Yang L, Yu H, Bian G (2023c) Wave-net: A lightweight deep network for retinal vessel segmentation from fundus images. *Computers in Biology and Medicine* 152:106,341
- Lu Z, Chen D, Xue D, Zhang S (2019) Weakly supervised semantic segmentation for optic disc of fundus image. *Journal of Electronic Imaging* 28(3):033,012
- Lu Z, Miao J, Dong J, Zhu S, Wang X, Feng J (2023) Automatic classification of retinal diseases with transfer learning-based lightweight convolutional neural network. *Biomedical Signal Processing and Control* 81:104,365
- Madadi Y, Abu-Serhan H, Yousefi S (2022) Domain adaptation-based deep learning models for forecasting and diagnosis of glaucoma disease. *TechRxiv*
- Madathil S, Padannayil SK (2022) Mc-dmd: A data-driven method for blood vessel enhancement in retinal images using morphological closing and dynamic mode decomposition. *Journal of King Saud University-Computer and Information Sciences* 34(8):5223–5239
- Maetschke S, Antony B, Ishikawa H, Wollstein G, Schuman J, Garnavi R (2019) A feature agnostic approach for glaucoma detection in OCT volumes. *PLOS ONE* 14(7):e0219,126, DOI 10.1371/journal.pone.0219126
- Mahapatra S, Agrawal S (????) An optimal statistical feature-based transformation function for enhancement of retinal images using adaptive enhanced leader particle swarm optimization. *International Journal of Imaging Systems and Technology*
- Mahmood MT, Lee IH (2022) Optic disc localization in fundus images through accumulated directional and radial blur analysis. *Computerized Medical Imaging and Graphics* 98:102,058
- Mai S, Li Q, Zhao Q, Gao M (2021) Few-shot transfer learning for hereditary retinal diseases recognition. In: *Medical Image Computing and Computer Assisted Intervention–MICCAI 2021: 24th International Conference, Strasbourg, France, September 27–October 1, 2021, Proceedings, Part VIII* 24, Springer, pp 97–107
- Makita S, Hong Y, Yamanari M, Yatagai T, Yasuno Y (2006) Optical coherence angiography. *Optics express* 14(17):7821–7840
- Man N, Guo S, Yiu K, Leung C (2023) Multi-layer segmentation of retina oct images via advanced u-net architecture. *Neurocomputing* 515:185–200
- Manoj S, Muralidharan SP, Sandeep M (2013) Neural network based classifier for retinal blood vessel segmentation. *International Journal of Recent Trends in Electrical & Electronics Engineering* 3(1):44–53
- Mansoori T, Viswanath K, Balakrishna N (2011) Ability of spectral domain optical coherence tomography peripapillary retinal nerve fiber layer thickness measurements to identify early glaucoma. *Indian Journal of Ophthalmology* 59(6):455
- Mantel I, Mosinska A, Bergin C, Polito MS, Guidotti J, Apostolopoulos S, Ciller C, De Zanet S (2021) Automated quantification of pathological fluids in neovascular age-related macular degeneration, and its repeatability using deep learning. *Translational Vision Science & Technology* 10(4):17–17
- Mariottoni EB, Jammal AA, Urata CN, Berchuck SI, Thompson AC, Estrela T, Medeiros FA (2020) Quantification of retinal nerve fibre layer thickness on optical coherence tomography with a deep learning segmentation-free approach. *Scientific Reports* 10(1), DOI 10.1038/s41598-019-57196-y
- Matta S, Lamard M, Conze PH, Le Guilcher A, Riquembourg V, Benyoussef AA, Massin P, Rottier JB, Cochener B, Quéllec G (2023) Meta learning for anomaly detection in fundus photographs. In: *Meta-Learning with Medical Imaging and Health Informatics Applications*, Elsevier, pp 301–329
- Mauschitz MM, Finger RP (2022) Age-related macular degeneration and cardiovascular diseases: revisiting the common soil theory. *The Asia-Pacific Journal of Ophthalmology* 11(2):94–99
- Mauschitz MM, Lohner V, Koch A, Stöcker T, Reuter M, Holz FG, Finger RP, Breteler MM (2022a) Retinal layer assessments as potential biomarkers for brain atrophy in the rhineland study. *Scientific reports* 12(1):2757
- Mauschitz MM, Schmitz MT, Verzijden T, Schmid M, Thee EF, Colijn JM, Delcourt C, Cougnard-Grégoire A, Merle BM, Korobelnik JF, et al. (2022b) Physical activity, incidence, and progression of age-related macular degeneration: A multicohort study. *American Journal of Ophthalmology* 236:99–106
- Mayer MA, Horneegger J, Mardin CY, Tornow RP (2010) Retinal nerve fiber layer segmentation on FD-OCT scans of normal subjects and glaucoma patients. *Biomedical Optics Express* 1(5):1358, DOI 10.1364/boe.1.001358

- Medeiros FA, Lisboa PR, Weinreb RN, Girkin CA, Liebmann JM, Zangwill LM (2012) A combined index of structure and function for staging glaucomatous damage. *Arch Ophthalmology* 130(9):1107–1116
- Melinscak M, Prentasac P, Loncaric S (2015) Retinal vessel segmentation using deep neural networks. In: *VISAPP* (1), pp 577–582
- Meng Q, Shin'ichi S (2020) Adinet: Attribute driven incremental network for retinal image classification. In: *Proceedings of the IEEE/CVF Conference on Computer Vision and Pattern Recognition*, pp 4033–4042
- Messidor (2017) Messidor: Methods to evaluate segmentation and indexing techniques in the field of retinal ophthalmology. <https://www.adcis.net/en/third-party/messidor/>
- Mikula E, Holland G, Bradford S, Khazaeinezhad R, Srass H, Suarez C, Jester JV, Juhasz T (2021) Intraocular pressure reduction by femtosecond laser created trabecular channels in perfused human anterior segments. *Translational vision science & technology* 10(9):22–22
- Mikula ER, Raksi F, Ahmed II, Sharma M, Holland G, Khazaeinezhad R, Bradford S, Jester JV, Juhasz T (2022) Femtosecond laser trabeculotomy in perfused human cadaver anterior segments: A novel, noninvasive approach to glaucoma treatment. *Translational vision science & technology* 11(3):28–28
- Milanowski P, Kosior-Jarecka E, Lukasik U, Wrobel-Dudzinska D, Milanowska J, Khor CC, Aung T, Kocki J, Zarnowski T (2022) Associations between opa1, mfn1, and mfn2 polymorphisms and primary open angle glaucoma in polish participants of european ancestry. *Ophthalmic Genetics* 43(1):42–47
- Mishra SS, Mandal B, Puhan NB (2021) Perturbed composite attention model for macular optical coherence tomography image classification. *IEEE Transactions on Artificial Intelligence* 3(4):625–635
- Mishra Z, Ganegoda A, Selicha J, Wang Z, Sadda SR, Hu Z (2020) Automated retinal layer segmentation using graph-based algorithm incorporating deep-learning-derived information. *Scientific Reports* 10(1):1–8
- Mistry S, Tonyushkina KN, Benavides VC, Choudhary A, Huerta-Saenz L, Patel NS, Mahmud FH, Libman I, Sperling MA (2022) A centennial review of discoveries and advances in diabetes: Children and youth. *Pediatric Diabetes*
- Mochida S, Yoshida T, Nomura T, Hatake R, Ohno-Matsui K (2022) Association between peripheral visual field defects and focal lamina cribrosa defects in highly myopic eyes. *Japanese Journal of Ophthalmology* 66(3):285–295
- Mohamed NA, Zulkifley MA, Zaki WMDW, Hussain A (2019) An automated glaucoma screening system using cup-to-disc ratio via simple linear iterative clustering superpixel approach. *Biomedical Signal Processing and Control* 53:101,454
- Moin K, Shrivastava M, Mishra A, Jena L, Nayak S (2023) Diabetic retinopathy detection using cnn model. In: *Ambient Intelligence in Health Care*, Springer, pp 133–143
- Moradi M, Chen Y, Du X, Seddon JM (2023) Deep ensemble learning for automated non-advanced amd classification using optimized retinal layer segmentation and sd-oct scans. *Computers in Biology and Medicine* p 106512
- Motamedi S, Gawlik K, Ayadi N, Zimmermann HG, Asseuer S, Bereuter C, Mikolajczak J, Paul F, Kadas EM, Brandt AU (2019) Normative data and minimally detectable change for inner retinal layer thicknesses using a semi-automated OCT image segmentation pipeline. *Frontiers in Neurology* 10, DOI 10.3389/fneur.2019.01117
- Mrad Y, Elloumi Y, Akil M, Bedoui M (2022) A fast and accurate method for glaucoma screening from smartphone-captured fundus images. *IRBM* 43(4):279–289
- Muhammad H, Fuchs TJ, Cuir ND, Moraes CGD, Blumberg DM, Liebmann JM, Ritch R, Hood DC (2017) Hybrid deep learning on single wide-field optical coherence tomography scans accurately classifies glaucoma suspects. *Journal of Glaucoma* 26(12):1086–1094, DOI 10.1097/ijg.0000000000000765
- Mukherjee S, De Silva T, Grisso P, Wiley H, Tiaran DK, Thavikulwat AT, Chew E, Cukras C (2022) Retinal layer segmentation in optical coherence tomography (oct) using a 3d deep-convolutional regression network for patients with age-related macular degeneration. *Biomedical Optics Express* 13(6):3195–3210
- Munteanu GZ, Munteanu ZVI, Daina CM, Daina LG, Coroi MC, Domnariu C, Badau D, Roiu G (2022) Study to identify and evaluate predictor factors for primary open-angle glaucoma in tertiary prophylactic actions. *Journal of Personalized Medicine* 12(9):1384
- Muramatsu D, Shimura M, Kitano S, Sakamoto T (2018) Survey of treatment for diabetic macular edema (streat-dme) study: Results by treatment options from real world data in japan. *Investigative Ophthalmology & Visual Science* 59(9):1895–1895
- Murugan R, Roy P (2022) Micronet: microaneurysm detection in retinal fundus images using convolutional neural network. *Soft Computing* 26(3):1057–

1066

- Murugappan M, Prakash N, Jeya R, Mohanarathinam A, Hemalakshmi G, Mahmud M (2022) A novel few-shot classification framework for diabetic retinopathy detection and grading. *Measurement* 200:111,485
- Muthukannan P, et al. (2022) Optimized convolution neural network based multiple eye disease detection. *Computers in Biology and Medicine* p 105648
- Mvoulana A, Kachouri R, Akil M (2019) Fully automated method for glaucoma screening using robust optic nerve head detection and unsupervised segmentation based cup-to-disc ratio computation in retinal fundus images. *Computerized Medical Imaging and Graphics* 77:101,643
- Mwanza JC, Chang RT, Budenz DL, Durbin MK, Gendy MG, Shi W, Feuer WJ (2010) Reproducibility of peripapillary retinal nerve fiber layer thickness and optic nerve head parameters measured with cirrus hd-oct in glaucomatous eyes. *Investigative ophthalmology & visual science* 51(11):5724–5730
- Nair AT, Muthuvel K, Haritha K (2022) Effectual evaluation on diabetic retinopathy. In: *Information and Communication Technology for Competitive Strategies (ICTCS 2020)*, Springer, pp 559–567
- Nashine S, Cohen P, Wan J, Kenney MC (2022) Effect of humanin g (hng) on inflammation in age-related macular degeneration (amd). *Aging (Albany NY)* 14(10):4247
- Naveed M, Ramzan A, Akram MU (2017) Clinical and technical perspective of glaucoma detection using oct and fundus images: A review. In: *2017 1st International Conference on Next Generation Computing Applications (NextComp)*, pp 157–162, DOI 10.1109/NEXTCOMP.2017.8016192
- Nawaz M, Nazir T, Javed A, Tariq U, Yong HS, Khan MA, Cha J (2022) An efficient deep learning approach to automatic glaucoma detection using optic disc and optic cup localization. *Sensors* 22(2):434
- Nicholson B, Noble J, Forooghian F, Meyerle C (2013) Central serous chorioretinopathy: update on pathophysiology and treatment. *Survey of ophthalmology* 58(2):103–126
- Nithya R, Venkateswaran N (2015) Analysis of segmentation algorithms in colour fundus and OCT images for glaucoma detection. *Indian Journal of Science and Technology* 8(24), DOI 10.17485/ijst/2015/v8i24/80151
- Niu S, Chen Q, de Sisternes L, Rubin DL, Zhang W, Liu Q (2014) Automated retinal layers segmentation in SD-OCT images using dual-gradient and spatial correlation smoothness constraint. *Computers in Biology and Medicine* 54:116–128, DOI 10.1016/j.combiomed.2014.08.028
- Nuzzi R, Boscia G, Marolo P, Ricardi F (2021) The impact of artificial intelligence and deep learning in eye diseases: A review. *Frontiers in Medicine* 8
- Ometto G, Moghul I, Montesano G, Hunter A, Pontikos N, Jones PR, Keane PA, Liu X, Denniston AK, Crabb DP (2019) ReLayer: a free, online tool for extracting retinal thickness from cross-platform OCT images. *Translational Vision Science & Technology* 8(3):25, DOI 10.1167/tvst.8.3.25
- O'Neill HC, Limnios IJ, Barnett NL (2020) Advancing a stem cell therapy for age-related macular degeneration. *Current stem cell research & therapy* 15(2):89–97
- Ong JX, Fawzi AA (2022) Perspectives on diabetic retinopathy from advanced retinal vascular imaging. *Eye* pp 1–9
- Oraby H, Elshaer S, Rashed L, Eldesoky N (2022) Microrna-499 gene expression in egyptian type 2 diabetes mellitus patients with and without coronary heart disease. *Azhar International Journal of Pharmaceutical and Medical Sciences* 2(1):73–81
- O'Fee JR, Juliano J, Moshfeghi AA (2022) Factors associated with diabetic macular edema in patients with proliferative diabetic retinopathy. *Graefe's Archive for Clinical and Experimental Ophthalmology* pp 1–10
- Pacaud D, Schwandt A, de Beaufort C, Casteels K, Bertrand J, Birkebaek NH, Campagnoli M, Bratina N, Limbert C, MP O'Riordan S, et al. (2016) A description of clinician reported diagnosis of type 2 diabetes and other non-type 1 diabetes included in a large international multicentered pediatric diabetes registry (sweet). *Pediatric Diabetes* 17:24–31
- Panda R, Puhan N, Panda G (2017) Robust and accurate optic disk localization using vessel symmetry line measure in fundus images. *Biocybernetics and Biomedical Engineering* 37(3):466–476
- Panwar N, Huang P, Lee J, Keane PA, Chuan TS, Richhariya A, Teoh S, Lim TH, Agrawal R (2016) Fundus photography in the 21st century—a review of recent technological advances and their implications for worldwide healthcare. *Telemedicine and e-Health* 22(3):198–208
- Park HYL, Park CK (2013) Diagnostic capability of lamina cribrosa thickness by enhanced depth imaging and factors affecting thickness in patients with glaucoma. *Ophthalmology* 120(4):745–752, DOI 10.1016/j.ophtha.2012.09.051
- Park JJ, Soetikno BT, Fawzi AA (2016) Characterization of the middle capillary plexus using optical coherence tomography angiography in healthy and diabetic eyes. *Retina (Philadelphia, Pa)* 36(11):2039

- Park KB, Choi SH, Lee JY (2020) M-gan: Retinal blood vessel segmentation by balancing losses through stacked deep fully convolutional networks. *IEEE Access* 8:146,308–146,322
- Parra-Mora E, da Silva Cruz LA (2022) Loctseg: A lightweight fully convolutional network for end-to-end optical coherence tomography segmentation. *Computers in Biology and Medicine* 150:106,174
- Parthiban K, Kamarasan M (2022) Efficientnet with optimal wavelet neural network for dr detection and grading. In: 2022 4th International Conference on Smart Systems and Inventive Technology (ICSSIT), IEEE, pp 1081–1086
- Pascolini D, Mariotti S (2012) Global estimates of visual impairment: 2010. *Br J Ophthalmol* 96(5):614–8, DOI 10.1136/bjophthalmol-2011-300539
- Pasini E, Corsetti G, Assanelli D, Testa C, Romano C, Dioguardi FS, Aquilani R (2019) Effects of chronic exercise on gut microbiota and intestinal barrier in human with type 2 diabetes. *Minerva medica* 110(1):3–11
- Patel KD, Silva LB, Park Y, Shakouri T, Keskin-Erdogan Z, Sawadkar P, Cho KJ, Knowles JC, Chau DY, Kim HW (2022) Recent advances in drug delivery systems for glaucoma treatment. *Materials Today Nano* p 100178
- Pavithra K, Kumar P, Geetha M, Bhandary SV (2023) Computer aided diagnosis of diabetic macular edema in retinal fundus and oct images: A review. *Biocybernetics and Biomedical Engineering*
- Pead E, Megaw R, Cameron J, Fleming A, Dhillon B, Trucco E, MacGillivray T (2019) Automated detection of age-related macular degeneration in color fundus photography: a systematic review. *survey of ophthalmology* 64(4):498–511
- Peled A, Raz I, Zucker I, Derazne E, Megreli J, Pinhas-Hamiel O, Einan-Lifshitz A, Morad Y, Pras E, Lutski M, et al. (2022) Myopia and early-onset type 2 diabetes: A nationwide cohort study. *The Journal of Clinical Endocrinology & Metabolism* 107(2):e663–e671
- Petchyim S, Subhadhirasakul S, Sakiyalak D, Vessadapan P, Ruangvaravate N (2022) Clinical characteristics and outcome of bleb-related infection in glaucoma patients. *Siriraj Medical Journal* 74(9):555–561
- Philippi D, Rothaus K, Castelli M (2023) A vision transformer architecture for the automated segmentation of retinal lesions in spectral domain optical coherence tomography images. *Scientific Reports* 13(1):517
- Pole C, Ameri H (2021) Fundus Autofluorescence and Clinical Applications. *J Ophthalmic Vis Res*
- Prager AJ, Kang JM, Tanna AP (2021) Advances in perimetry for glaucoma. *Current opinion in ophthalmology* 32(2):92–97
- Prashanth G, Vastrad B, Tengli A, Vastrad C, Kotturshetti I (2021) Investigation of candidate genes and mechanisms underlying obesity associated type 2 diabetes mellitus using bioinformatics analysis and screening of small drug molecules. *BMC Endocrine Disorders* 21(1):1–48
- Pujar M, Vastrad B, Kavatagimath S, Vastrad C, Kotturshetti S (2022) Identification of candidate biomarkers and pathways associated with type 1 diabetes mellitus using bioinformatics analysis. *Scientific Reports* 12(1):1–27
- Qin X, Zou H (2022) The role of lipopolysaccharides in diabetic retinopathy. *BMC ophthalmology* 22(1):1–14
- Qomariah D, Nopember I, Tjandrasa H, Fatichah C (2021) Segmentation of microaneurysms for early detection of diabetic retinopathy using mresunet. *International Journal of Intelligent Engineering and Systems* 14(3):359–373
- Qomariah DUN, Tjandrasa H, Fatichah C (2019) Classification of diabetic retinopathy and normal retinal images using cnn and svm. In: 2019 12th International Conference on Information & Communication Technology and System (ICTS), IEEE, pp 152–157
- Qu Z, Zhuo L, Cao J, Li X, Yin H, Wang Z (2023) Tp-net: Two-path network for retinal vessel segmentation. *IEEE Journal of Biomedical and Health Informatics*
- Qummar S, Khan FG, Shah S, Khan A, Shamshirband S, Rehman ZU, Khan IA, Jadoon W (2019) A deep learning ensemble approach for diabetic retinopathy detection. *Ieee Access* 7:150,530–150,539
- Qureshi RJ, Kovacs L, Harangi B, Nagy B, Peto T, Hajdu A (2012) Combining algorithms for automatic detection of optic disc and macula in fundus images. *Computer Vision and Image Understanding* 116(1):138–145
- Raghavendra U, Fujita H, Bhandary SV, Gudigar A, Tan JH, Acharya UR (2018) Deep convolution neural network for accurate diagnosis of glaucoma using digital fundus images. *Information Sciences* 441:41–49
- Raja H, Akram MU, Khawaja SG, Arslan M, Ramzan A, Nazir N (2020a) Data on oct and fundus images for the detection of glaucoma. *Data in brief* 29:105,342
- Raja H, Akram MU, Shaukat A, Khan SA, Alghamdi N, Khawaja SG, Nazir N (2020b) Extraction of retinal layers through convolution neural network (cnn) in an oct image for glaucoma diagnosis. *Journal of Digital Imaging* 33(6):1428–1442

- Raja H, Hassan T, Akram MU, Werghi N (2020c) Clinically verified hybrid deep learning system for retinal ganglion cells aware grading of glaucomatous progression. *IEEE Transactions on Biomedical Engineering*
- Raja H, Hassan T, Akram MU, Werghi N (2020d) Clinically verified hybrid deep learning system for retinal ganglion cells aware grading of glaucomatous progression. *IEEE Transactions on Biomedical Engineering* 68(7):2140–2151
- Raja H, Akram MU, Hassan T, Ramzan A, Aziz A, Raja H (2022) Glaucoma detection using optical coherence tomography images: A systematic review of clinical and automated studies. *IETE Journal of Research* pp 1–21
- Rakhlin A (2018) Diabetic retinopathy detection through integration of deep learning classification framework. *BioRxiv* p 225508
- Ramakanth SA, Babu RV (2014) Approximate nearest neighbour field based optic disk detection. *Computerized medical imaging and graphics* 38(1):49–56
- Rashno A, Koozekanani DD, Drayna PM, Nazari B, Sadri S, Rabbani H, Parhi KK (2017) Fully automated segmentation of fluid/cyst regions in optical coherence tomography images with diabetic macular edema using neutrosophic sets and graph algorithms. *IEEE Transactions on Biomedical Engineering* 65(5):989–1001
- Rasti R, Rabbani H, Mehridehnavi A, Hajizadeh F (2017) Macular oct classification using a multi-scale convolutional neural network ensemble. *IEEE transactions on medical imaging* 37(4):1024–1034
- Rasti R, Mehridehnavi A, Rabbani H, Hajizadeh F (2018) Automatic diagnosis of abnormal macula in retinal optical coherence tomography images using wavelet-based convolutional neural network features and random forests classifier. *Journal of biomedical optics* 23(3):035,005
- Rathore S, Aswal A, Saranya P (2021) Bright lesion detection in retinal fundus images for diabetic retinopathy detection using machine learning approach. *Annals of the Romanian Society for Cell Biology* pp 4360–4367
- Ravichandran C, Raja JB (2014) A fast enhancement/thresholding based blood vessel segmentation for retinal image using contrast limited adaptive histogram equalization. *Journal of medical imaging and health informatics* 4(4):567–575
- REFUGE (2020) Refuge: Retinal fundus glaucoma challenge. <https://refuge.grand-challenge.org/>.
- Rehman ZU, Naqvi SS, Khan TM, Arsalan M, Khan MA, Khalil M (2019) Multi-parametric optic disc segmentation using superpixel based feature classification. *Expert Systems with Applications* 120:461–473
- RIGA (2018) Retinal fundus images for glaucoma analysis: Riga dataset. https://deepblue.lib.umich.edu/data/concern/data_sets/3b591905z
- RIMONE (2011) Rimone database. <https://medimrg.webs.uill.es/research/downloads/>.
- RIONS-DB (2009) Drions-db: Digital retinal images for optic nerve segmentation database. <http://www.ia.uned.es/~ejcarmona/DRIONS-DB.html>
- RKromer, Rahman S, Filev F, Klemm M (2017) An approach for automated segmentation of retinal layers in peripapillary spectralis sd-oct images using curve regularisation. *Insights in Ophthalmology* 1(7):1–6
- Ro JS, Moon JY, Park TK, Lee SH (2022) Association between chronic kidney disease and open-angle glaucoma in south korea: a 12-year nationwide retrospective cohort study. *Scientific Reports* 12(1):1–9
- Robert N (1995) Diabetic retinopathy. *Robert N Frank* 14(2):361–392
- Roisman L, Goldhardt R (2017) Oct angiography: an upcoming non-invasive tool for diagnosis of age-related macular degeneration. *Current ophthalmology reports* 5:136–140
- Roshini R, Alex JSR (2022) Automatic segmentation of optic cup and optic disc using multiresnet for glaucoma classification from fundus image. In: *Intelligent Vision in Healthcare*, Springer, pp 33–44
- Roy AG, Conjeti S, Karri SPK, Sheet D, Katouzian A, Wachinger C, Navab N (2017) Relaynet: retinal layer and fluid segmentation of macular optical coherence tomography using fully convolutional networks. *Biomedical optics express* 8(8):3627–3642
- Roychowdhury S, Koozekanani DD, Parhi KK (2013) Automated denoising and segmentation of optical coherence tomography images. In: *2013 Asilomar Conference on Signals, Systems and Computers*, IEEE, DOI 10.1109/acssc.2013.6810272
- Rübsam A, Wernecke L, Rau S, Pohlmann D, Müller B, Zeitz O, Joussen AM (2021) Behavior of sd-oct detectable hyperreflective foci in diabetic macular edema patients after therapy with anti-vegf agents and dexamethasone implants. *Journal of diabetes research* 2021
- Saeed E, Gołaszewska K, Dmuchowska DA, Zalewska R, Konopińska J (2023) The preserflo microshunt in the context of minimally invasive glaucoma surgery: A narrative review. *International Journal of Environmental Research and Public Health* 20(4):2904
- Saha S, Nassisi M, Wang M, Lindenberg S, Sadda S, Hu ZJ, et al. (2019) Automated detection and classification of early amd biomarkers using deep learning. *Scientific reports* 9(1):1–9

- Saleh GA, Batouty NM, Haggag S, Elnakib A, Khalifa F, Taher F, Mohamed MA, Farag R, Sandhu H, Sewelam A, et al. (2022) The role of medical image modalities and ai in the early detection, diagnosis and grading of retinal diseases: A survey. *Bioengineering* 9(8):366
- Salehi MA, Mohammadi S, Gouravani M, Rezaghali F, Arevalo JF (2022) Retinal and choroidal changes in amd: A systematic review and meta-analysis of spectral-domain optical coherence tomography studies. *Survey of Ophthalmology*
- Sarki R, Ahmed K, Wang H, Zhang Y (2020) Automatic detection of diabetic eye disease through deep learning using fundus images: A survey. *IEEE Access* 8:151,133–151,149
- Saßmannshausen M, Behning C, Isselmann B, Schmid M, Finger RP, Holz FG, Schmitz-Valckenberg S, Pfau M, Thiele S (2022) Relative ellipsoid zone reflectivity and its association with disease severity in age-related macular degeneration: a macustar study report. *Scientific Reports* 12(1):1–12
- Sawa M, Ober MD, Spaide RF (2006) Autofluorescence and retinal pigment epithelial atrophy after subretinal hemorrhage. *Retina* 26(1):119–120
- Schaal KB, Rosenfeld PJ, Gregori G, Yehoshua Z, Feuer WJ (2016) Anatomic clinical trial endpoints for nonexudative age-related macular degeneration. *Ophthalmology* 123(5):1060–1079
- Schaal KB, Munk MR, Wyssmueller I, Berger LE, Zinkernagel MS, Wolf S (2019) Vascular abnormalities in diabetic retinopathy assessed with swept-source optical coherence tomography angiography widefield imaging. *Retina* 39(1):79–87
- Schlegl T, Waldstein SM, Bogunovic H, Endstraßer F, Sadeghipour A, Philip AM, Podkowinski D, Gerasdas BS, Lings G, Schmidt-Erfurth U (2018) Fully automated detection and quantification of macular fluid in oct using deep learning. *Ophthalmology* 125(4):549–558
- Schmitz-Valckenberg S, Pfau M, Fleckenstein M, Staurenghi G, Sparrow JR, Bindewald-Wittich A, Spaide RF, Wolf S, Sadda SR, Holz FG (2021) Fundus autofluorescence imaging. *Progress in retinal and eye research* 81:100,893
- Schreur V, Larsen MB, Sobrin L, Bhavsar AR, den Hollander AI, Klevering BJ, Hoyng CB, de Jong EK, Grauslund J, Peto T (2022) Imaging diabetic retinal disease: clinical imaging requirements. *Acta ophthalmologica*
- Sedai S, Antony B, Rai R, Jones K, Ishikawa H, Schuman J, Gadi W, Garnavi R (2019) Uncertainty guided semi-supervised segmentation of retinal layers in oct images. In: *International Conference on Medical Image Computing and Computer-Assisted Intervention*, Springer, pp 282–290
- Selçuk T, Beyoğlu A, Alkan A (2022) Automatic detection of exudates and hemorrhages in low-contrast color fundus images using multi semantic convolutional neural network. *Concurrency and Computation: Practice and Experience* 34(6):e6768
- Seltman W (2021 (accessed March 5, 2022)) Age-related macular degeneration overview. <https://www.webmd.com/eye-health/macular-degeneration/age-related-macular-degeneration-overview>
- Septiarini A, Harjoko A, Pulungan R, Ekantini R (2018) Automated detection of retinal nerve fiber layer by texture-based analysis for glaucoma evaluation. *Healthcare informatics research* 24(4):335–345
- Sethuraman S, PALAKUZHIL GOPI V (2022) Staircase-net: a deep learning based architecture for retinal blood vessel segmentation. *Sādhanā* 47(4):1–9
- Sevastopolsky A (2017) Optic disc and cup segmentation methods for glaucoma detection with modification of u-net convolutional neural network. *Pattern Recognition and Image Analysis* 27(3):618–624
- Shah A, Abramoff MD, Wu X (2017) Simultaneous multiple surface segmentation using deep learning. In: *Deep Learning in Medical Image Analysis and Multimodal Learning for Clinical Decision Support*, Springer International Publishing, pp 3–11, DOI 10.1007/978-3-319-67558-9_1
- Shah A, Zhou L, Abramoff MD, Wu X (2018) Multiple surface segmentation using convolution neural nets: application to retinal layer segmentation in OCT images. *Biomedical Optics Express* 9(9):4509, DOI 10.1364/boe.9.004509
- Shahriari MH, Sabbaghi H, Asadi F, Hosseini A, Khorrami Z (2022) Artificial intelligence in screening, diagnosis, and classification of diabetic macular edema: A systematic review. *Survey of Ophthalmology*
- Shankaranarayana SM, Ram K, Mitra K, Sivaprakasam M (2019) Fully convolutional networks for monocular retinal depth estimation and optic disc-cup segmentation. *IEEE journal of biomedical and health informatics* 23(4):1417–1426
- Sharma R, Nappi V, Empeslidis T (2023) The developments in amniotic membrane transplantation in glaucoma and vitreoretinal procedures. *International Ophthalmology* pp 1–13
- Sharma S, Tripathi P (2019) Gut microbiome and type 2 diabetes: where we are and where to go? *The Journal of nutritional biochemistry* 63:101–108
- Sheikh S, Qidwai U (2020) Smartphone-based diabetic retinopathy severity classification using convolution neural networks. In: *Proceedings of SAI Intelligent*

- Systems Conference, Springer, pp 469–481
- Shi Z, Wang T, Huang Z, Xie F, Liu Z, Wang B, Xu J (2021) Md-net: A multi-scale dense network for retinal vessel segmentation. *Biomedical Signal Processing and Control* 70:102,977
- Siesky B, Harris A, Belamkar A, Zukerman R, Horn A, Vercellin AV, Mendoza KA, Sidoti PA, Oddone F (2022) Glaucoma treatment outcomes in open angle glaucoma patients of african descent. *Journal of Glaucoma* 31(7):479–487
- Singh A, Dutta MK, ParthaSarathi M, Uher V, Burget R (2016) Image processing based automatic diagnosis of glaucoma using wavelet features of segmented optic disc from fundus image. *Computer methods and programs in biomedicine* 124:108–120
- Singh RP, Elman MJ, Singh SK, Fung AE, Stoilov I (2019) Advances in the treatment of diabetic retinopathy. *Journal of Diabetes and its Complications* 33(12):107,417
- Sjølie AK, Stephenson J, Aldington S, Kohner E, Janka H, Stevens L, Fuller J, Karamanos B, Tountas C, Kofinis A, et al. (1997) Retinopathy and vision loss in insulin-dependent diabetes in europe: the eurodiab iddm complications study. *Ophthalmology* 104(2):252–260
- Smitha A, Jidesh P (2022) Detection of retinal disorders from oct images using generative adversarial networks. *Multimedia Tools and Applications* pp 1–23
- Son J, Park SJ, Jung KH (2019) Towards accurate segmentation of retinal vessels and the optic disc in fundoscopic images with generative adversarial networks. *Journal of digital imaging* 32(3):499–512
- Son T, Ma J, Toslak D, Rossi A, Kim H, Chan RP, Yao X (2022) Light color efficiency-balanced transpalpebral illumination for widefield fundus photography of the retina and choroid. *Scientific Reports* 12(1):13,850
- Song R, Cao P, Yang J, Zhao D, Zaiane OR (2020) A domain adaptation multi-instance learning for diabetic retinopathy grading on retinal images. In: 2020 IEEE international conference on bioinformatics and biomedicine (BIBM), IEEE, pp 743–750
- Sousa JA, Paiva A, Silva A, Almeida JD, Braz Junior G, Diniz JO, Figueredo WK, Gattass M (2021) Automatic segmentation of retinal layers in oct images with intermediate age-related macular degeneration using u-net and dexined. *Plos one* 16(5):e0251,591
- Sreng S, Maneerat N, Hamamoto K, Win KY (2020) Deep learning for optic disc segmentation and glaucoma diagnosis on retinal images. *Applied Sciences* 10(14):4916
- Srinivasan PP, Heflin SJ, Izatt JA, Arshavsky VY, Farsiu S (2014a) Automatic segmentation of up to ten layer boundaries in SD-OCT images of the mouse retina with and without missing layers due to pathology. *Biomedical Optics Express* 5(2):348, DOI 10.1364/boe.5.000348
- Srinivasan PP, Kim LA, Mettu PS, Cousins SW, Comer GM, Izatt JA, Farsiu S (2014b) Fully automated detection of diabetic macular edema and dry age-related macular degeneration from optical coherence tomography images. *Biomedical optics express* 5(10):3568–3577
- Srivastava O, Tennant M, Grewal P, Rubin U, Seamone M (2023) Artificial intelligence and machine learning in ophthalmology: A review. *Indian Journal of Ophthalmology* 71(1):11–17
- STARE (2000) Structured analysis of the retina. <http://cecas.clemson.edu/~ahoover/stare/>
- Stoica SA, Valentini G, Dolci M, D’Agostino S (2022) Diabetes and non-surgical periodontal therapy: What can we hope for? *Hygiene* 2(2):85–93
- Stolte S, Fang R (2020) A survey on medical image analysis in diabetic retinopathy. *Medical image analysis* 64:101,742
- Strisciuglio N, Azzopardi G, Vento M, Petkov N (2016) Supervised vessel delineation in retinal fundus images with the automatic selection of b-cosfire filters. *Machine Vision and Applications* 27(8):1137–1149
- Suciu CI, Suciu VI, Cuțaș A, Nicoară SD (2022) Interleaved optical coherence tomography: Clinical and laboratory biomarkers in patients with diabetic macular edema. *Journal of Personalized Medicine* 12(5):765
- Sufyan M, Ashfaq UA, Ahmad S, Noor F, Saleem MH, Aslam MF, El-Serehy HA, Aslam S (2021) Identifying key genes and screening therapeutic agents associated with diabetes mellitus and hcv-related hepatocellular carcinoma by bioinformatics analysis. *Saudi Journal of Biological Sciences* 28(10):5518–5525
- Sugmk J, Kiattisin S, Leelasantham A (2014) Automated classification between age-related macular degeneration and diabetic macular edema in oct image using image segmentation. In: The 7th 2014 biomedical engineering international conference, IEEE, pp 1–4
- Sui X, Zheng Y, Wei B, Bi H, Wu J, Pan X, Yin Y, Zhang S (2017) Choroid segmentation from optical coherence tomography with graph-edge weights learned from deep convolutional neural networks. *Neurocomputing* 237:332–341, DOI 10.1016/j.neucom.2017.01.023
- Sun JD, Yao C, Liu J, Liu W, Yu ZK (2022) Gnas-u2 net: A new optic cup and optic disc segmentation architecture with genetic neural architecture search. *IEEE Signal Processing Letters* 29:697–701

- Sun X, Xu Y, Zhao W, You T, Liu J (2018) Optic disc segmentation from retinal fundus images via deep object detection networks. In: 2018 40th annual international conference of the IEEE engineering in medicine and biology society (EMBC), IEEE, pp 5954–5957
- Sun Y, Zhang H, Yao X (2020) Automatic diagnosis of macular diseases from oct volume based on its two-dimensional feature map and convolutional neural network with attention mechanism. *Journal of Biomedical Optics* 25(9):096,004
- Surendiran J, Theetchenya S, Benson Mansingh P, Sekar G, Dhipa M, Yuvaraj N, Arulkarthick V, Suresh C, Sriram A, Srihari K, et al. (2022) Segmentation of optic disc and cup using modified recurrent neural network. *BioMed Research International* 2022
- Suzuki N, Hirano Y, Yoshida M, Tomiyasu T, Uemura A, Yasukawa T, Ogura Y (2016) Microvascular abnormalities on optical coherence tomography angiography in macular edema associated with branch retinal vein occlusion. *American journal of ophthalmology* 161:126–132
- Swarnalatha K, Nayak UA, Benny NA, Bharath H, Shetty D, Kumar SD (2023) Detection of diabetic retinopathy using convolution neural network. In: *Emerging Research in Computing, Information, Communication and Applications*, Springer, pp 427–439
- Tan JH, Acharya UR, Bhandary SV, Chua KC, Sivaprasad S (2017) Segmentation of optic disc, fovea and retinal vasculature using a single convolutional neural network. *Journal of Computational Science* 20:70–79
- Tan Y, Yang KF, Zhao SX, Li YJ (2022) Retinal vessel segmentation with skeletal prior and contrastive loss. *IEEE Transactions on Medical Imaging* 41(9):2238–2251
- Terry L, Cassels N, Lu K, Acton JH, Margrain TH, North RV, Fergusson J, White N, Wood A (2016) Automated retinal layer segmentation using spectral domain optical coherence tomography: Evaluation of inter-session repeatability and agreement between devices. *PLOS ONE* 11(9):e0162,001, DOI 10.1371/journal.pone.0162001
- Tham YC, Li X, Wong TY, Quigley HA, Aung T, Cheng CY (2014) Global prevalence of glaucoma and projections of glaucoma burden through 2040: a systematic review and meta-analysis. *Ophthalmology* 121(11):2081–2090
- Thomas D, Duguid G (2004) Optical coherence tomography—a review of the principles and contemporary uses in retinal investigation. *Eye* 18(6):561–570
- Tian Y, Krishnan D, Isola P (2019) Contrastive representation distillation. *arXiv preprint arXiv:1910.10699*
- Tian Z, Zheng Y, Li X, Du S, Xu X (2020) Graph convolutional network based optic disc and cup segmentation on fundus images. *Biomedical Optics Express* 11(6):3043–3057
- Toptaş B, Hanbay D (2021) Retinal blood vessel segmentation using pixel-based feature vector. *Biomedical Signal Processing and Control* 70:103,053
- Tosur M, Philipson LH (2022) Precision diabetes: Lessons learned from maturity-onset diabetes of the young (mody). *Journal of Diabetes Investigation* 13(9):1465–1471
- Touahri R, Azizi N, Hammami NE, Benaida F, Zemmal N, Gasmi I (2022) An improved disc segmentation based on u-net architecture for glaucoma diagnosis. *International Journal of Ambient Computing and Intelligence (IJACI)* 13(1):1–18
- Tran K, Mendel TA, Holbrook KL, Yates PA (2012) Construction of an inexpensive, hand-held fundus camera through modification of a consumer “point-and-shoot” camera. *Investigative ophthalmology & visual science* 53(12):7600–7607
- Treister AD, Nesper PL, Fayed AE, Gill MK, Mirza RG, Fawzi AA (2018) Prevalence of subclinical cnv and choriocapillaris nonperfusion in fellow eyes of unilateral exudative amd on oct angiography. *Translational Vision Science & Technology* 7(5):19–19
- Tulsani A, Kumar P, Pathan S (2021) Automated segmentation of optic disc and optic cup for glaucoma assessment using improved unet++ architecture. *Biocybernetics and Biomedical Engineering* 41(2):819–832
- Uemura A, Fruttiger M, D’Amore PA, De Falco S, Joussen AM, Sennlaub F, Brunck LR, Johnson KT, Lambrou GN, Rittenhouse KD, et al. (2021) Vegfr1 signaling in retinal angiogenesis and microinflammation. *Progress in retinal and eye research* 84:100,954
- Usman A, Khitran SA, Usman Akram M, Nadeem Y (2014) A robust algorithm for optic disc segmentation from colored fundus images. In: *International conference image analysis and recognition*, Springer, pp 303–310
- Usman M, Fraz MM, Barman SA (2017) Computer vision techniques applied for diagnostic analysis of retinal oct images: a review. *Archives of Computational Methods in Engineering* 24(3):449–465
- Van Rijssen TJ, Van Dijk EH, Yzer S, Ohno-Matsui K, Keunen JE, Schlingemann RO, Sivaprasad S, Querques G, Downes SM, Fauser S, et al. (2019) Central serous chorioretinopathy: towards an evidence-based treatment guideline. *Progress in Retinal and Eye Research* 73:100,770

- Vazquez LE, Bye A, Aref AA (2021) Recent developments in the use of optical coherence tomography for glaucoma. *Current opinion in ophthalmology* 32(2):98–104
- Vergroesen JE, Thee EF, Ahmadizar F, van Duijn CM, Stricker BH, Kavousi M, Klaver CC, Ramdas WD (2022) Association of diabetes medication with open-angle glaucoma, age-related macular degeneration, and cataract in the rotterdam study. *JAMA ophthalmology*
- Viedma IA, Alonso-Caneiro D, Read SA, Collins MJ (2022) Oct retinal and choroidal layer instance segmentation using mask r-cnn. *Sensors* 22(5):2016
- Vujosevic S, Parra MM, Hartnett ME, O'Toole L, Nuzzi A, Limoli C, Villani E, Nucci P (2023) Optical coherence tomography as retinal imaging biomarker of neuroinflammation/neurodegeneration in systemic disorders in adults and children. *Eye* 37(2):203–219
- Wan S, Liang Y, Zhang Y (2018) Deep convolutional neural networks for diabetic retinopathy detection by image classification. *Computers & Electrical Engineering* 72:274–282
- Wändell P, Carlsson AC, Ljunggren G (2022) Systemic diseases and their association with open-angle glaucoma in the population of stockholm. *International ophthalmology* 42(5):1481–1489
- Wang C, Zhao Z, Ren Q, Xu Y, Yu Y (2019a) Dense u-net based on patch-based learning for retinal vessel segmentation. *Entropy* 21(2):168
- Wang C, Zhao Z, Yu Y (2021a) Fine retinal vessel segmentation by combining nest u-net and patch-learning. *Soft Computing* 25(7):5519–5532
- Wang J, He Y, Fang W, Chen Y, Li W, Shi G (2021b) Unsupervised domain adaptation model for lesion detection in retinal oct images. *Physics in Medicine & Biology* 66(21):215,006
- Wang J, Li W, Chen Y, Fang W, Kong W, He Y, Shi G (2021c) Weakly supervised anomaly segmentation in retinal oct images using an adversarial learning approach. *Biomedical optics express* 12(8):4713–4729
- Wang J, Li YJ, Yang KF (2021d) Retinal fundus image enhancement with image decomposition and visual adaptation. *Computers in Biology and Medicine* 128:104,116
- Wang L, Liu H, Lu Y, Chen H, Zhang J, Pu J (2019b) A coarse-to-fine deep learning framework for optic disc segmentation in fundus images. *Biomedical signal processing and control* 51:82–89
- Wang L, Li X, Chen Y, Han D, Wang M, Zeng Y, Zhong J, Wang X, Ji Y, Xiong H, et al. (2022a) Automated retinal layer segmentation in optical coherence tomography images with intraretinal fluid. *Journal of Innovative Optical Health Sciences* 15(03):2250,019
- Wang S, Yin Y, Cao G, Wei B, Zheng Y, Yang G (2015) Hierarchical retinal blood vessel segmentation based on feature and ensemble learning. *Neurocomputing* 149:708–717
- Wang Y, Huang L (2022) Optic disc segmentation in retinal fundus images using improved ce-net. In: *Fourteenth International Conference on Digital Image Processing (ICDIP 2022)*, SPIE, vol 12342, pp 417–426
- Wang Y, Zhang Y, Yao Z, Zhao R, Zhou F (2016) Machine learning based detection of age-related macular degeneration (amd) and diabetic macular edema (dme) from optical coherence tomography (oct) images. *Biomedical optics express* 7(12):4928–4940
- Wang Y, Lin Z, Zhai G, Ding XX, Wen L, Li D, Zou B, Feng KM, Liang YB, Xie C (2022b) Prevalence of and risk factors for diabetic retinopathy and diabetic macular edema in patients with early-and late-onset diabetes mellitus. *Ophthalmic research* 65(3):293–299
- Wang Z, Wiggs JL, Aung T, Khawaja AP, Khor CC (2022c) The genetic basis for adult onset glaucoma: Recent advances and future directions. *Progress in Retinal and Eye Research* p 101066
- Warner EF, Boyd K, Whitehead M, Widdowson PS, Binley K, Osborne A (2022) Design of novel multicistronic aav2 gene therapy constructs for the treatment of diabetic macular edema. *Investigative Ophthalmology & Visual Science* 63(7):3470–3470
- Wei H, Peng P (2020) The segmentation of retinal layer and fluid in sd-oct images using mutex dice loss based fully convolutional networks. *IEEE Access* 8:60,929–60,939
- Wei Z, Yuhua P, Jianhang J, Jikun Y, Weiqi B, Yugen Y, Wenle W (2022) Rmsdsc-net: A robust multiscale feature extraction with depthwise separable convolution network for optic disc and cup segmentation. *International Journal of Intelligent Systems*
- Weinhaus RS, Burke JM, Delori FC, Snodderly DM (1995) Comparison of fluorescein angiography with microvascular anatomy of macaque retinas. *Experimental eye research* 61(1):1–16
- Wilkins GR, Houghton OM, Oldenburg AL (2012) Automated segmentation of intraretinal cystoid fluid in optical coherence tomography. *IEEE Transactions on Biomedical Engineering* 59(4):1109–1114
- Willoughby CE, Ponzin D, Lobo SFA, Landau K, Omid Y (2010) Anatomy and physiology of the human eye: effects of mucopolysaccharidoses disease on structure and function – a review. *Clinical and Experimental Ophthalmology* 38:2–11
- Wolfgang D, G F (2008) State-of-the-art retinal optical coherence tomography. *Prog Retin Eye Res*

- 27(1):45–88
- Wong RV ((accessed April 5, 2022)) Macular edema: so many types. <https://retinaeyedoctor.com/2010/02/what-is-macular-edema/>
- Wu Y, Xia Y, Song Y, Zhang Y, Cai W (2020) Nfn+: a novel network followed network for retinal vessel segmentation. *Neural Networks* 126:153–162
- Wu Y, Szymanska M, Hu Y, Fazal MI, Jiang N, Yetisen AK, Cordeiro MF (2022) Measures of disease activity in glaucoma. *Biosensors and Bioelectronics* 196:113,700
- Xiang D, Tian H, Yang X, Shi F, Zhu W, Chen H, Chen X (2018) Automatic segmentation of retinal layer in oct images with choroidal neovascularization. *IEEE Transactions on Image Processing* 27(12):5880–5891
- Xie S, Tu Z (2015) Holistically-nested edge detection. In: *Proceedings of the IEEE international conference on computer vision*, pp 1395–1403
- Xiong H, Liu S, Sharan RV, Coiera E, Berkovsky S (2022a) Weak label based bayesian u-net for optic disc segmentation in fundus images. *Artificial Intelligence in Medicine* 126:102,261
- Xiong K, Wang L, Li W, Wang W, Meng J, Gong X, Lu P, Liang X, Huang J, Huang W (2022b) Risk of acute angle-closure and changes in intraocular pressure after pupillary dilation in patients with diabetes. *Eye* pp 1–6
- Xiong L, Li H (2016) An approach to locate optic disc in retinal images with pathological changes. *Computerized Medical Imaging and Graphics* 47:40–50
- Xu R, Zhao J, Ye X, Wu P, Wang Z, Li H, Chen YW (2022) Local-region and cross-dataset contrastive learning for retinal vessel segmentation. In: *Medical Image Computing and Computer Assisted Intervention–MICCAI 2022: 25th International Conference, Singapore, September 18–22, 2022, Proceedings, Part II*, Springer, pp 571–581
- Xu S, Chen Z, Cao W, Zhang F, Tao B (2021) Retinal vessel segmentation algorithm based on residual convolution neural network. *Frontiers in Bioengineering and Biotechnology* 9
- Yang G, Wei J, Liu P, Zhang Q, Tian Y, Hou G, Meng L, Xin Y, Jiang X (2021) Role of the gut microbiota in type 2 diabetes and related diseases. *Metabolism* 117:154,712
- Yang Q, Reisman CA, Wang Z, Fukuma Y, Hangai M, Yoshimura N, Tomidokoro A, Araie M, Raza AS, Hood DC, Chan K (2010) Automated layer segmentation of macular OCT images using dual-scale gradient information. *Optics Express* 18(20):21,293, DOI 10.1364/oe.18.021293
- Yang S, Zhou X, Wang J, Xie G, Lv C, Gao P, Lv B (2020) Unsupervised domain adaptation for cross-device oct lesion detection via learning adaptive features. In: *2020 IEEE 17Th international symposium on biomedical imaging (ISBI)*, IEEE, pp 1570–1573
- Yang SF, Cheng CH (2014) Fast computation of hessian-based enhancement filters for medical images. *Computer Methods and Programs in Biomedicine* 116(3):215–225
- Yao X, Son T, Ma J (2022) Developing portable wide-field fundus camera for teleophthalmology: Technical challenges and potential solutions. *Experimental Biology and Medicine* 247(4):289–299
- Ye EZ, Ye J, Ye EH (2023) Applications of vision transformers in retinal imaging: A systematic review. *Autheoria*
- Yi S, Wei Y, Zhang G, Wang T, She F, Yang X (2023) Segmentation of retinal vessels based on mranet. *Heliyon* 9(1):e12,361
- Yin P, Cai H, Wu Q (2022) Df-net: Deep fusion network for multi-source vessel segmentation. *Information Fusion* 78:199–208
- Yongpeng Z, Yaxing W, Jinqiong Z, Qian W, Yanni Y, Xuan Y, Jingyan Y, Wenjia Z, Ping W, Chang S, et al. (2022) The association between diabetic retinopathy and the prevalence of age-related macular degeneration—the kailuan eye study. *Frontiers in Public Health* 10
- Yoo TK, Choi JY, Kim HK (2021) Feasibility study to improve deep learning in oct diagnosis of rare retinal diseases with few-shot classification. *Medical & Biological Engineering & Computing* 59:401–415
- Yoshitake T, Murakami T, Suzuma K, Dodo Y, Fujimoto M, Tsujikawa A (2020) Hyperreflective foci in the outer retinal layers as a predictor of the functional efficacy of ranibizumab for diabetic macular edema. *Scientific reports* 10(1):1–8
- Yu M, Lin C, Weinreb RN, Lai G, Chiu V, Leung CKS (2016) Risk of visual field progression in glaucoma patients with progressive retinal nerve fiber layer thinning: a 5-year prospective study. *Ophthalmology* 123(6):1201–1210
- Yuksel Elgin C, Chen D, Al-Aswad LA (2022) Ophthalmic imaging for the diagnosis and monitoring of glaucoma: A review. *Clinical & Experimental Ophthalmology* 50(2):183–197
- Zaaboub N, Sandid F, Douik A, Solaiman B (2022) Optic disc detection and segmentation using saliency mask in retinal fundus images. *Computers in Biology and Medicine* 150:106,067
- Zago GT, Andreão RV, Dorizzi B, Salles EOT (2020) Diabetic retinopathy detection using red lesion localization and convolutional neural networks. *Computers in biology and medicine* 116:103,537

- Zaharia AC, Dumitrescu OM, Radu M, Rogoz RE (2022) Adherence to therapy in glaucoma treatment—a review. *Journal of Personalized Medicine* 12(4):514
- Zang P, Wang J, Hormel TT, Liu L, Huang D, Jia Y (2019) Automated segmentation of peripapillary retinal boundaries in oct combining a convolutional neural network and a multi-weights graph search. *Biomedical optics express* 10(8):4340–4352
- Zhang L, Zhu W, Shi F, Chen H, Chen X (2015) Automated segmentation of intraretinal cystoid macular edema for retinal 3d oct images with macular hole. In: 2015 IEEE 12th International Symposium on Biomedical Imaging (ISBI), IEEE, pp 1494–1497
- Zhang S, Webers CA, Berendschot TT (2022a) A double-pass fundus reflection model for efficient single retinal image enhancement. *Signal Processing* 192:108,400
- Zhang X, Li D, Wei Q, Han X, Zhang B, Chen H, Zhang Y, Mo B, Hu B, Ding D, et al. (2022b) Automated detection of severe diabetic retinopathy using deep learning method. *Graefe's Archive for Clinical and Experimental Ophthalmology* 260(3):849–856
- Zhang X, Song QJ, Wang RC, Zhou Z (2022c) Convolutional autoencoder joint boundary and mask adversarial learning for fundus image segmentation. *Frontiers in Human Neuroscience* p 834
- Zhang Y, Fang J, Chen Y, Jia L (2022d) Edge-aware u-net with gated convolution for retinal vessel segmentation. *Biomedical Signal Processing and Control* 73:103,472
- Zhang Y, He M, Chen Z, Hu K, Li X, Gao X (2022e) Bridge-net: Context-involved u-net with patch-based loss weight mapping for retinal blood vessel segmentation. *Expert Systems with Applications* 195:116,526
- Zhang YP, Wang YX, Zhou JQ, Qian W, Yan YN, Xuan Y, Yang JY, Zhou WJ, Ping W, Chang S, et al. (2022f) The influence of diabetes, hypertension, and hyperlipidemia on the onset of age-related macular degeneration in north china: The kailuan eye study. *Biomedical and Environmental Sciences* 35(7):613–621
- Zhang Z, Yin FS, Liu J, Wong WK, Tan NM, Lee BH, Cheng J, Wong TY (2010) Origa-light: An online retinal fundus image database for glaucoma analysis and research. In: 2010 Annual international conference of the IEEE engineering in medicine and biology, IEEE, pp 3065–3068
- Zhao R, Chen X, Liu X, Chen Z, Guo F, Li S (2019) Direct cup-to-disc ratio estimation for glaucoma screening via semi-supervised learning. *IEEE journal of biomedical and health informatics* 24(4):1104–1113
- Zhao Y, Liu Y, Wu X, Harding SP, Zheng Y (2015) Correction: Retinal vessel segmentation: An efficient graph cut approach with retinex and local phase. *Plos one* 10(4):e0127,486
- Zhu H, Zhu X, Liu Y, Jiang F, Chen M, Cheng L, Cheng X (2020) Gene expression profiling of type 2 diabetes mellitus by bioinformatics analysis. *Computational and Mathematical Methods in Medicine* 2020
- Zhuang J, Chen Z, Zhang J, Zhang D, Cai Z (2019) Domain adaptation for retinal vessel segmentation using asymmetrical maximum classifier discrepancy. In: *Proceedings of the ACM Turing Celebration Conference-China*, pp 1–6